Spring 2003

Multi-Symplectic Integrators for Nonlinear Wave Equations

Alvaro Lucas Islas
Old Dominion University

MULTI-SYMPLECTIC INTEGRATORS FOR NONLINEAR WAVE EQUATIONS

by

Alvaro Lucas Islas
B.S. September 1981, National University of Mexico
M.S. June 1985, New York University

A Dissertation Submitted to the Faculty of
Old Dominion University in Partial Fulfillment of the
Requirement for the Degree of

DOCTOR OF PHILOSOPHY

MATHEMATICS AND STATISTICS

OLD DOMINION UNIVERSITY
May 2003

Approved by:

Constance M. Schober (Director)

David G. Lasseigne

Fang Q. Hu

David E. Keves

Chester E. Grosch

ABSTRACT

MULTI-SYMPLECTIC INTEGRATORS FOR NONLINEAR WAVE EQUATIONS

Alvaro Lucas Islas
Old Dominion University, 2003
Director: Dr. Constance M. Schober

Symplectic (area-preserving) integrators for Hamiltonian ordinary differential equations have shown to be robust, efficient and accurate in long-term calculations. In this thesis, we show how symplectic integrators have a natural generalization to Hamiltonian PDEs by introducing the concept of multi-symplectic partial differential equations (PDEs). In particular, we show that multi-symplectic PDEs have an underlying spatio-temporal multi-symplectic structure characterized by a multi-symplectic conservation law (MSCL). Then multi-symplectic integrators (MSIs) are numerical schemes that preserve exactly the MSCL. Remarkably, we demonstrate that, although not designed to do so, MSIs preserve very well other associated local conservation laws and global invariants, such as the energy and the momentum, for very long periods of time. We develop two types of MSIs, based on finite differences and Fourier spectral approximations, and illustrate their superior performance over traditional integrators by deriving new numerical schemes to the well known 1D nonlinear Schrödinger and sine-Gordon equations and the 2D Gross-Pitaevskii equation. In sensitive regimes, the spectral MSIs are not only more accurate but are better at capturing the spatial features of the solutions. In particular, for the sine-Gordon equation we show that its phase space, as measured by the nonlinear spectrum associated with it, is better preserved by spectral MSIs than by spectral non-symplectic Runge-Kutta integrators. Finally, to further understand the improved performance of MSIs, we develop a backward error analysis of the multi-symplectic centered-cell discretization for the nonlinear Schrödinger equation. We verify that the numerical solution satisfies to higher order a nearby modified multi-symplectic PDE and its modified multi-symplectic energy conservation law. This implies, that although the numerical solution is an approximation, it retains the key feature of the original PDE, namely its multi-symplectic structure.

ACKNOWLEDGMENTS

I would like to thank my wife for her invaluable and constant support and encouragement, my children for their patience and maturity, and my parents for their life-long example of hard work, faith and love of living.

TABLE OF CONTENTS

Page

LIST OF TABLES

Page

LIST OF FIGURES

CHAPTER I

INTRODUCTION

Symplectic (area-preserving) integrators, which are numerical integration methods that preserve the symplectic structure of Hamiltonian ODEs, have proven to be robust, efficient and accurate in long-time calculations. Although symplectic integrators (SIs) are not designed to preserve the Hamiltonian, they do, in fact, preserve the Hamiltonian very well over very long times. Insight into the performance of symplectic methods has been provided by a backward error analysis which shows that symplectic discretizations of a Hamiltonian system lead to modified differential equations that are also Hamiltonian. The Hamiltonian structure of the modified equations can then be used to show that a symplectic integrator almost preserves the total energy over an exponentially long period of time [10, 29].

These properties made it natural to consider SIs when developing structure preserving integrators for Hamiltonian PDEs. The question was how appropriately to generalize the concept of symplecticity to encompass PDEs. Until recently, the standard approach was to introduce a Hamiltonian semi-discretization of the PDE and then apply a symplectic scheme to integrate the semi-discrete system in time. This approach focuses on preserving global properties of the PDE as time evolves and met with varying degrees of success. Many Hamiltonian PDEs were found to be very sensitive to the manner in which space is discretized [2, 3]. However, the standard approach does not provide a method for finding an appropriate spatial discretization.

An alternate generalization of symplecticity to the PDE framework is the development of a local concept of symplecticity that treats space and time equally [12, 36, 37]. *Multi-symplectic* PDEs owe their name to the underlying *spatial-temporal* symplectic structure. An immediate consequence of the multi-symplectic (MS) structure is the existence of a *local*, rather than global, multi-symplectic conservation law where changes in time are exactly compensated by changes in space.

In this thesis, using the new space-time MS formulation of Hamiltonian PDEs, we develop several classes of MS integrators and explore their ability to preserve

This dissertation follows the style of the *Journal of Computational Physics*

local conservation laws as well as global invariants. In Chapter 2 we begin by reviewing the basic concepts associated with Hamiltonian ODEs, their symplectic structure, and symplectic discretizations. In Chapter 3 we introduce the concept of a multi-symplectic PDE and its associated multi-symplectic conservation law. We present several examples to illustrate how a MS formulation applies to well known nonlinear wave equations such as the nonlinear Schrödinger (NLS) and sine-Gordon (SG) equations. Multi-symplectic integrators are discretizations of the PDE which preserve exactly a discrete version of the MS conservation law. We derive, numerically implement, and examine the properties of a new class of integrators for the NLS equation: MS finite difference discretizations based on the Gauss-Legendre (G-L) family of schemes. In Chapter 4 we carry out a backward error analysis of the MS finite difference discretization of the NLS equation. This explains the preservation properties of the local conservation laws observed in the numerical experiments.

In Chapter 5 we show that spectral discretizations provide another class of multi-symplectic integrators and derive MS spectral discretizations for the NLS and SG equations. We compare the performance of MS spectral methods with non-symplectic spectral methods and find: (1) A significant improvement in the resolution of the qualitative features of solutions of the NLS equation is obtained with MS spectral methods. (2) MS spectral methods preserve the geometry of the sine-Gordon phase space better, as measured by preservation of the nonlinear spectrum.

Finally, we show that the concept of multi-symplecticity can easily be generalized to several space dimensions. In Chapter 6 we develop a MS formulation for a variable coefficient Gross-Pitaevskii equation in two space dimensions. We conclude in Chapter 7 and provide the necessary background material on integrable systems in the appendices.

Appendix A discusses the context in which our benchmark equations, the nonlinear Schrödinger (NLS), sine-Gordon (SG) and Gross-Pitaevskii equations, are related. We focus only on those elements of the integrable theory which are relevant for interpreting the ability of the symplectic and multi-symplectic numerical schemes that we develop to preserve phase space structures. Appendix B examines an alternate approach to discretizing the NLS equation. The NLS equation is an

integrable PDE and so we consider an integrable semi-discretization of the equation, the Ablowitz-Ladik (AL) system. An interesting feature of the AL system is that it has a non-canonical symplectic structure. Several symplectic integrators are developed, providing integrable-symplectic discretizations of the NLS equation. The results in this appendix provide a basis of comparison for the MS integrators.

CHAPTER II

BACKGROUND: SYMPLECTIC INTEGRATORS

Numerical integration methods for Hamiltonian ODEs which preserve the underlying symplectic structure by preserving the symplectic differential area, generally known as symplectic integrators, were first studied in a general setting by K. Feng [24]. Feng employed generating function techniques to construct the symplectic schemes [25]. Subsequently, other researchers investigated standard numerical methods, such as Runge-Kutta methods, to determine if they had subclasses which were symplectic [35, 46, 48, 57]. These ideas were then applied to develop specific integration methods for specific Hamiltonian problems [18, 45, 53].

In this chapter we review the basic concepts associated with Hamiltonian ODEs, their symplectic structure, and the symplectic discretizations used to solve them. A comprehensive treatment of Hamiltonian systems can be found in the text of Arnold [8] or that of Meyer and Hall [40], while symplectic discretizations of ODEs are surveyed in the articles [49, 59] and in the texts [30, 50]. In later chapters many of these ideas are extended to Hamiltonian PDEs, providing new insight into the structure of the PDE. This enables the further development of new structure-preserving integrators, or multi-symplectic integrators, for Hamiltonian PDEs.

II.1 HAMILTONIAN ODES

Consider a nonempty, open, connected subset $\Omega \subset \mathbb{R}^{2d}$ and an open interval $I \subset \mathbb{R}$. Let $(p,q) = (p_1,\ldots,p_d,q_1,\ldots,q_d) \in \Omega$ and let $H = H(p,q,t)$ be a sufficiently smooth real function defined in the product $\Omega \times I$. Then the *Hamiltonian system* of differential equations with Hamiltonian H is, by definition, given by

$$\begin{aligned} \frac{d}{dt}p_i &= -\frac{\partial H}{\partial q_i}, \\ \frac{d}{dt}q_i &= +\frac{\partial H}{\partial p_i}, \end{aligned} \tag{1}$$

for $i = 1,\ldots,d$. The integer d is called the *number of degrees of freedom* and Ω is the *phase space*. For existence and uniqueness theorems for (1), we assume that H is at least C^2. If H does not explicitly depend on t, (1) is an *autonomous* system.

To facilitate later calculations, it is convenient to write these equations in vector form. Let $z = (p,q) = (p_1,\ldots,p_d,q_1,\ldots,q_d)$. Then the Hamiltonian system of

equations becomes

$$\frac{d}{dt}z = \boldsymbol{J}^{-1}\nabla_z H(z), \tag{2}$$

where ∇_z is the *gradient* operator

$$\nabla_z = \left(\frac{\partial}{\partial p_1}, \ldots, \frac{\partial}{\partial p_d}, \frac{\partial}{\partial q_1}, \ldots, \frac{\partial}{\partial q_d}\right)^T$$

and $\boldsymbol{J}$ is the $2d \times 2d$ skew-symmetric matrix

$$\boldsymbol{J} = \begin{pmatrix} \mathbf{0} & \boldsymbol{I}_d \\ -\boldsymbol{I}_d & \mathbf{0} \end{pmatrix},$$

with $\boldsymbol{I}_d$ and $\mathbf{0}$ being the $d \times d$ unit and zero matrices, respectively. ($\boldsymbol{J}$ is significant enough that $\boldsymbol{J}^{-1}$ is used in the Hamiltonian system (2) instead of another symbol).

Associated with (1) we have the *variational* system of equations

$$\begin{aligned} \frac{d}{dt}dp_i &= -\frac{\partial^2 H}{\partial q \partial p}dp - \frac{\partial H}{\partial q^2}dq, \\ \frac{d}{dt}dq_i &= +\frac{\partial H}{\partial p^2}dp + \frac{\partial^2 H}{\partial p \partial q}dq, \end{aligned}$$

or in vector form

$$\frac{d}{dt}dz = \boldsymbol{J}^{-1}\boldsymbol{H}_{zz}(z)\,dz, \tag{3}$$

where $\boldsymbol{H}_{zz}$ is the $2d \times 2d$ symmetric matrix

$$\boldsymbol{H}_{zz} = \begin{pmatrix} \frac{\partial H^2}{\partial p^2} & \frac{\partial^2 H}{\partial p \partial q} \\ \frac{\partial^2 H}{\partial p \partial q} & \frac{\partial H^2}{\partial q^2} \end{pmatrix}.$$

Another useful concept is that of a Poisson bracket. The Poisson bracket between two functions, G and H is defined by

$$\{G,\, H\} = (\nabla G)^T \boldsymbol{J}^{-1} \nabla H,$$

or equivalently

$$\{G,\, H\} = \sum_{i=1}^{d} \frac{\partial H}{\partial p_i}\frac{\partial G}{\partial q_i} - \frac{\partial H}{\partial q_i}\frac{\partial G}{\partial p_i}.$$

Then, Hamiltonian equations can be written in yet another form, as

$$\frac{d}{dt}z = \{z,\, H\}.$$

The flow, ψ, generated by the Hamiltonian system is a transformation mapping the phase space Ω into itself in such a way that

$$(p(t), q(t)) = \psi(p^0, q^0) \tag{4}$$

is the solution of (1) at time t for the initial condition $(p(t_0), q(t_0)) = (p^0, q^0)$. When (p^0, q^0) is kept fixed and t is varied, then the solution of the Hamiltonian system is recovered. On the other hand, when t is kept fixed and (p^0, q^0) is varied, then ψ defines a map of Ω into itself, assuming that the solutions using initial values (p^0, q^0) exist at time t.

Conservation of energy

Let $z(t)$ be a solution of (2). Then, using the fact that J is skew-symmetric, we have that

$$\begin{aligned} \frac{d}{dt}H(z(t),t) &= (\nabla_z H)^T \frac{d}{dt}z + \frac{\partial H}{\partial t} \\ &= (\nabla_z H)^T J^{-1} \nabla_z H + \frac{\partial H}{\partial t} \\ &= \frac{\partial H}{\partial t}. \end{aligned}$$

In particular, if H is autonomous, then

$$\frac{d}{dt}H = 0.$$

That is, along the solution $z(t)$, $H(z(t)) = H(z_0)$ is a constant. In many applications, this corresponds physically to the conservation of energy.

A consequence of energy conservation is that autonomous planar Hamiltonian systems are *integrable*. Away from fixed points where

$$\frac{\partial H}{\partial p} = 0 \quad \text{and} \quad \frac{\partial H}{\partial q} = 0,$$

the implicit function theorem ensures that we can either solve for $p = p(q; p_0, q_0)$ or $q = q(p; p_0, q_0)$. This can be used to eliminate one of the variables in the planar system, reducing it to a single quadrature.

Preservation of area

The most fundamental or characteristic property of Hamiltonian systems is that they are area-preserving: *A system of ODEs has an area-preserving property if*

and only if it is Hamiltonian. For simplicity assume that $d = 1$. It follows directly from (1) that the vector field $(-\partial H/\partial q, \partial H/\partial p)^T$ is divergence-free, i.e.,

$$\frac{\partial}{\partial p}\left(-\frac{\partial H}{\partial q}\right) + \frac{\partial}{\partial q}\left(\frac{\partial H}{\partial p}\right) = 0.$$

As a consequence, for each fixed t, the flow ψ is an area-preserving transformation in Ω, i.e., for each bounded $D \subset \Omega$, D and $\psi(D)$ have the same oriented area. On the other hand, if ψ is an area-preserving solution operator for the the system

$$\frac{d}{dt}p = f(p,q,t), \qquad \frac{d}{dt}q = g(p,q,t), \tag{5}$$

then, by Liouville's theorem [8], for each fixed t, the vector field $(f,g)^T$ is divergence-free

$$\frac{\partial f}{\partial p} + \frac{\partial g}{\partial q} = 0$$

which is a necessary and sufficient condition for the field $(g,-f)^T$ to be the the gradient of a scalar function H (assuming also that Ω is simply connected). That is, (5) is Hamiltonian.

Consequences of area preservation

Area preservation has a marked impact on the long time dynamics of (planar) Hamiltonian systems. For instance, asymptotically stable equilibrium (fixed) points or limit cycles are not allowed – in their vicinity area has to shrink. This has an important consequence.

Recall the Poincarè-Bendixon theorem for general planar dynamical systems of the form (5): an orbit which remains bounded for all time ($t > 0$) and does not have a fixed point, approaches a closed orbit (limit cycle) [8]. We have excluded limit cycles for planar Hamiltonian systems, therefore, the only possibility for planar Hamiltonian orbits not containing any fixed points, is periodicity.

The matrix J

One approach to verifying that a map is area-preserving is to use the Jacobian determinant of the transformation. Let ψ be a map that advances the solution from (p,q) at t to (p^*,q^*) at t^*. That is, let ψ satisfy (4). Then ψ is area-preserving if and only if its Jacobian

$$\psi' = \frac{\partial(p^*,q^*)}{\partial(p,q)} = \begin{pmatrix} \frac{\partial p^*}{\partial p} & \frac{\partial p^*}{\partial q} \\ \frac{\partial q^*}{\partial p} & \frac{\partial q^*}{\partial q} \end{pmatrix}$$

has a determinant equal to one, i.e.,

$$\frac{\partial p^*}{\partial p}\frac{\partial q^*}{\partial q} - \frac{\partial p^*}{\partial q}\frac{\partial q^*}{\partial p} = 1. \tag{6}$$

This relation can be expressed using the symplectic matrix $\boldsymbol{J}$ Specifically, if ψ is an area-preserving map then relation (6) can be rewritten as

$$\psi'^T \boldsymbol{J} \psi' = \boldsymbol{J}. \tag{7}$$

This can be established by direct matrix multiplication, i.e., let

$$\psi' = \begin{pmatrix} a & b \\ c & d \end{pmatrix}$$

with determinant $ad - bc = 1$. Then

$$\begin{aligned} \psi'^T \boldsymbol{J} \psi' &= \begin{pmatrix} a & c \\ b & d \end{pmatrix} \begin{pmatrix} 0 & 1 \\ -1 & 0 \end{pmatrix} \begin{pmatrix} a & b \\ c & d \end{pmatrix} \\ &= \begin{pmatrix} a & c \\ b & d \end{pmatrix} \begin{pmatrix} c & d \\ -a & -b \end{pmatrix} = \begin{pmatrix} 0 & 1 \\ -1 & 0 \end{pmatrix} = \boldsymbol{J}. \end{aligned}$$

The matrix $\boldsymbol{J}$ is important because, given two vectors u, $v \in \mathbb{R}^2$, the quantity $u^T \boldsymbol{J} v$ is *the oriented area of the parallelogram determined by u and v*. Now given the transformation $\psi : \Omega \in \mathbb{R}^2 \longrightarrow \Omega$, the parallelogram $\mathcal{P}$ with sides u, v gets mapped into the parallelogram $\psi(\mathcal{P})$ with curved sides that can be approximated by the parallelogram with sides $\psi' u$, $\psi' v$. Equation (7) says that these parallelograms have the same area, since

$$(\psi' u)^T \boldsymbol{J}\, \psi' v = u^T \psi'^T \boldsymbol{J}\, \psi' v = u^T \boldsymbol{J} v.$$

The straightforward generalization of area preservation to higher dimensions, i.e., volume preservation, does not necessarily define a Hamiltonian flow. Relation (7) yields the appropriate generalization of area preservation to higher dimensions.

Higher dimensional Hamiltonian systems

For planar systems we observed that Hamiltonian flows preserve the area and that area preservation is the definitive property of planar Hamiltonian systems. The analogous property for higher dimensional Hamiltonian systems is a straightforward generalization of (7). It has a simple geometric interpretation: the sum of

the oriented areas obtained by projecting $D \subset \Omega$ onto the d 2-dimensional planes (p_i, q_i), $i = 1, \ldots, d$ is preserved by the flow $\psi(D)$. It can be shown that this is again the definitive property of Hamiltonian system: any differential system with this property is Hamiltonian.

Differential forms and exterior products

An alternative approach, involving differential forms and their exterior product, can be used to establish whether a map is symplectic or area-preserving [8]. The use of differential forms considerably simplifies the calculation of symplecticity, so we therefore comment very briefly on their properties. A more complete treatment of differential forms and how they measure areas can be found in [52].

Briefly, the exterior or wedge product, denoted by "$\wedge$", is a skew-symmetric operator,

$$du \wedge dv = -dv \wedge du, \tag{8}$$

between differentials that can be interpreted as a measure of two-dimensional areas in the following sense: Let $(p, q) = (p(u, v), q(u, v))$. Then

$$\begin{aligned} dp &= p_u du + p_v dv, \\ dq &= q_u du + q_v dv. \end{aligned}$$

Using the skew-symmetric property of the exterior product, we find that

$$\begin{aligned} dp \wedge dq &= (p_u q_v - p_v q_u) du \wedge dv \\ &= \left| \frac{\partial(p, q)}{\partial(u, v)} \right| du \wedge dv. \end{aligned}$$

Therefore, $dp \wedge dq$ can be interpreted as a two-dimensional area element.

When p and q are vectors, we are still interested in two-dimensional areas. Let $z = (p_1, \ldots, p_d, q_1, \ldots, q_d)^T$. Then, using (8), we have that

$$\begin{aligned} \tfrac{1}{2}\, dz \wedge \boldsymbol{J} dz &= \tfrac{1}{2}\, (dp_1, \cdots, dp_d, dq_1, \cdots, dq_d)^T \wedge (dq_1, \cdots, dq_d, -dp_1, \cdots, -dp_d)^T \\ &= dp_1 \wedge dq_1 + \cdots + dp_d \wedge dq_d \\ &= dp \wedge dq, \end{aligned} \tag{9}$$

can be interpreted as the sum of the two-dimensional areas $dp_i \wedge dq_i$, $i = 1, \ldots, d$.

It also holds in general, from (9), that if A is any matrix, then

$$dp \wedge \boldsymbol{A} dq = \boldsymbol{A}^T dp \wedge dq.$$

In particular, if $\boldsymbol{A}$ is symmetric, then

$$\boldsymbol{A}dp \wedge dp = dp \wedge \boldsymbol{A}^T dp = dp \wedge \boldsymbol{A}dp = -\boldsymbol{A}dp \wedge dp$$

or

$$\boldsymbol{A}dp \wedge dp = 0.$$

It is straightforward now to check whether a map is area-preserving using differential forms and exterior products. Let ψ be an area-preserving map such that $z^* = \psi(z)$ and $dz^* = \boldsymbol{\psi}'(z)\, dz$. Then

$$dz^* \wedge \boldsymbol{J}dz^* = \boldsymbol{\psi}' dz \wedge \boldsymbol{J}\boldsymbol{\psi}' dz = dz \wedge \boldsymbol{\psi}'^{\boldsymbol{T}} \boldsymbol{J}\boldsymbol{\psi}' dz = dz \wedge \boldsymbol{J}dz$$

or

$$dz^* \wedge \boldsymbol{J}dz^* = dz \wedge \boldsymbol{J}dz. \tag{10}$$

Integrability

Autonomous Hamiltonian systems in R^2 have the additional feature that they are integrable. From

$$\frac{d}{dt}H = 0,$$

it follows that $H(p(t), q(t)) = H(p^0, q^0)$ along the solution curves. Provided that $\frac{\partial H}{\partial p}$ and $\frac{\partial H}{\partial q}$ are not simultaneously zero (we are away from the fixed points of the system), the implicit function theorem can be used to solve for either $p = p(q; p^0, q^0)$ or $q = q(p; p^0, q^0)$. This is then used to eliminate one of the variables in the 2-dimensional system, reducing the solution to a single quadrature.

For a general $2n$-dimensional (n degrees of freedom) system to be integrable, normally $2n - 1$ independent constants of motion are needed to reduce the system to a single quadrature. Hamiltonian systems are special in that only n independent constants of motion (which commute under the Poisson bracket) are needed for a $2n$-dimensional Hamiltonian system to be integrable. These n independent constants of motion allow one to find (locally) a symplectic transformation to a new coordinate system, $(I_1, ..., I_n, \theta_1, ..., \theta_n)$ such that the Hamiltonian in the new coordinate system depends only on the actions, $\boldsymbol{I}$, i.e., $H = H(\boldsymbol{I})$. In the new coordinate system the equations of motion become

$$\begin{aligned} \frac{d}{dt}I_i &= -\frac{\partial H}{\partial \theta_i} = 0, \\ \frac{d}{dt}\theta_i &= +\frac{\partial H}{\partial I_i} \equiv \omega_i(\boldsymbol{I}). \end{aligned}$$

The actions, I_i, are constants of the motion. In addition, the conjugate variables, θ_i, are referred to as the angle coordinates and are only defined mod 2π. The ω_i are the frequencies and geometrically these coordinates correspond to an n-dimensional torus, which may be defined only locally. Another important structure associated with Hamiltonian systems is that of a homoclinic orbit. An interesting question that can be asked is what happens to phase space structure (i.e., to the tori and homoclinic orbits) under small perturbations. The answer depends on many things, such as the type of perturbation, and the geometry and the dimension of the phase space.

II.2 SYMPLECTIC DISCRETIZATIONS

In this thesis we study structure-preserving integrators – symplectic and multi-symplectic numerical schemes and how they compare with non-symplectic schemes. But what exactly does it mean for a discretization to be symplectic? To precisely define this, we first need to introduce the symplectic conservation law.

Symplectic conservation law

Result (10) is significant enough that it should be expressed as a conservation law. Let

$$\omega = \frac{1}{2} dz \wedge \boldsymbol{J} dz,$$

where dz satisfies the variational system of equations (3). Then

$$\begin{aligned} (dz \wedge \boldsymbol{J} dz)_t &= dz_t \wedge \boldsymbol{J} dz + dz \wedge \boldsymbol{J} dz_t \\ &= -\boldsymbol{J} dz_t \wedge dz - \boldsymbol{J} dz_t \wedge dz \\ &= -2\boldsymbol{H}_{zz} dz \wedge dz \\ &= 0 \end{aligned}$$

since $\boldsymbol{H}_{zz}$ is a symmetric matrix. That is,

$$\frac{d}{dt}\omega = 0. \tag{11}$$

Equation (11) is known as the *symplectic* conservation law (SCL). We are now in the position to define a symplectic discretization.

Definition 1 *A discretization of the Hamiltonian system of equations (2) is said to be symplectic if its solution exactly satisfies a discretization of the SCL (11).*

This is a strong requirement and, as we have discussed, is the requirement that actually distinguishes the Hamiltonian flow. Once the SCL is satisfied, we can examine how other invariants, such as the energy, are being preserved. The SCL, together with the energy conservation law (ECL),

$$\frac{d}{dt}H = 0,$$

form an important pair of constants of the motion. Until recently, numerical schemes were designed to preserve the energy H and did not take into account symplecticity. As a result symplecticity was not preserved and the numerical solution can be viewed as the solution of a nearby perturbed non-Hamiltonian system (see Chapter IV on backward error analysis). The focus has now shifted to designing numerical schemes that preserve symplecticity rather than the energy and the results have been very encouraging. In fact, in certain situations, symplectic methods (that preserve symplecticity) perform better at preserving the energy in long-time calculations than those schemes designed to preserve the energy [62].

Implicit midpoint rule

Symplectic schemes have been developed which are applicable in relatively general situations. One such class is the class of symplectic Runge-Kutta methods (note that not all Runge-Kutta (R-K) methods are symplectic) [48]. In this section we briefly describe symplectic R-K schemes, concentrating on the well known implicit midpoint rule. The implicit midpoint rule is then used in later chapters when developing multi-symplectic finite difference and (pseudo) spectral discretizations.

We now show that the implicit midpoint rule provides a symplectic discretization of the Hamiltonian system (2). To do so, let F denote the right hand side of equation (2). Then the implicit midpoint rule scheme is given by the two steps

$$\begin{aligned} Z^{1/2} &= z^0 + \tfrac{1}{2}hF(Z^{1/2}), \\ z^1 = &= z^0 + hF(Z^{1/2}). \end{aligned} \tag{12}$$

By eliminating $F(Z^{1/2})$ we find that $Z^{1/2} = \frac{1}{2}\left(z^0 + z^1\right)$. To show that the scheme is symplectic, we need to show that a discretization of the SCL is satisfied. Let us start by rewriting equation (12) as

$$J\left(z^1 - z^0\right) = h\nabla_z H(Z^{1/2}).$$

Taking its differential we get

$$\boldsymbol{J}\left(dz^1 - dz^0\right) = h\boldsymbol{H}_{zz}dZ^{1/2}.$$

Multiplying it by $dZ^{1/2}$ yields zero on the right-hand side

$$hdZ^{1/2} \wedge \boldsymbol{H}_{zz}dZ^{1/2} = 0,$$

since $\boldsymbol{H}_{zz}$ is symmetric. The left-hand side gives

$$\begin{aligned} 0 = dZ^{1/2} \wedge \boldsymbol{J}\left(dz^1 - dz^0\right) &= \tfrac{1}{2}\left(dz^1 + dz^0\right) \wedge \boldsymbol{J}\left(dz^1 - dz^0\right) \\ &= \tfrac{1}{2}\left(dz^1 \wedge \boldsymbol{J}dz^1 - dz^0 \wedge \boldsymbol{J}dz^0\right). \end{aligned}$$

This shows that the solution obtained from applying an implicit midpoint step satisfies the discrete SCL

$$dz^{n+1} \wedge \boldsymbol{J}dz^{n+1} = dz^n \wedge \boldsymbol{J}dz^n.$$

The implicit midpoint rule is one member of the family of symplectic Runge-Kutta methods for nonlinear Hamiltonian systems. Higher order symplectic RK methods can readily be obtained using the Baker-Campbell-Hausdorff formula [60].

CHAPTER III

MULTI-SYMPLECTIC INTEGRATORS

Once the advantages of using symplectic methods for Hamiltonian ODEs became apparent, the question naturally arose as to how appropriately to generalize symplectic integrators to a Hamiltonian PDE framework. What are the relevant geometric features for a PDE integrator to preserve? One long standing approach has been to introduce a Hamiltonian semi-discretization of the PDE using, e.g., spectral methods or finite differencing, and then to apply a symplectic scheme to integrate the semi-discrete system in time [1, 20, 38]. This met with varying degrees of success as the numerical results were found to be highly dependent on the particular discretization used to discretize the spatial derivatives [2, 3].

Recently a generalization of symplecticity to the PDE framework (multi-symplectic PDEs) was proposed that involves a local concept of symplecticity and an equal treatment of the spatial and temporal variables [12, 36, 37]. In this chapter we introduce the concept of a multi-symplectic PDE and present several examples to illustrate how it applies to well known nonlinear wave equations. Specifically, we provide a multi-symplectic formulation of the nonlinear Schrödinger (NLS) and sine-Gordon (SG) equations. Multi-symplectic integrators are discretizations of the PDE which preserve a multi-symplectic conservation law (similar to the conservation of symplecticity for Hamiltonian ODEs) and can be constructed using symplectic discretizations both in space and time. We derive a new class of integrators for the NLS equation – multi-symplectic finite difference discretizations which can be constructed by employing the Gauss-Legendre (G-L) family of schemes. We numerically implement the second order member of the G-L family of integrators for the NLS equation and examine the preservation of the local conservation laws and global invariants. As our numerical experiments demonstrate, multi-symplectic methods have remarkable preservation properties. For instance, we show that the local and global energy are preserved far better than expected, given the order of the scheme. In addition, the global invariants, the norm and momentum, are preserved within roundoff.

III.1 MULTI-SYMPLECTIC PDES

We begin by defining multi-symplectic PDEs for the "1 + 1" case of one spatial and one temporal dimension [12]:

Definition 2 *A PDE is said to be multi-symplectic if it can be written in the form*

$$\boldsymbol{M} z_t + \boldsymbol{K} z_x = \nabla_z S, \tag{13}$$

where $\boldsymbol{M}$ *and* $\boldsymbol{K}$ *are skew-symmetric matrices* ($\boldsymbol{M}^T = -\boldsymbol{M}$) *on* $\mathbb{R}^{d\times d}$ *and* $S : \mathbb{R}^d \mapsto \mathbb{R}$ *is a smooth function of the state variable*

$$z = (z_1, \ldots, z_d)^T.$$

The gradient operator ∇_z *is defined as*

$$\nabla_z = \left(\frac{\partial}{\partial z_1}, \ldots, \frac{\partial}{\partial z_d}\right)^T.$$

The term multi-symplectic is applied to system (13) in the sense that associated with $\boldsymbol{M}$ and $\boldsymbol{K}$ are the 2-forms

$$\omega = \frac{1}{2}(dz \wedge \boldsymbol{M} dz), \qquad \kappa = \frac{1}{2}(dz \wedge \boldsymbol{K} dz), \tag{14}$$

such that ω and κ define a symplectic space-time structure (symplectic with respect to more than one independent variable).

Multi-symplectic conservation law

Symplecticity is a global property for Hamiltonian ODEs. In contrast, an important aspect of the multi-symplectic structure is that symplecticity is now a local property, i.e., symplecticity may vary from point to point and from time to time. This local feature is expressed through the following multi-symplectic conservation law (MSCL) [12]:

Proposition 1 *Let* ω *and* κ *be defined as in (14). Then they satisfies the multi-symplectic conservation law (MSCL):*

$$\frac{\partial \omega}{\partial t} + \frac{\partial \kappa}{\partial x} = 0. \tag{15}$$

Proof:

$$\begin{aligned} 2\omega_t = (dz \wedge \boldsymbol{M} dz)_t &= dz_t \wedge \boldsymbol{M} dz + dz \wedge \boldsymbol{M} dz_t \\ &= -(\boldsymbol{M} dz_t) \wedge dz + dz \wedge \boldsymbol{M} dz_t \\ &= -(\boldsymbol{S}_{zz} dz - \boldsymbol{K} dz_x) \wedge dz + dz \wedge (\boldsymbol{S}_{zz} dz - \boldsymbol{K} dz_x) \\ &= -(dz_x \wedge \boldsymbol{K} dz + dz \wedge \boldsymbol{K} dz_x) \\ &= -(dz \wedge \boldsymbol{K} dz)_x = -2\kappa_x \end{aligned}$$

since $\boldsymbol{M}$, $\boldsymbol{K}$ are skew-symmetric and $\boldsymbol{H}_{zz}$ is symmetric.

The MSCL (15) is a local equation and expresses the fact that symplecticity for Hamiltonian PDEs can vary over the spatial domain. However, the MSCL (15) is the appropriate generalization of preservation of the 2-form, $\omega_t = 0$, for Hamiltonian ODEs. In fact, let

$$z = (p_1, \ldots, p_N, q_1, \ldots, q_N), \quad \boldsymbol{M} \equiv \boldsymbol{J} = \begin{pmatrix} 0 & -\boldsymbol{I}_N \\ \boldsymbol{I}_N & 0 \end{pmatrix},$$

where all p_j, q_j are spatially independent, then $\partial_x dz \equiv 0$ leads to $\partial_x \kappa = \partial_x [dz \wedge \boldsymbol{K} dz] \equiv 0$ and (15) reduces to

$$\omega_t = \partial_t [\tfrac{1}{2} dz \wedge \boldsymbol{J} dz] = \partial_t [dp \wedge dq] = 0,$$

recovering the familiar notion of preservation of the canonical symplectic structure by the phase flow. As symplectic integrators are discretizations preserving the 2-form ω, multi-symplectic integrators are approximations to (13) which similarly conserve a discretization of the multi-symplectic conservation law (15). As we will show later in the numerical experiments, just as symplectic schemes conserve the Hamiltonian extremely well over very long times, multi-symplectic schemes conserve the related local energy and momentum conservation laws very well over long times.

Local and global conservation laws

In this section we present a treatment of the local conservation laws which is applicable to a broad class of Hamiltonian PDEs, not just to the equations of AKNS type (for a derivation of the local conservation laws of the AKNS equations, see

Appendix A). When the Hamiltonian $S(z)$ is independent of x and t, each independent variable gives rise to a conservation law [11]. Conservation of energy and momentum are associated with translation invariance in time and space, respectively.

Local energy conservation law

Multiplying (13) with z_t^T from the left provides the energy conservation law. Since $U^T M U = 0 \; \forall U$, we have

$$\begin{aligned} z_t^T K z_x = z_t^T \nabla_z S \;\; &\Rightarrow \;\; \frac{\partial S}{\partial t} - \frac{\partial z^T K z_x}{\partial t} + z^T K z_{xt} = 0 \\ &\Rightarrow \;\; \frac{\partial S - z^T K z_x}{\partial t} + \frac{\partial z^T K z_t}{\partial x} - z_x^T K z_t = 0 \\ &\Rightarrow \;\; \frac{\partial S - z^T K z_x}{\partial t} + \frac{\partial z^T K z_t}{\partial x} + \frac{\partial S}{\partial t} = 0, \end{aligned}$$

which gives the energy conservation law (ECL)

$$\partial_t E(z) + \partial_x F(z) = 0, \tag{16}$$

where the energy and flux densities are given by

$$E(z) = S(z) - \frac{1}{2} z^T K z_x, \tag{17}$$

$$F(z) = \frac{1}{2} z^T K z_t. \tag{18}$$

Local momentum conservation law

Similarly, multiplying (13) with z_x^T from the left yields

$$\begin{aligned} z_x^T M z_t = z_x^T \nabla_z S \;\; &\Rightarrow \;\; \frac{\partial S}{\partial x} - \frac{\partial z^T M z_t}{\partial x} + z^T M z_{xt} = 0 \\ &\Rightarrow \;\; \frac{\partial S - z^T M z_t}{\partial x} + \frac{\partial z^T M z_x}{\partial x} - z_t^T M z_x = 0 \\ &\Rightarrow \;\; \frac{\partial S - z^T M z_t}{\partial x} + \frac{\partial z^T M z_x}{\partial x} + \frac{\partial S}{\partial x} = 0, \end{aligned}$$

which gives the momentum conservation law (MCL)

$$\partial_t I(z) + \partial_x G(z) = 0, \tag{19}$$

where

$$\begin{aligned} G(z) &= S(z) - \frac{1}{2} z^T M z_t, \\ I(z) &= \frac{1}{2} z^T M z_x. \end{aligned}$$

Note that $S(z)$ itself is not preserved.

Global conservation laws

Integrating the densities $E(z)$, $I(z)$ and $N(z)$ over the spatial domain (with periodic boundary conditions) leads to the following global conservation laws

$$\begin{aligned} \frac{d}{dt}\mathcal{E}(z) &= 0, \qquad \mathcal{E}(z) = \int_0^L E(z)\,dx \\ \frac{d}{dt}\mathcal{I}(z) &= 0, \qquad \mathcal{I}(z) = \int_0^L I(z)\,dx \\ \frac{d}{dt}\mathcal{N}(z) &= 0, \qquad \mathcal{N}(z) = \int_0^L N(z)\,dx. \end{aligned} \tag{20}$$

In the numerical experiments we monitor both the local and global conservation of energy, momentum, and the norm and find that the global momentum and norm are preserved within roundoff. This substantiates that global conservation properties are weaker conditions, i.e., that global conservation of energy or momentum (20) is a necessary but not sufficient condition for local conservation of energy or momentum (16)–(19).

Example: multi-symplectic formulation of the NLS equation

The focusing one dimensional nonlinear Schrödinger (NLS) equation,

$$iu_t + u_{xx} + 2|u|^2 u = 0, \tag{21}$$

can be written in multi-symplectic form by letting $u = p + iq$ and introducing the new variables $v = p_x$, $w = q_x$. Separating (21) into real and imaginary parts, we obtain the system

$$\begin{aligned} q_t - v_x &= 2\left(p^2 + q^2\right) p \\ -p_t - w_x &= 2\left(p^2 + q^2\right) q \\ p_x &= v \\ q_x &= w, \end{aligned} \tag{22}$$

which is equivalent to the multi-symplectic form (eq. (13) with $N = 1$) for the NLS equation with

$$z = \begin{pmatrix} p \\ q \\ v \\ w \end{pmatrix}, \qquad M = \begin{pmatrix} 0 & 1 & 0 & 0 \\ -1 & 0 & 0 & 0 \\ 0 & 0 & 0 & 0 \\ 0 & 0 & 0 & 0 \end{pmatrix}, \qquad K = \begin{pmatrix} 0 & 0 & -1 & 0 \\ 0 & 0 & 0 & -1 \\ 1 & 0 & 0 & 0 \\ 0 & 1 & 0 & 0 \end{pmatrix},$$

and Hamiltonian

$$S(z) = \frac{1}{2}\left[\left(p^2+q^2\right)^2 + \left(v^2+w^2\right)\right].$$

The multi-symplectic conservation law is given by

$$\partial_t[dp \wedge dq] - \partial_x[dp \wedge dv + dq \wedge dw] = 0. \tag{23}$$

Implementing relations (16)–(19) for the NLS equation yields the energy conservation law (ECL)

$$\partial_t\left[\frac{1}{2}\left(\left(p^2+q^2\right)^2 - v^2 - w^2\right)\right] + \partial_x\left(vp_t + wq_t\right) = 0 \tag{24}$$

and the momentum conservation law (MCL)

$$\partial_t\left[\frac{1}{2}\left(pw - qv\right)\right] + \partial_x\left[\frac{1}{2}\left(\left(p^2+q^2\right)^2 + v^2 + w^2 - \left(pq_t - p_tq\right)\right)\right] = 0. \tag{25}$$

Another conservation law, which we call the norm conservation law, is given by

$$\partial_t\left[\frac{1}{2}\left(p^2+q^2\right)\right] + \partial_x(qv - pw) = 0. \tag{26}$$

These three equations, when integrated with respect to x, yield the classic global conservation of energy (Hamiltonian), momentum and norm (for an alternative derivation, see Appendix A, equations (112)).

Example: multi-symplectic formulation of the SG equation

Another example is provided by the sine-Gordon equation, given by

$$u_{tt} - u_{xx} + \sin u = 0. \tag{27}$$

The sine-Gordon equation can be cast in multi-symplectic form by introducing the variables $v = u_t$ and $w = u_x$. This results in the system of equations

$$\begin{aligned} -v_t + w_x &= \sin u \\ u_t \quad\;\; &= v \\ -u_x &= -w. \end{aligned} \tag{28}$$

System (28) can be written in standard multi-symplectic form with

$$z = \begin{pmatrix} u \\ v \\ w \end{pmatrix}, \quad M = \begin{pmatrix} 0 & -1 & 0 \\ 1 & 0 & 0 \\ 0 & 0 & 0 \end{pmatrix}, \quad K = \begin{pmatrix} 0 & 0 & 1 \\ 0 & 0 & 0 \\ -1 & 0 & 0 \end{pmatrix},$$

and Hamiltonian

$$S = -\cos u + \tfrac{1}{2}\left(v^2 - w^2\right). \tag{29}$$

The multi-symplectic conservation law is given by

$$\partial_t[du \wedge dv] - \partial_x[du \wedge dw] = 0. \tag{30}$$

The energy and flux are given by

$$E = S - \tfrac{1}{2} z^T \boldsymbol{K} z_x = -\cos u + \tfrac{1}{2}\left(v^2 - w^2 - u w_x + u_x w\right),$$

$$F = \tfrac{1}{2} z^T \boldsymbol{K} z_t = \tfrac{1}{2}\left(u w_t - u_t w\right).$$

Thus the energy conservation law can be simplified to

$$E_t + F_x = \left(-\cos u + \tfrac{1}{2}(v^2 + w^2)\right)_t - (vw)_x = 0. \tag{31}$$

Similarly, the momentum conservation law is given by

$$I_t + G_x = \left(\cos u + \tfrac{1}{2}(v^2 + w^2)\right)_x - (vw)_t = 0. \tag{32}$$

III.2 MULTI-SYMPLECTIC DISCRETIZATIONS

Symplectic integrators are designed to preserve the symplectic 2-form and underlying symplectic geometry associated with the Hamiltonian ODE. In a similar spirit, we are interested in developing discretizations that preserve the multi-symplectic structure associated with Hamiltonian PDEs. Using the framework of [12], we provide the following definition. Specifically, let the discretization of the multi-symplectic PDE (13) and the conservation law of multi-symplecticity be written schematically as

$$M \partial_t^{i,j} z_i^j + K \partial_x^{i,j} z_i^j = \left(\nabla_z S(z_i^j)\right)_i^j, \tag{33}$$

and

$$\partial_t^{i,j} \omega_i^j + \partial_x^{i,j} \kappa_i^j = 0 \tag{34}$$

respectively, where $z_i^j = z(x_i, t_j)$, $\partial_t^{i,j}$ and $\partial_x^{i,j}$ are discretizations of the corresponding derivatives ∂_t and ∂_x, and

$$\omega_i^j = \frac{1}{2}(dz_i^j \wedge \boldsymbol{M} dz_i^j), \qquad \kappa_i^j = \frac{1}{2}(dz_i^j \wedge \boldsymbol{K} dz_i^j).$$

Definition 3 *Discretization (33) is a multi-symplectic discretization of the multi-symplectic PDE (13) if its solution satisfies (34), the discretization of the multi-symplectic conservation law (15).*

Multi-symplectic PDEs have a symplectic structure associated with both the temporal and spatial variables. Thus, a natural starting point for developing multi-symplectic schemes is to examine schemes which are known to be symplectic in the traditional sense. One possibility is to discretize both in space and time using the implicit midpoint scheme, which is the simplest symplectic scheme in the Gauss-Legendre family of Runge-Kutta schemes [44].

The implicit midpoint rule

In this subsection we show that implementing an implicit midpoint discretization both in space and time yields a multi-symplectic discretization of the PDE (15). We provide a new, simpler proof which also generalizes an earlier result obtained specifically for the sine-Gordon equation [44] and which is a prelude to our results for higher order multi-symplectic discretizations of the NLS equation (22) given in Proposition 3.

Proposition 2 *Applying the implicit midpoint rule to both time and space derivatives of (13) results in a multi-symplectic discretization.*

Proof: Applying a midpoint discretization on both time and space yields

$$\boldsymbol{M}\left(\frac{z_{1/2}^1 - z_{1/2}^0}{\Delta t}\right) + \boldsymbol{K}\left(\frac{z_1^{1/2} - z_0^{1/2}}{\Delta x}\right) = \nabla_z S\left(z_{1/2}^{1/2}\right),$$

where

$$\begin{aligned}
z_{1/2}^j &= \tfrac{1}{2}\left(z_0^j + z_1^j\right), \\
z_i^{1/2} &= \tfrac{1}{2}\left(z_i^0 + z_i^1\right), \\
z_{1/2}^{1/2} &= \frac{1}{4}\left(z_0^0 + z_0^1 + z_1^0 + z_1^1\right) \\
&= \tfrac{1}{2}\left(z_{1/2}^0 + z_{1/2}^1\right) \\
&= \tfrac{1}{2}\left(z_0^{1/2} + z_1^{1/2}\right).
\end{aligned}$$

To show we have a multi-symplectic discretization we proceed as follows. Take the differential of the midpoint discretization

$$\boldsymbol{M}\left(\frac{dz_{1/2}^{1}-dz_{1/2}^{0}}{\Delta t}\right)+\boldsymbol{K}\left(\frac{dz_{1}^{1/2}-dz_{0}^{1/2}}{\Delta x}\right)=\boldsymbol{S}_{zz}\,dz_{1/2}^{1/2}.$$

Take the wedge product with $dz_{1/2}^{1/2}$. Since $\boldsymbol{S}_{zz}$ is symmetric, the right-hand side becomes zero. The first term of the left-hand side becomes

$$\begin{aligned} dz_{1/2}^{1/2}\wedge\boldsymbol{M}\left(dz_{1/2}^{1}-dz_{1/2}^{0}\right) &= \tfrac{1}{2}\left(dz_{1/2}^{1}+dz_{1/2}^{0}\right)\wedge\boldsymbol{M}\left(dz_{1/2}^{1}-dz_{1/2}^{0}\right)\\ &= \tfrac{1}{2}\left(dz_{1/2}^{1}\wedge\boldsymbol{M}dz_{1/2}^{1}-dz_{1/2}^{0}\wedge\boldsymbol{M}dz_{1/2}^{0}\right)\\ &= \omega_{1/2}^{1}-\omega_{1/2}^{0}. \end{aligned}$$

Similarly, the second term becomes

$$\begin{aligned} dz_{1/2}^{1/2}\wedge\boldsymbol{K}\left(dz_{1}^{1/2}-dz_{0}^{1/2}\right) &= \tfrac{1}{2}\left(dz_{1}^{1/2}+dz_{0}^{1/2}\right)\wedge\boldsymbol{K}\left(dz_{1}^{1/2}-dz_{0}^{1/2}\right)\\ &= \tfrac{1}{2}\left(dz_{1}^{1/2}\wedge\boldsymbol{K}dz_{1}^{1/2}-dz_{0}^{1/2}\wedge\boldsymbol{K}dz_{0}^{1/2}\right)\\ &= \kappa_{1}^{1/2}-\kappa_{0}^{1/2}. \end{aligned}$$

Therefore we have a discretization of the multi-symplectic conservation law

$$\left(\frac{\omega_{1/2}^{1}-\omega_{1/2}^{0}}{\Delta t}\right)+\left(\frac{\kappa_{1}^{1/2}-\kappa_{0}^{1/2}}{\Delta x}\right)=0.$$

The previous result can be summarized as follows: Implementing an implicit midpoint discretization both in space and time yields the following centered-cell discretization of the PDE,

$$\boldsymbol{M}\left(\frac{z_{i+\frac{1}{2}}^{j+1}-z_{i+\frac{1}{2}}^{j}}{\Delta t}\right)+\boldsymbol{K}\left(\frac{z_{i+1}^{j+\frac{1}{2}}-z_{i}^{j+\frac{1}{2}}}{\Delta x}\right)=\nabla_{z}S\left(z_{i+\frac{1}{2}}^{j+\frac{1}{2}}\right), \tag{35}$$

where

$$z_{i+\frac{1}{2}}^{j}=\frac{1}{2}\left(z_{i}^{j}+z_{i+1}^{j}\right),\quad z_{i}^{j+\frac{1}{2}}=\frac{1}{2}\left(z_{i}^{j}+z_{i}^{j+1}\right),$$

and

$$z_{i+\frac{1}{2}}^{j+\frac{1}{2}}=\frac{1}{4}\left(z_{i}^{j}+z_{i+1}^{j}+z_{i}^{j+1}+z_{i+1}^{j+1}\right).$$

The centered-cell discretization is *multi-symplectic* for any PDE which possesses the multi-symplectic formulation (13), i.e., in each cell the discretization satisfies

$$\left(\frac{\omega_{i+\frac{1}{2}}^{j+1}-\omega_{i+\frac{1}{2}}^{j}}{\Delta t}\right)+\left(\frac{\kappa_{i+1}^{j+\frac{1}{2}}-\kappa_{i}^{j+\frac{1}{2}}}{\Delta x}\right)=0$$

exactly, where ω_{i}^{j} and κ_{i}^{j} are given by (14).

III.3 MS FINITE-DIFFERENCE DISCRETIZATIONS FOR THE NLS EQUATION

Applying the centered-cell discretization to the NLS equation (22) we obtain the following multi-symplectic scheme:

$$\frac{q_{i+1/2}^{j+1}-q_{i+1/2}^{j}}{\Delta t}-\frac{v_{i+1}^{j+1/2}-v_{i}^{j+1/2}}{\Delta x} = 2\left(\left(p_{i+1/2}^{j+1/2}\right)^2+\left(q_{i+1/2}^{j+1/2}\right)^2\right)p_{i+1/2}^{j+1/2}, \quad (36)$$

$$-\frac{p_{i+1/2}^{j+1}-p_{i+1/2}^{j}}{\Delta t}-\frac{w_{i+1}^{j+1/2}-w_{i}^{j+1/2}}{\Delta x} = 2\left(\left(p_{i+1/2}^{j+1/2}\right)^2+\left(q_{i+1/2}^{j+1/2}\right)^2\right)q_{i+1/2}^{j+1/2}, \quad (37)$$

$$\frac{p_{i+1}^{j+1/2}-p_{i}^{j+1/2}}{\Delta x} = v_{i+1/2}^{j+1/2}, \quad (38)$$

$$\frac{q_{i+1}^{j+1/2}-q_{i}^{j+1/2}}{\Delta x} = w_{i+1/2}^{j+1/2}, \quad (39)$$

where the following notation, as above in (35), has been used,

$$f_{i+1/2}^{j}=\frac{1}{2}\left(f_{i+1}^{j}+f_{i}^{j}\right), \qquad f_{i}^{j+1/2}=\frac{1}{2}\left(f_{i}^{j+1}+f_{i}^{j}\right),$$

$$f_{i+1/2}^{j+1/2}=\frac{1}{4}\left(f_{i+1}^{j+1}+f_{i}^{j+1}+f_{i+1}^{j}+f_{i}^{j}\right).$$

For the NLS equation, the corresponding discretization of the multi-symplectic conservation law (23) is

$$\frac{dp_{i+1/2}^{j+1}\wedge dq_{i+1/2}^{j+1}-dp_{i+1/2}^{j}\wedge dq_{i+1/2}^{j}}{\Delta t} -$$

$$\frac{dp_{i+1}^{j+1/2}\wedge dv_{i+1}^{j+1/2}-dp_{i}^{j+1/2}\wedge dv_{i}^{j+1/2}}{\Delta x} -$$

$$\frac{dq_{i+1}^{j+1/2}\wedge dw_{i+1}^{j+1/2}-dq_{i}^{j+1/2}\wedge dw_{i}^{j+1/2}}{\Delta x} = 0. \quad (40)$$

Scheme (36)–(39) is a *new* numerical scheme for the NLS equation which is second order in space and time. We can write scheme (36)–(39) in terms of $u=p+iq$. We first eliminate v from (36) and (38),

$$\frac{q_{i+3/2}^{j+1}-q_{i+3/2}^{j}+q_{i+1/2}^{j+1}-q_{i+1/2}^{j}}{\Delta t}-2\frac{p_{i+2}^{j+1/2}-2p_{i+1}^{j+1/2}+p_{i}^{j+1/2}}{\Delta x^2}$$

$$=2\left(\left(p_{i+3/2}^{j+1/2}\right)^2+\left(q_{i+3/2}^{j+1/2}\right)^2\right)p_{i+3/2}^{j+1/2}+2\left(\left(p_{i+1/2}^{j+1/2}\right)^2+\left(q_{i+1/2}^{j+1/2}\right)^2\right)p_{i+1/2}^{j+1/2}, \quad (41)$$

and then eliminate w from (37) and (39)

$$\frac{p_{i+3/2}^{j+1}-p_{i+3/2}^{j}+p_{i+1/2}^{j+1}-p_{i+1/2}^{j}}{\Delta t}-2\frac{q_{i+2}^{j+1/2}-2q_{i+1}^{j+1/2}+q_{i}^{j+1/2}}{\Delta x^2}$$

$$=2\left(\left(p_{i+3/2}^{j+1/2}\right)^2+\left(q_{i+3/2}^{j+1/2}\right)^2\right)q_{i+3/2}^{j+1/2}+2\left(\left(p_{i+1/2}^{j+1/2}\right)^2+\left(q_{i+1/2}^{j+1/2}\right)^2\right)q_{i+1/2}^{j+1/2}. \quad (42)$$

Combining (41) and (42) we obtain a new six-point difference scheme for the NLS equation (we denote this discretization by MS-CC in the numerical experiments).

$$
\begin{aligned}
& i\frac{\left(u_{i-1}^{j+1}+2u_i^{j+1}+u_{i+1}^{j+1}\right)-\left(u_{i-1}^{j}+2u_i^{j}+u_{i+1}^{j}\right)}{2\Delta t} \\
& +\frac{u_{i-1}^{j}+u_{i-1}^{j+1}-2\left(u_i^{j}+u_i^{j+1}\right)+u_{i+1}^{j}+u_{i+1}^{j+1}}{\Delta x^2} \\
& +2\left|\frac{u_{i-1}^{j}+u_i^{j}+u_{i-1}^{j+1}+u_i^{j+1}}{4}\right|^2\frac{u_{i-1}^{j}+u_i^{j}+u_{i-1}^{j+1}+u_i^{j+1}}{4} \\
& +2\left|\frac{u_i^{j}+u_{i+1}^{j}+u_i^{j+1}+u_{i+1}^{j+1}}{4}\right|^2\frac{u_i^{j}+u_{i+1}^{j}+u_i^{j+1}+u_{i+1}^{j+1}}{4} \\
& =0. \qquad (43)
\end{aligned}
$$

Higher order multi-symplectic schemes can be obtained by concatenating higher order members in the Gauss-Legendre family. We prove that a concatenated pair of s- and r-stage (G-L) methods yields a multi-symplectic integrator for the NLS equation.

Proposition 3 *Let (22) be discretized in space and in time by a pair of Gauss-Legendre collocation methods with s and r stages, respectively. The resulting discretization is a multi-symplectic integrator for the NLS equation.*

Proof: We begin by discretizing in space and apply an implicit s-stage Runge-Kutta scheme to the multi-symplectic formulation of NLS (22) to obtain the following spatial semi-discretization:

$$
\begin{aligned}
P_i &= p_k+\Delta x\sum_{j=1}^{s}a_{ij}V_j, \\
V_i &= v_k+\Delta x\sum_{j=1}^{s}a_{ij}\left(-\partial_t Q_j-2\left(P_j^2+Q_j^2\right)P_j\right), \\
Q_i &= q_k+\Delta x\sum_{j=1}^{s}a_{ij}W_j, \\
W_i &= w_k+\Delta x\sum_{j=1}^{s}a_{ij}\left(\partial_t P_j-2\left(P_j^2+Q_j^2\right)Q_j\right), \\
p_{k+1} &= p_k+\Delta x\sum_{j=1}^{s}b_jV_j, \\
v_{k+1} &= v_k+\Delta x\sum_{j=1}^{s}b_j\left(-\partial_t Q_j-2\left(P_j^2+Q_j^2\right)P_j\right),
\end{aligned}
$$

$$
\begin{aligned}
q_{k+1} &= q_k + \Delta x \sum_{j=1}^{s} b_j W_j, \\
w_{k+1} &= w_k + \Delta x \sum_{j=1}^{s} b_j \left(\partial_t P_j - 2\left(P_j^2 + Q_j^2\right) Q_j\right),
\end{aligned} \tag{44}
$$

which is defined for all t. The standard notation $u_k(t) \approx u(x_k, t)$ is employed and for convenience we set $k = 0$ and assume that $x_k = 0$. The corresponding semi-discretization of conservation law (40) is given by

$$
\begin{aligned}
[dp_1 \wedge dv_1 - dp_0 \wedge dv_0] &+ [dq_1 \wedge dw_1 - dq_0 \wedge dw_0] \\
&- \sum_{i=1}^{s} b_i \partial_t [dP_i \wedge dQ_i] \Delta x = 0.
\end{aligned} \tag{45}
$$

Solving the first four equations of (44) for $\partial_t P_j,\ \partial_t Q_j,\ j = 1, \ldots, s$, we next implement an r-stage Runge-Kutta discretization in time

$$
\begin{aligned}
P_{i,m} &= p_i^0 + \Delta t \sum_{n=1}^{r} \tilde{a}_{mn}\, \partial_t P_{i,n}, \qquad Q_{i,m} = q_i^0 + \Delta t \sum_{n=1}^{r} \tilde{a}_{mn}\, \partial_t Q_{i,n}, \\
p_i^1 &= p_i^0 + \Delta t \sum_{n=1}^{r} \tilde{b}_m\, \partial_t P_{i,m}, \qquad q_i^1 = q_i^0 + \Delta t \sum_{n=1}^{r} \tilde{b}_m\, \partial_t Q_{i,m},
\end{aligned}
$$

with the corresponding conservation property

$$
\begin{aligned}
\left[dp_i^1 \wedge dq_i^1 - dp_i^0 \wedge dq_i^0\right] - \sum_{m=1}^{r} \tilde{b}_m \ [\ & \partial_t dP_{i,m} \wedge dQ_{i,m} \\
&+ dP_{i,m} \wedge \partial_t dQ_{i,m} \ ] \Delta t = 0.
\end{aligned} \tag{46}
$$

Combining (45) and (46), the discretized multi-symplectic conservation law is given by

$$
\begin{aligned}
\sum_{i=1}^{s} b_i \left[dp_i^1 \wedge dq_i^1 - dp_i^0 \wedge dq_i^0\right] \Delta x &- \sum_{m=1}^{r} \tilde{b}_m \left[\, dp_1^m \wedge dv_1^m - dp_0^m \wedge dv_0^m \right. \\
&+ \left. dq_1^m \wedge dw_1^m - dq_0^m \wedge dw_0^m \,\right] \Delta t = 0,
\end{aligned}
$$

which is a discretization of (40) integrated over the domain $[0,\ \Delta x] \times [0,\ \Delta t]$. This establishes that the concatenated G-L integrator is multi-symplectic.

Another interesting property of the Gauss-Legendre multi-symplectic integrators when periodic boundary conditions are imposed, is the following:

Proposition 4 *Let the Gauss-Legendre multi-symplectic integrator for the NLS equation be specified as in Proposition 3. When periodic boundary conditions*

are imposed, the discretization (in particular MS-CC) yields a finite-dimensional Hamiltonian truncation of the NLS equation in space with the underlying symplectic structure $da \wedge Bdb$ and a symplectic discretization of this finite-dimensional system in time. It should be noted that multi-symplectic schemes are not automatically symplectic in the global sense.

Proof: To examine a global property such as symplecticity, sum over the k lattice points:

$$\sum_{k=1}^{M} \Big(\sum_{i=1}^{s} b_i \quad [\quad dp_{i,k}^1 \wedge dq_{i,k}^1 - dp_{i,k}^0 \wedge dq_{i,k}^0 \,] \, \Delta x$$
$$- \sum_{m=1}^{r} \tilde{b}_m \quad [\quad dp_{k+1}^m \wedge dv_{k+1}^m - dp_k^m \wedge dv_k^m$$
$$+ \quad dq_{k+1}^m \wedge dw_{k+1}^m - dq_k^m \wedge dw_k^m \,] \, \Delta t \, \Big) = 0.$$

Expanding the outer sum and noting that for periodic boundary conditions $p_{M+1}^m = p_1^m$ and $v_{M+1}^m = v_1^m$, we find that

$$\sum_{k=1}^{M} \sum_{m=1}^{r} \tilde{b}_m \left[dp_{k+1}^m \wedge dv_{k+1}^m - dp_k^m \wedge dv_k^m \right] \Delta t \;\; =$$
$$\sum_{m=1}^{r} \tilde{b}_m \left[dp_{M+1}^m \wedge dv_{M+1}^m - dp_1^m \wedge dv_1^m \right] \Delta t \;\; = \;\; 0.$$

Similarly,

$$\sum_{k=1}^{M} \sum_{m=1}^{r} \tilde{b}_m \left[dq_{k+1}^m \wedge dw_{k+1}^m - dq_k^m \wedge dw_k^m \right] \Delta t = 0.$$

Therefore,

$$\sum_{k=1}^{M} \sum_{i=1}^{s} b_i \left[dp_{i,k}^1 \wedge dq_{i,k}^1 \right] = \sum_{k=1}^{M} \sum_{i=1}^{s} b_i \left[dp_{i,k}^0 \wedge dq_{i,k}^0 \right].$$

This is conservation of symplecticity in time with respect to the state variables $p = \{p_{i,k}\}$ and $q = \{q_{i,k}\}$ and the wedge product $dp \wedge \boldsymbol{B} dq$ where $\boldsymbol{B}$ is a diagonal matrix with entries $\{b_i\}$.

Discrete conservation laws

Using the centered-cell discretization we can write a discrete form of the local conservation laws (16)–(19) in the general form

$$\left(\frac{A_{i+\frac{1}{2}}^{j+1} - A_{i+\frac{1}{2}}^{j}}{\Delta t} \right) + \left(\frac{B_{i+1}^{j+\frac{1}{2}} - B_{i}^{j+\frac{1}{2}}}{\Delta x} \right) = 0,$$

which, when applied to (24)–(26), gives the discrete versions of the local conservation laws for the NLS equation. The discrete energy conservation law is given by

$$\frac{E_{i+1/2}^{j+1} - E_{i+1/2}^{j}}{\Delta t} + \frac{F_{i+1}^{j+1/2} - F_{i}^{j+1/2}}{\Delta x} = 0, \tag{47}$$

where

$$\begin{aligned} E_{i+1/2}^{j} &= \frac{1}{2}\left[\left(\left(p_{i+1/2}^{j}\right)^2 + \left(q_{i+1/2}^{j}\right)^2\right)^2 - \left(\left(v_{i+1/2}^{j}\right)^2 + \left(w_{i+1/2}^{j}\right)^2\right)\right], \\ F_{i}^{j+1/2} &= v_{i}^{j+1/2}\left(\frac{p_{i}^{j+1} - p_{i}^{j}}{\Delta t}\right) + w_{i}^{j+1/2}\left(\frac{q_{i}^{j+1} - q_{i}^{j}}{\Delta t}\right). \end{aligned}$$

The discrete momentum conservation law takes the form

$$\frac{I_{i+1/2}^{j+1} - I_{i+1/2}^{j}}{\Delta t} + \frac{G_{i+1}^{j+1/2} - G_{i}^{j+1/2}}{\Delta x} = 0, \tag{48}$$

where

$$\begin{aligned} I_{i+1/2}^{j} &= \frac{1}{2}\left(p_{i+1/2}^{j}\, w_{i+1/2}^{j} - q_{i+1/2}^{j}\, v_{i+1/2}^{j}\right), \\ G_{i}^{j+1/2} &= \frac{1}{2}\left[\left(\left(p_{i}^{j+1/2}\right)^2 + \left(q_{i}^{j+1/2}\right)^2\right)^2 + \left(v_{i}^{j+1/2}\right)^2 + \left(w_{i}^{j+1/2}\right)^2 \right. \\ &\quad \left. - \left(p_{i}^{j+1/2}\left(\frac{q_{i}^{j+1} - q_{i}^{j}}{\Delta t}\right) - q_{i}^{j+1/2}\left(\frac{p_{i}^{j+1} - p_{i}^{j}}{\Delta t}\right)\right)\right]. \end{aligned}$$

Finally, a discrete version of the norm conservation law is given by

$$\frac{N_{i+1/2}^{j+1} - N_{i+1/2}^{j}}{\Delta t} + \frac{M_{i+1}^{j+1/2} - M_{i}^{j+1/2}}{\Delta x} = 0,$$

where

$$\begin{aligned} N_{i+1/2}^{j} &= \frac{1}{2}\left(\left(p_{i+1/2}^{j}\right)^2 + \left(q_{i+1/2}^{j}\right)^2\right), \\ M_{i}^{j+1/2} &= q_{i}^{j+1/2}\, v_{i}^{j+1/2} - p_{i}^{j+1/2}\, w_{i}^{j+1/2}. \end{aligned}$$

Analogous to symplectic Gauss-Legendre schemes preserving the Hamiltonian exactly for linear Hamiltonian ODEs [50], it has been shown that multi-symplectic Gauss-Legendre schemes preserve both the discrete energy and momentum conservation laws exactly for linear Hamiltonian PDEs [12]. In the present situation, for nonlinear wave equations, the local conservation of energy and momentum will not be exact for the NLS using (22) since $S(z)$ is not quadratic. However the numerical experiments show that the local conservation laws (24)–(25) are preserved very well over long times.

III.4 NUMERICAL EXPERIMENTS FOR THE NLS EQUATION

We are interested in simulating multi-phase quasi-periodic (in time) solutions of the NLS equation under periodic boundary conditions $u(x+L,t) = u(x,t)$. We consider initial conditions of the form

$$u_0(x) = a(1 + \epsilon \cos \mu x), \tag{49}$$

where $a = 0.5$, $\epsilon = 0.1$, $\mu = 2\pi/L$ and L is either (a) $L = 2\sqrt{2}\pi$ or (b) $L = 4\sqrt{2}\pi$ Initial data (a) and (b) correspond to multi-phase solutions, near the plane wave, which are characterized by either one or two excited modes, respectively. We refer to these cases as the one-mode and two-mode cases.

We consider the multi-symplectic scheme MS-CC. We use initial conditions (49a) and examine the performance of the scheme for different mesh sizes and time-steps. The multi-symplectic discretization (43) is implicit and is solved using an iteration scheme. All the local conservation laws are of the general form

$$\partial_t A + \partial_x B = 0,$$

and multiplying the discrete conservation laws (47)-(48) by $\Delta x \Delta t$, they can be written as

$$\left(A_{i+1/2}^{j+1} - A_{i+1/2}^{j}\right) \Delta x + \left(B_{i+1}^{j+1/2} - B_{i}^{j+1/2}\right) \Delta t = 0. \tag{50}$$

In addition to the local energy and momentum conservation laws, we monitor the error in the global invariants $\mathcal{E}(t)$, $\mathcal{I}(t)$ and $\mathcal{N}(t)$. Once the local conservation laws (47)-(48) have been evaluated, we obtain a second order approximation to the global conserved quantities by implementing (50) and summing in space and time.

Figure 1 provides the results obtained using MS-CC for initial data (49a), with $N = 64$ and $\Delta t = 5 \times 10^{-3}$ over the time interval [0,500]. For clarity, in the surface plots we only show the time slice [450,500]. The surface of the one mode multi-phase solution (Figure 1) clearly displays quasi-periodic behavior in time. Figure 2 shows the errors in the local energy and momentum conservation laws as given by (47)–(48). The error in the MCL is $\mathcal{O}(10^{-3})$ and in the ECL is $\mathcal{O}(10^{-6})$. The errors in the local conservation laws are concentrated in the regions of the multi-phase solution where there are steep gradients. Further, it is clear that the error in the local conservation laws exhibit bounded oscillations as is expected from

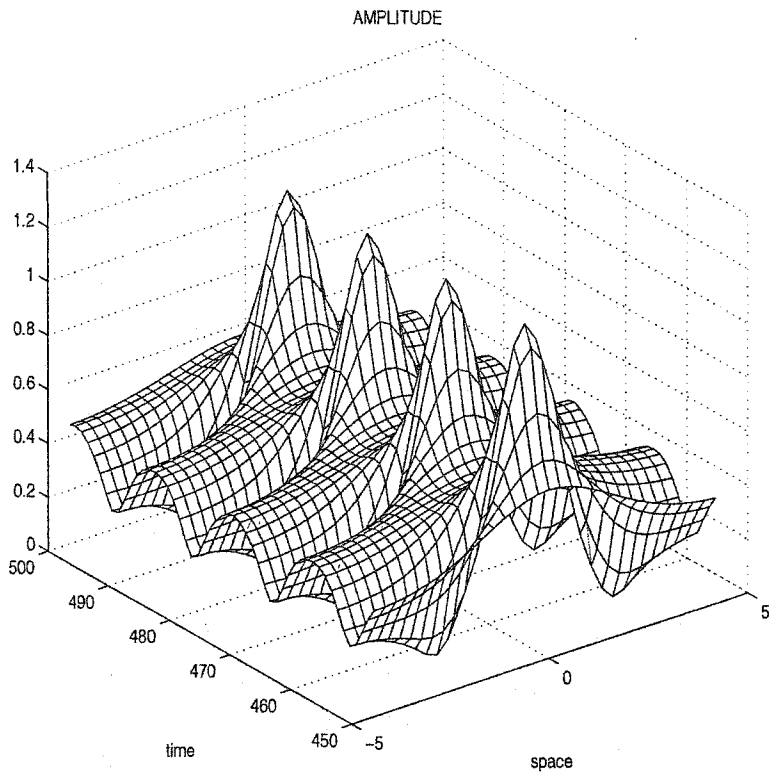

FIG. 1: MS-CC surface. $N = 64$ and $\Delta t = 5 \times 10^{-3}$.

a symplectic discretization. A drift in the error of the LCL's is not observed. The corresponding error in the global energy and momentum over the time interval [0,500] are given in Figure 3. There, the picks in the global energy correspond to the picks in the surface. It is worth noting that the global momentum and norm are conserved *exactly* (up to the error criterion of 10^{-14} in the iteration procedure in the implicit MS scheme) since they are quadratic invariants! Clearly, this is a very attractive feature of the MS scheme. Further, the error in the global energy oscillates in a bounded fashion as is typical of the behavior of a symplectic integrator (recall Proposition 1, where MS is shown to be symplectic).

The maximum error in the local energy and momentum and global energy and momentum for MS-CC is summarized in Table I for mesh sizes $N = 32$ and 64, each for three time steps. From the experiments it is readily seen that the error in the local energy conservation law (47) depends only on the time-step Δt and that the the error is second order in Δt (successively halving the time-step decreases the LE error each time by a factor of 2^{-2}). In contrast the error in the local

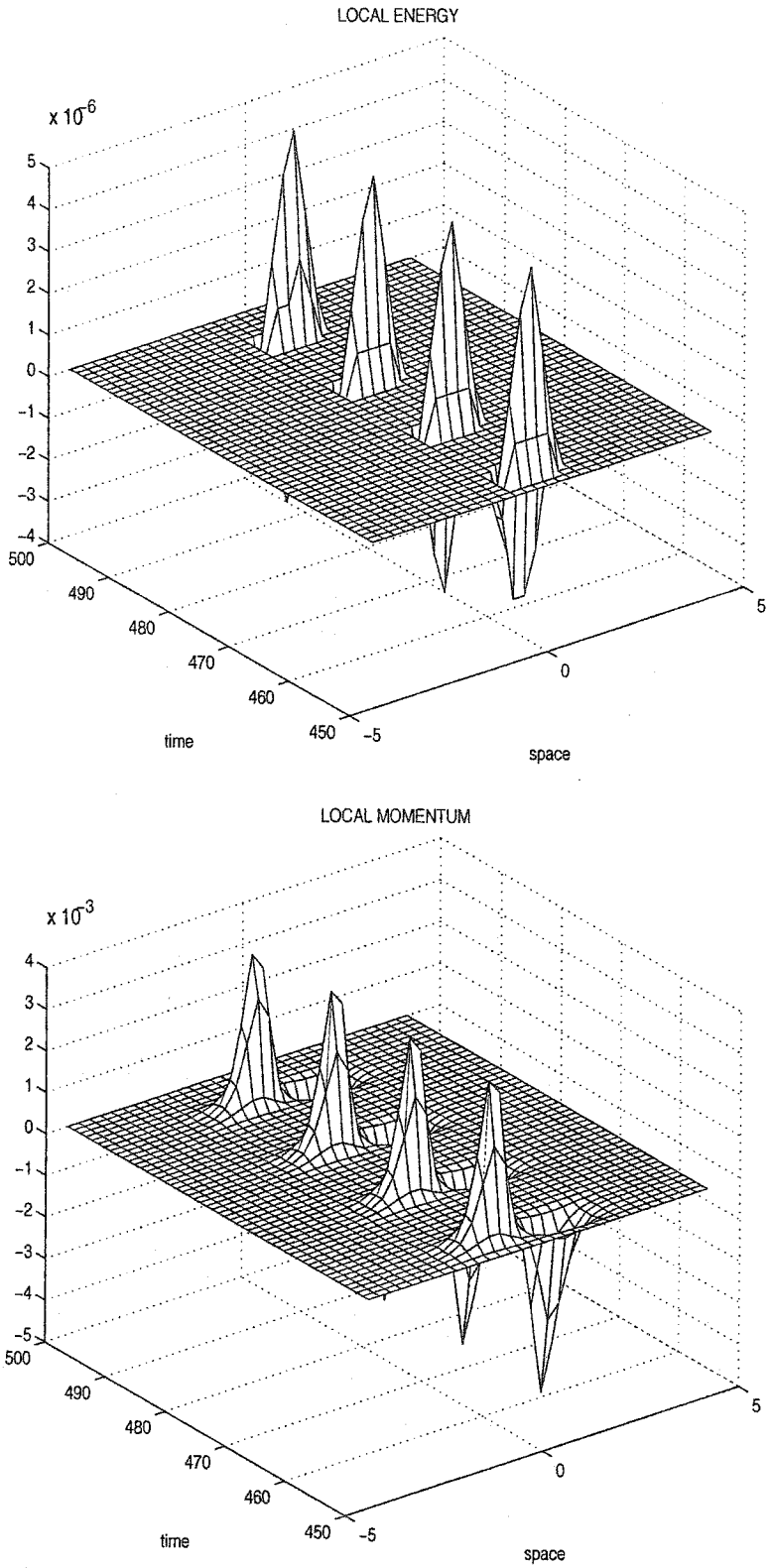

FIG. 2: MS-CC local ECL and MCL. $N = 64$ and $\Delta t = 5 \times 10^{-3}$.

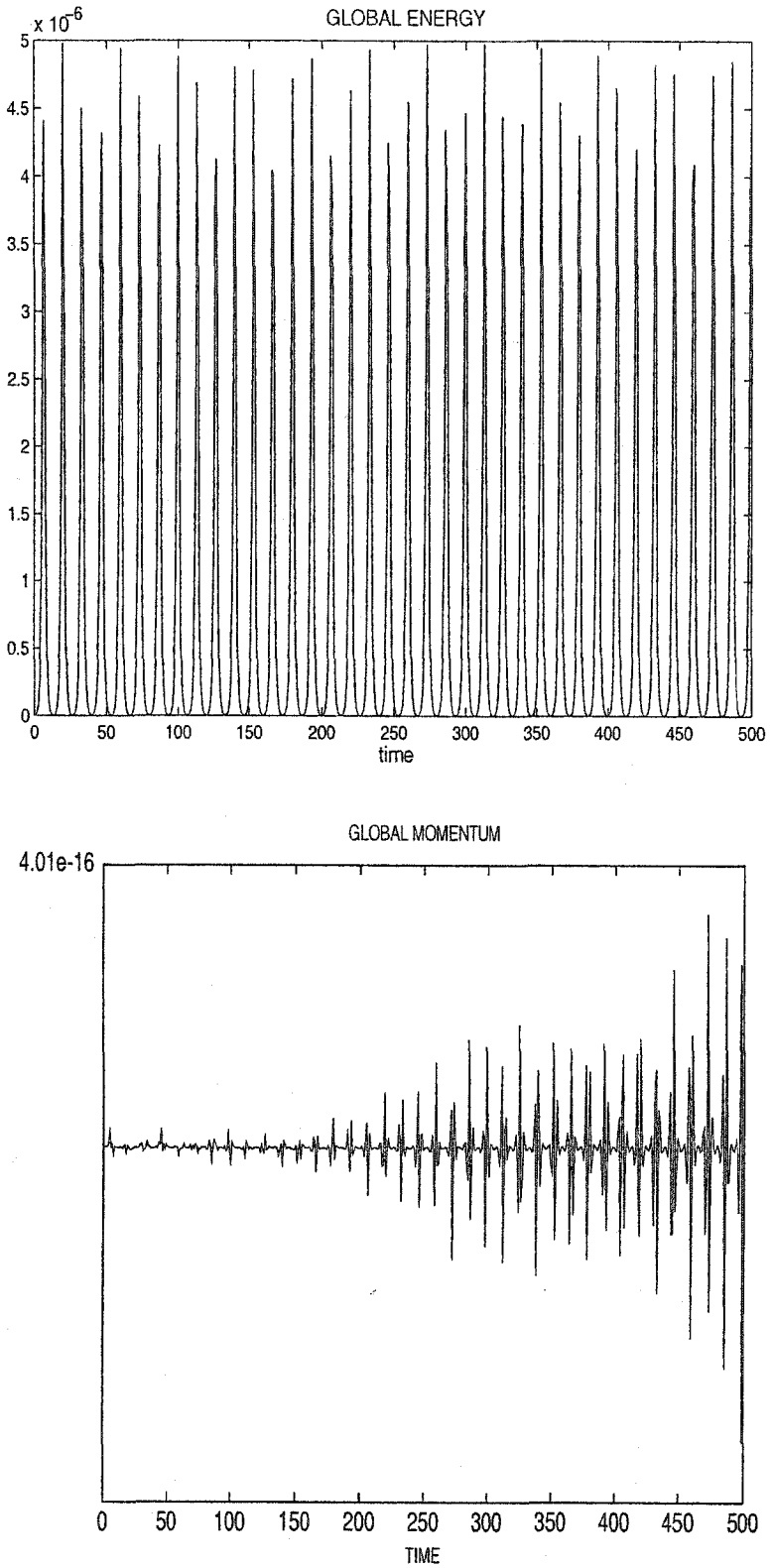

FIG. 3: MS-CC global ECL and MCL. $N = 64$ and $\Delta t = 5 \times 10^{-3}$.

TABLE I: Error in LE,LM, GE and GM for MS-CC.

N	32	32	32	64	64	64
Δt	2.0E-02	1.0E-02	5.0E-03	2.0E-02	1.0E-02	5.0E-03
LE	6.0E-05	1.5E-05	4.0E-06	8.0E-05	2.0E-05	5.0E-06
LM	1.7E-02	1.7E-02	1.7E-02	4.8E-03	4.8E-03	4.8E-03
GE	7.3E-05	2.0E-05	5.0E-06	7.6E-05	2.2E-05	5.0E-06
GM	1.2E-13	2.5E-14	2.0E-13	1.3E-13	1.0E-13	4.5E-13

momentum conservation law (48) depends only on the spatial mesh size N and, as anticipated, the error in LM is second order in h.

The approximation to the global energy, GE, obtained using the MS-CC scheme and the Hamiltonian for the AL system both provide a second order approximation to the NLS Hamiltonian. In comparing the error in the GE in Table I with the errors in the Hamiltonian in Tables II and III (found in Appendix B), we see that the multi-symplectic scheme preserves the global energy better than both S2 and CS2. So in addition to having very good resolution of the local conservation laws, the multi-symplectic scheme preserves the global energy extremely well (and the global momentum and norm exactly!). Another important feature of the MS-CC method is that it is significantly faster than the symplectic schemes S2 and CS2.

A final issue to consider is the preservation of the qualitative properties of the solution. Since we consider S2 to be the most robust of the symplectic integrators for the AL system, we compare the performance of MS-CC with that of S2. As mentioned before, the surface of the waveform obtained using MS-CC for initial data (49a) with discretization parameters $N = 64$, $\Delta t = 5 \times 10^{-3}$ is given in Figure 1 for the time frame $450 < t < 500$. Implementing S2 with the same discretization parameters and for the same initial data, the surface of the waveform appears identical to Figure 1. This is initial data for a stable multi-phase solution of NLS and, although "near" the unstable plane wave solution, it is not "too close" (as measured in spectral space, see [6]). It is expected that when simulating other stable solutions of NLS, e.g., solitons (which are actually limiting cases of the multi-phase solutions with $L \to \infty$), the MS-CC and S2 schemes will comparably

preserve the qualitative features of the waveform. However, when examining more complex solutions there can be a striking difference in the S2 and MS-CC results. In highly sensitive regimes, where spurious numerical solutions become an important computational issue, the integrability of the AL discretization becomes crucial. Figure 4(a-b) shows the surface of the waveform and Figure 5(a-b) the error in the global energy obtained using the S2 and the MS-CC discretization, respectively for initial data (49b) with discretization parameters $N = 64$, $\Delta t = 5 \times 10^{-3}$ and $T = 500$. Notice that the AL based S2 scheme accurately captures the quasi-periodic motion. On the other hand, using the MS-CC integrator the onset of numerically induced temporal chaos, as typified by a random switching in time of the location of the spatial excitations in the waveform, is clearly visible. The numerical chaos is observed even though the MS scheme preserves the global energy better than the AL discretization (see Figure 5(a-b)) and indicates that preservation of global invariants is a weaker property than preservation of local conservation laws.

As a consequence, when examining sensitive regimes using finite difference schemes, the significant improvement in the qualitative features of the waveform obtained with the integrable AL - S2 scheme justifies the computational expense. The advantages of the MS scheme are as follows – when considering non-sensitive regimes such as soliton solutions or the one-mode multi-phase solution, it is faster, there is no loss of conjugacy, it handles a wide range of mesh sizes and it preserves the local conservation laws and global invariants as well or better than the AL based scheme.

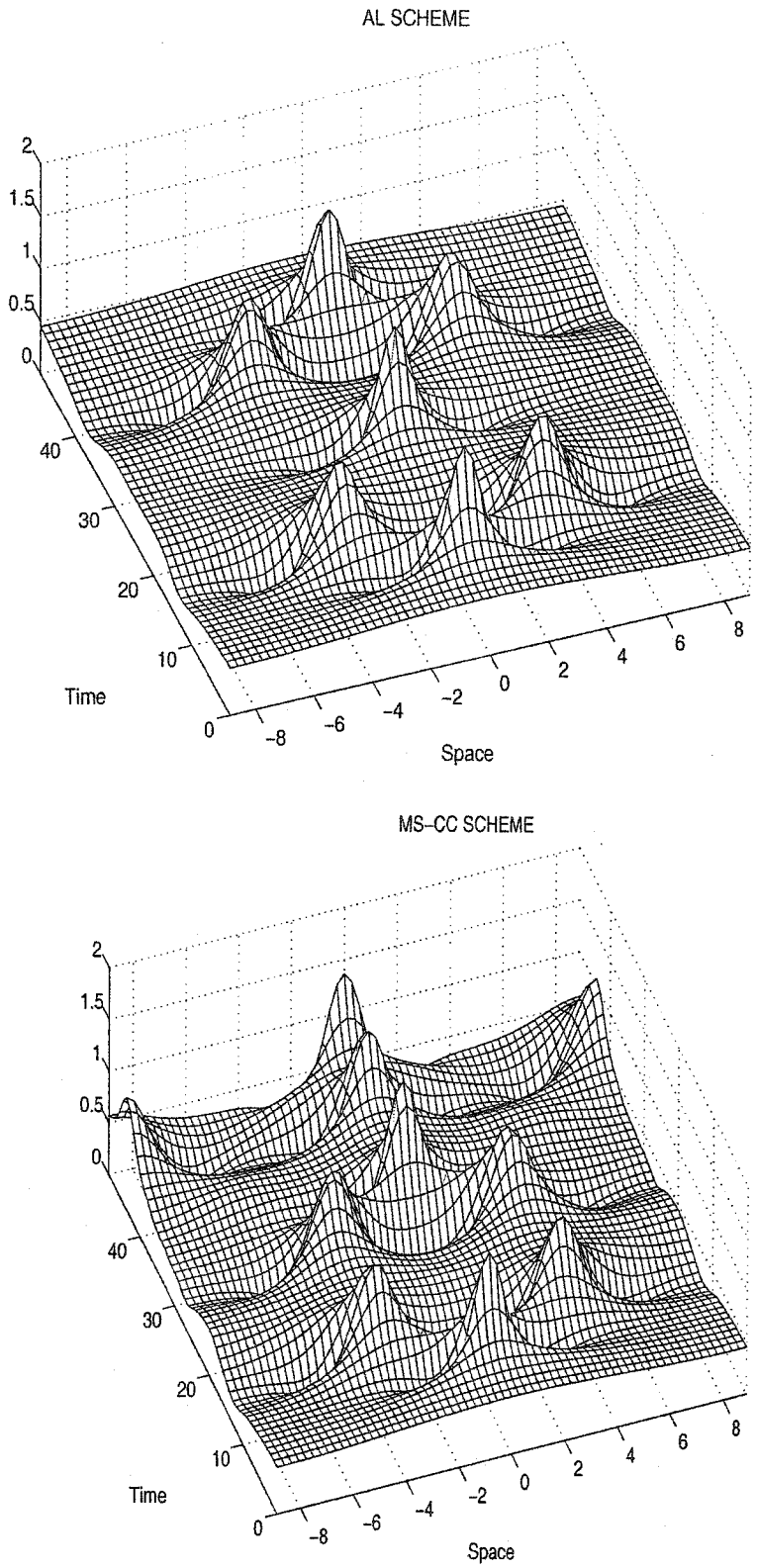

FIG. 4: S2 and MS-CC two-mode multi-phase surfaces.

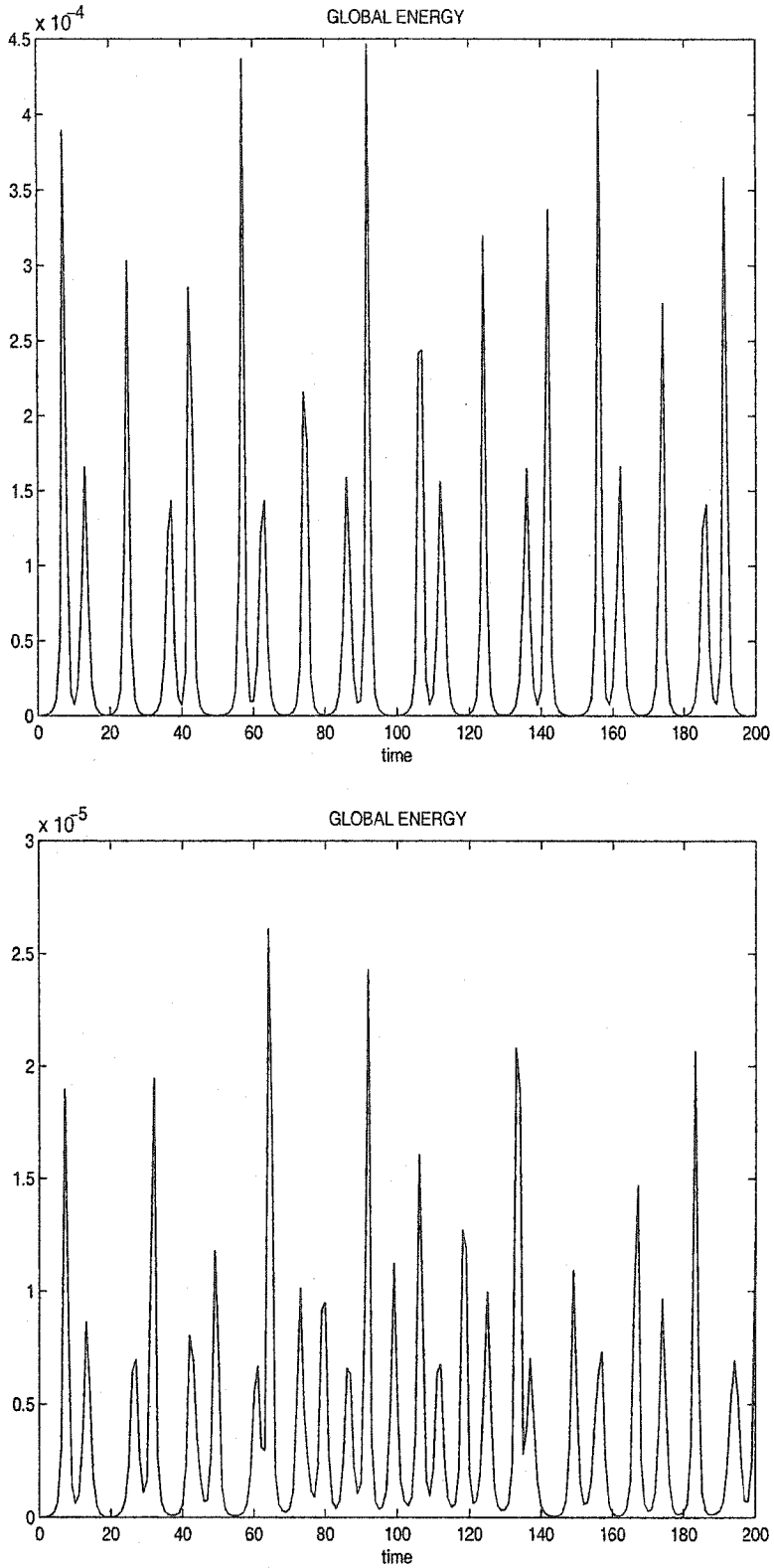

FIG. 5: S2 and MS-CC two-mode multi-phase global energies.

CHAPTER IV

BACKWARD ERROR ANALYSIS

Multi-symplectic integrators are approximations that preserve a discrete version of the multi-symplectic conservation law. In other words, MS integrators have been designed to preserve the multi-symplectic structure, but not necessarily other invariants such as the local energy and momentum, or the nonlinear spectrum. The question that arises then is, in practice, to what extent are these other invariants preserved? The numerical experiments on the NLS, SG and GP equations have shown that in addition to preserving the discrete MSCL exactly, multi-symplectic schemes preserve these other invariants very well (although not exactly) over long times.

This is reminiscent of the behavior of symplectic schemes for Hamiltonian ODEs. Symplectic integrators are designed to preserve the symplectic structure, not to preserve the energy. In fact, for general Hamiltonian systems, conservation of the symplectic structure and conservation of energy are conflicting requirements that, in general, are not solved simultaneously by a symplectic scheme [62]. Even so, the Hamiltonian is preserved extremely well over very long times (for numerical experiments substantiating this, see [17, 53]). Insight into this feature of symplectic methods has been provided by a backward error analysis of the problem [28, 29, 43]. In backward error analysis of ordinary differential equations, one interprets the numerical solution as the exact solution of a modified differential equation. The modified equation is given in terms of a series in powers of the mesh size and is typically truncated at successive powers to obtain a sequence of modified equations that the numerical solution approximates to higher and higher order. In the case of Hamiltonian ODEs, it has been shown that symplectic discretizations lead to modified differential equations which are also Hamiltonian [28]. The Hamiltonian structure of the modified equation can then be used to show that a symplectic integrator almost preserves the total energy over an exponentially long period of time [10].

In this chapter we implement a formal backward error analysis of the multi-symplectic centered-cell discretization of the NLS equation. We show that this allows the numerical solution to be interpreted as the exact solution of a perturbed PDE which is again multi-symplectic. In the numerical experiments we verify

that the modified conservation laws are preserved to higher order by the numerical solution. This helps to explain the preservation properties of the local conservation laws observed in the numerical experiments and the improved long time numerical solution. We begin by reviewing backward error analysis for ODEs.

IV.1 BACKWARD ERROR ANALYSIS FOR ODES

Backward error analysis can be applied to general ODEs, not just Hamiltonian ODEs [56]. We examine one-step integrators such as Runge-Kutta methods. For a smooth function F, consider the ODE (we label it S_1)

$$\frac{d}{dt}u = F(u), \tag{51}$$

and, e.g., the explicit first order forward Euler discretization

$$u_{i+1} = u_i + hF, \tag{52}$$

where h is the time step. The exact solution of (51) and the numerical solution computed using (52) differ by $\mathcal{O}(h)$ terms. The question arises: can the numerical solution be interpreted as the exact solution of a perturbed differential equation? As a first step in answering this question, one can ask if there is another ODE, S_2^h (h appears as a parameter in the modified ODE), so that (52) differs with S_2^h by $\mathcal{O}(h^2)$ terms? A Taylor series expansion in t about t_i generates

$$u_{i+1} = u_i + hu_t + \frac{h^2}{2}u_{tt} + \cdots \tag{53}$$

Substituting this expansion into (52) and neglecting $\mathcal{O}(h^2)$ terms, yields the modified equation S_2^h:

$$\begin{aligned} \frac{d}{dt}u &= F - \frac{h}{2}u_{tt} \\ &= F - \frac{h}{2}F'(u)\frac{d}{dt}u \\ &= F - \frac{h}{2}F'(u)F. \end{aligned} \tag{54}$$

So although the numerical solution is a first order approximation to (51), it can be interpreted as a second order approximation to the solution of the modified differential equation (54). Keeping higher order terms in the Taylor expansion (53) leads to higher order modified equations, S_r^h. The numerical solution can formally

be interpreted, with increasing index r, as the increasingly accurate solution of the modified equations. The details and explicit formulas for the modified differential equations for general integration methods are derived in [30]. These results are extended to Hamiltonian ODEs in the works of Hairer and Lubich [29], Sanz-Serna and Calvo[50] and Benettin and Giorgilli [10].

Example

Since our primary concern is in the numerical solution of Hamiltonian systems, we apply these ideas to the pendulum equation

$$\frac{d}{dt}u = \frac{d}{dt}\begin{pmatrix} p \\ q \end{pmatrix} = \begin{pmatrix} -\sin q \\ p \end{pmatrix} = \begin{pmatrix} F_1 \\ F_2 \end{pmatrix}, \tag{55}$$

with Hamiltonian $H = 1/2p^2 - \cos q$. The pendulum equation arises when considering the special case of spatially uniform solutions of the sine-Gordon solution, i.e., let $u = u(t)$ in (27). Using the forward Euler discretization, the modified equation is given by

$$\frac{d}{dt}u = F - \frac{h}{2}F'(u)F = \begin{pmatrix} -\sin q + \frac{h}{2}p\cos q \\ p + \frac{h}{2}\sin q \end{pmatrix}. \tag{56}$$

Figure 6 shows exact and numerical solutions for these equations. For the initial condition $p(0) = 0, q(0) = 2$, it shows the exact solutions to the original (circles) and the modified (crosses) equations together with the numerical solution (solid line) obtained using the first order forward Euler discretization. The forward Euler is implemented with a time step of $h = 0.5$. The numerical solution is clearly "closer" to the solution of the modified equation ($\mathcal{O}(h^3)$ close) than to the solution of the original equation ($\mathcal{O}(h^2)$ close).

Unfortunately, the modified ODE is not Hamiltonian. This happens because the forward Euler discretization is *not symplectic*. In fact negative dissipation has been introduced into the system. This can be seen by rewriting (56) as a perturbation of a Hamiltonian system, i.e.

$$\frac{d}{dt}u = \begin{pmatrix} -\sin q - \frac{h}{2}p\cos q \\ p + \frac{h}{2}\sin q \end{pmatrix} + \begin{pmatrix} hp\cos q \\ 0 \end{pmatrix}.$$

The phase plane portrait for the pendulum equation has a center at (0,0) with periodic orbits nested about this center. The initial data (0,2) is initial data

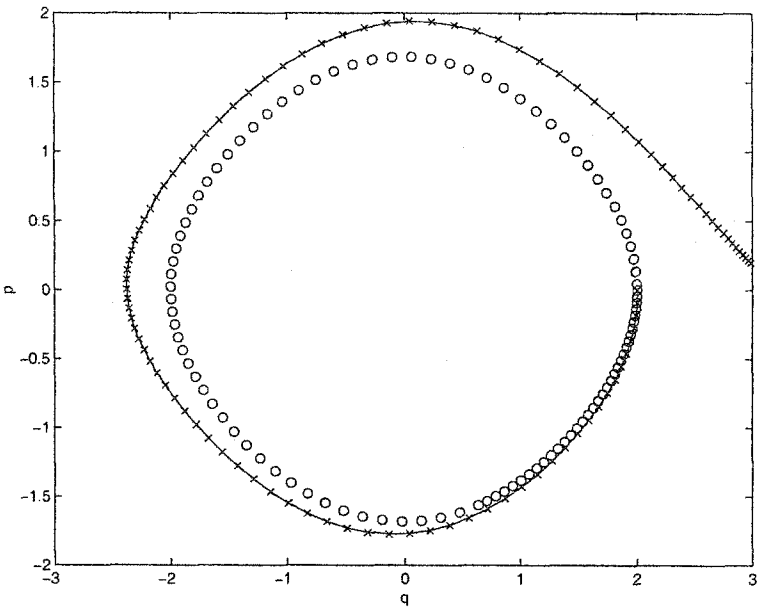

FIG. 6: Numerical (-) and exact original (o) and modified (x) solutions.

for a periodic orbit but the forward Euler discretization produces a non-periodic, outwardly spiraling solution.

We now consider the first order symplectic discretization

$$\begin{aligned} p_{i+1} &= p_i + hF_1(q_{i+1}), \\ q_{i+1} &= q_i + hF_2(p_i). \end{aligned} \tag{57}$$

Substituting the Taylor series expansions for (57) into (55), and truncating at $\mathcal{O}(h^2)$, we find that the modified system remains Hamiltonian and is given by

$$\frac{d}{dt}u = F - \frac{h}{2}F'(u)F = \begin{pmatrix} -\sin q - \frac{h}{2}p\cos q \\ p + \frac{h}{2}\sin q \end{pmatrix},$$

with Hamiltonian $H_1 = p^2/2 - \cos q + h/2p\sin q$. In fact, symplectic discretizations always lead to modified ODEs which are Hamiltonian. The fact that the modified equation, now labeled as $S_{H_2^h}$, is in the same Hamiltonian class as the original equation, has significant consequences for the numerical solution. Note that the subscript H in the notation for the modified equation indicates that the modified equation is Hamiltonian.

Figure 7 shows the exact solutions to the original pendulum equation and the Hamiltonian modified equation as well as the numerical solution obtained with the

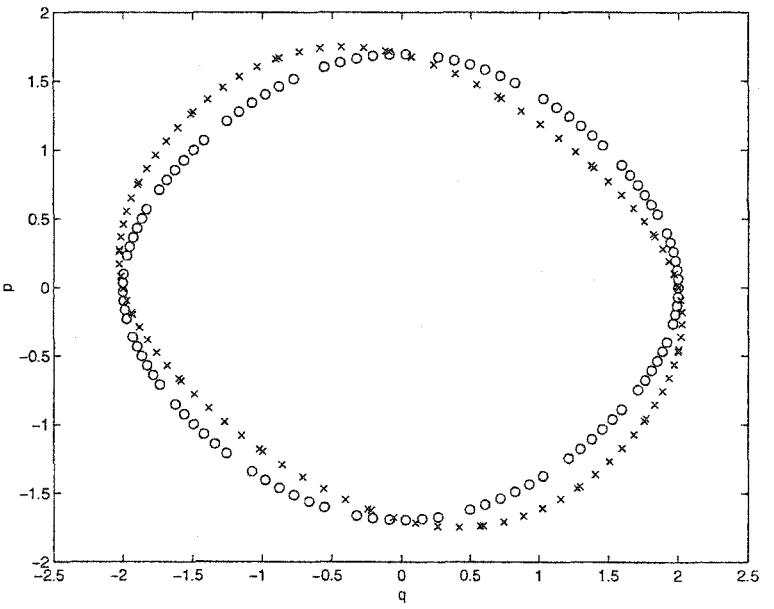

FIG. 7: Numerical (x) and exact original (o) solution.

symplectic scheme (57). As before we see that the numerical solution is closer to the solution of the modified equation than the original equation. However, since the modified equation is Hamiltonian, in this case the numerical solution shows the appropriate periodic behavior and (0,0) remains a center.

As before, keeping higher order terms in the Taylor expansion (53) leads to a sequence of modified equations, $S_{H_r^h}$ (each Hamiltonian), which are satisfied by the numerical solution to $\mathcal{O}(h^r)$ (or the numerical solution differs from the solution of the modified equation in terms of $\mathcal{O}(h^{r+1})$).

This example illustrates how the modified equations obtained by backward error analysis provide an explanation for the improved performance of symplectic discretizations. Although the numerical solution obtained using an m-th order symplectic discretization produces a solution that is accurate to the given order, it can be viewed as the numerical solution of arbitrarily high order of a nearby Hamiltonian system and so preserves the *qualitative* features of the system to arbitrarily high order.

The backward error analysis argument or interpretation given in this last example is possible for every symplectic integration method applied to an autonomous Hamiltonian system. More precisely: For an arbitrary autonomous Hamiltonian

system with a smooth Hamiltonian H and any positive integer r, a modified autonomous Hamiltonian system $S_{H_r^h}$ can be found such that the numerical solution differs from the exact solution of the modified equation in $\mathcal{O}(h^{r+1})$ terms. If the numerical method belongs to one of the standard classes of methods, including the Runge-Kutta methods which we are interested in, the formulas for the computation of the modified equations is given by, e.g., Hairer [28] and Calvo, Murura and Sanz-Serna [15]. The question of the closeness of the numerical approximations and the solutions of the modified equations is addressed in the papers of Hairer and Lubich [29] and Benettin and Giorgilli [10]. It is shown in these papers that the difference between the numerical solution Ψ_h and the solutions of the modified equations can be made exponentially small in the step size h; i.e.

$$\|\Phi_{h,\tilde{X}_{i_*}}(x) - \Psi_h(x)\| \leq c_1 h e^{-c_2/h},$$

provided the original system and the numerical method are analytic. Here c_1, $c_2 > 0$ are appropriate constants, $\Phi_{h,\tilde{X}_{i_*}}$ denotes the time flow map of the modified vector field $\tilde{X}_{i_*}$, and the index $i_*(h)$ has been chosen such that the difference is minimized.

Vector backward error analysis for Hamiltonian ODEs

We would like to extend these results to Hamiltonian PDEs, but first let us reformulate the case for Hamiltonian ODEs and symplectic discretizations in a form that seems natural for extending it to the study of PDEs.

We start by recalling the vector form of a Hamiltonian ODE. Let $z = (p, q)$ satisfy

$$\boldsymbol{J}\frac{d}{dt}z = \nabla_z H(z), \qquad \boldsymbol{J} = \begin{pmatrix} 0 & 1 \\ -1 & 0 \end{pmatrix}.$$

Then apply the symplectic Euler scheme

$$\boldsymbol{J}_+\delta_t^+ z^j + \boldsymbol{J}_-\delta_t^- z^j = \nabla_z H(z^j), \tag{58}$$

where

$$\boldsymbol{J}_+ = \begin{pmatrix} 0 & -1 \\ 0 & 0 \end{pmatrix}, \qquad \boldsymbol{J}_- = \begin{pmatrix} 0 & 0 \\ 1 & 0 \end{pmatrix}, \tag{59}$$

and

$$\delta_t^+ z^j = \frac{z^{j+1} - z^j}{\Delta t}, \qquad \delta_t^- z^j = \frac{z^j - z^{j-1}}{\Delta t}. \tag{60}$$

Since expansions of z^{j+1} and z^{j-1} about t_j yield

$$\begin{aligned}\delta_t^+ z^j &= z_t + \frac{\Delta t}{2} z_{tt} + \frac{\Delta t^2}{6} z_{ttt} + \cdots, \\ \delta_t^- z^j &= z_t - \frac{\Delta t}{2} z_{tt} + \frac{\Delta t^2}{6} z_{ttt} - \cdots,\end{aligned}$$

then, to first order, the modified system of equations becomes

$$\boldsymbol{J} z_t + \frac{\Delta t}{2} \left(\boldsymbol{J}_+ - \boldsymbol{J}_-\right) z_{tt} = \nabla_z H(z). \tag{61}$$

So far nothing new has been added. But just as we cast PDEs into multi-symplectic form by defining new variables, the same can be done now. Let $q = z_t$. Then (61) can be cast into the modified Hamiltonian system

$$\tilde{\boldsymbol{J}} \frac{d}{dt} \tilde{z} = \nabla_{\tilde{z}} \tilde{H}_1(\tilde{z}),$$

where

$$\tilde{z} = \begin{pmatrix} z \\ q \end{pmatrix}, \qquad \tilde{\boldsymbol{J}} = \begin{pmatrix} \boldsymbol{J} & \Delta t \boldsymbol{A} \\ -\Delta t \boldsymbol{A} & 0 \end{pmatrix}, \qquad \boldsymbol{A} = \frac{1}{2}\left(\boldsymbol{J}_+ - \boldsymbol{J}_-\right),$$

and

$$\tilde{H}_1(\tilde{z}) = H(z) - \frac{\Delta t}{2} q^T \boldsymbol{A} q = H(z) - \frac{\Delta t}{2} z_t^T \boldsymbol{A} z_t.$$

Higher order modifications are found in the same way.

IV.2 BACKWARD ERROR ANALYSIS FOR MULTI-SYMPLECTIC PDES

This form of the backward error analysis can be extended to multi-symplectic PDEs in both time and space. Consider the multi-symplectic PDE

$$\boldsymbol{M} z_t + \boldsymbol{K} z_x = \nabla_z S(z). \tag{62}$$

Applying the symplectic Euler discretization (58) to both time and space and using the definitions (59) and (60), to first order, we first obtain the modified PDE

$$\boldsymbol{M} z_t + \frac{\Delta t}{2} \left(\boldsymbol{M}_+ - \boldsymbol{M}_-\right) z_{tt} + \boldsymbol{K} z_x + \frac{\Delta x}{2} \left(\boldsymbol{K}_+ - \boldsymbol{K}_-\right) z_{xx} = \nabla_z S(z),$$

and then, by augmenting the system with the variables $r = z_t$ and $s = z_x$, we obtain the modified multi-symplectic PDE

$$\tilde{\boldsymbol{M}} \tilde{z}_t + \tilde{\boldsymbol{K}} \tilde{z}_x = \nabla_{\tilde{z}} \tilde{S}_1(\tilde{z}),$$

where

$$\tilde{z} = \begin{pmatrix} z \\ r \\ s \end{pmatrix}, \quad \tilde{M} = \begin{pmatrix} M & \Delta t A & 0 \\ -\Delta t A & 0 & 0 \\ 0 & 0 & 0 \end{pmatrix}, \quad \tilde{K} = \begin{pmatrix} K & 0 & \Delta x B \\ 0 & 0 & 0 \\ -\Delta x B & 0 & 0 \end{pmatrix},$$

$$A = \frac{1}{2}(M_+ - M_-), \qquad B = \frac{1}{2}(K_+ - K_-),$$

and

$$\tilde{S}_1(\tilde{z}) = S(z) - \frac{\Delta t}{2} r^T A r - \frac{\Delta x}{2} s^T B s = S(z) - \frac{\Delta t}{2} z_t^T A z_t - \frac{\Delta x}{2} z_x^T B z_x.$$

Now a modified local energy conservation law can be derived from this new multi-symplectic formulation.

IV.3 BACKWARD ERROR ANALYSIS FOR THE NLS EQUATION

A backward error analysis of the multi-symplectic PDE (62) yields modified equations which are also multi-symplectic and satisfy modified local conservation laws. The modified multi-symplectic PDE is satisfied by the numerical solution to higher order. We begin by noting that the forward difference operators can also be expanded as follows

$$\begin{aligned} \delta_t^+ z(t^j) &= z_t(t^{j+1/2}) + \frac{\Delta t^2}{6} z_{ttt}(t^{j+1/2}) + \mathcal{O}(\Delta t^4), \\ \delta_x^+ z(x_i) &= z_x(x_{i+1/2}) + \frac{\Delta x_2}{6} z_{xxx}(x_{i+1/2}) + \mathcal{O}(\Delta x^4). \end{aligned}$$

Substituting into (62), and truncating these expansions at $\mathcal{O}(\Delta t^4 + \Delta x^4)$, one obtains the modified equation

$$M z_t + \frac{\Delta t^2}{6} M z_{ttt} + K z_x + \frac{\Delta x^2}{6} K z_{xxx} = \nabla_z S(z),$$

which we will show is satisfied by the numerical solution up to $\mathcal{O}(\Delta t^4 + \Delta x^4)$. Letting

$$\tilde{z} = (z, p, q, r, s)^T = (z, z_t, z_{tt}, z_x, z_{xx})^T, \qquad \tilde{S} = S + \frac{\Delta t^2}{6} q^T M p + \frac{\Delta x^2}{6} s^T K r,$$

$$\tilde{M} = \begin{pmatrix} M & 0 & \frac{\Delta t^2}{6} M & 0 & 0 \\ 0 & \frac{\Delta t^2}{6} M & 0 & 0 & 0 \\ \frac{\Delta t^2}{6} M & 0 & 0 & 0 & 0 \\ 0 & 0 & 0 & 0 & 0 \\ 0 & 0 & 0 & 0 & 0 \end{pmatrix},$$

and

$$\tilde{K} = \begin{pmatrix} K & 0 & 0 & 0 & \frac{\Delta x^2}{6}K \\ 0 & 0 & 0 & 0 & 0 \\ 0 & 0 & 0 & 0 & 0 \\ 0 & 0 & 0 & \frac{\Delta x^2}{6}K & 0 \\ \frac{\Delta x^2}{6}K & 0 & 0 & 0 & 0 \end{pmatrix},$$

the modified multi-symplectic equation can be written in the standard form

$$\tilde{M}\tilde{z}_t + \tilde{K}\tilde{z}_x = \nabla_{\tilde{z}}\tilde{S}(\tilde{z}).$$

The modified PDE can be used to derive modified conservation laws of energy and momentum. Substituting $\tilde{z}$, $\tilde{M}$, $\tilde{K}$ and $\tilde{S}$, into (16) and (19), the modified LECL and LMCL are found to be, respectively,

$$\left(E + \frac{\Delta t^2}{6} z_{tt}^T M z_t\right)_t + \left(F - \frac{\Delta x^2}{3} z_t^T K z_{xx} - \frac{\Delta x^2}{6} z_{xt}^T K z_x\right)_x = 0$$

and

$$\left(G + \frac{\Delta x^2}{6} z_{xx}^T K z_x\right)_x + \left(I - \frac{\Delta t^2}{3} z_x^T M z_{tt} - \frac{\Delta t^2}{6} z_{xt}^T M z_t\right)_t = 0.$$

Numerical verification of preservation of the local conservation laws

We next examine whether the modified LECL obtained from the multi-symplectic discretization of the NLS is preserved to higher order in space and time (similarly for the LMCL). Using the MS centered-cell box scheme, we solve the discrete system of equations at each time step and use this to evaluate the local residual $R_i^j = \tilde{E}_i^j + \tilde{F}_i^j$ at each grid point. Note that each derivative in $\tilde{E}$ and $\tilde{F}$ must be evaluated using a higher order discretization (at least fourth-order) so that the estimate of the error is not miscalculated. The residual, $R = \max_{i,j} R_i^j$, is the maximum of R_i^j over the entire space-time mesh.

To check the order of the convergence for the modified (and unmodified) LECL, the residual R is evaluated for different spatial meshes Δx and time steps Δt. The numerical results in Table I show that the residuals for the unmodified LECL and LMCL converge quadratically in Δx and Δt. The data we obtained for the modified LECL shows fourth-order convergence in Δx and Δt. For example, for a fixed $N = 64$, we view R as a function of Δt. We find that for $\Delta t = .02$, $R = 7.0 \times 10^{-7}$; $\Delta t = .01$, $R = 4.0 \times 10^{-8}$; $\Delta t = .005$, $R = 2.6 \times 10^{-9}$. Hence, R

exhibits fourth order convergence to $C\Delta x^4$ as $\Delta t \to 0$. We further find that for $\Delta t \approx 0$, $R \to 0$ like Δx^4. The modified LECL is satisfied by the numerical solution up to $\mathcal{O}(\Delta t^4) + \mathcal{O}(\Delta x^4)$. Thus we see that the modified local conservation law is preserved to higher order along the numerical solution than the original LECL.

CHAPTER V

A MULTI-SYMPLECTIC SPECTRAL SCHEME

The MS-CC discretization of the NLS equation has demonstrated that multi-symplectic finite difference schemes can have difficulty in resolving spatial structures in sensitive regimes. On the other hand, spectral methods have proven to be highly effective methods for solving evolution equations with simple boundary conditions. As the number N of basis functions used to approximate the solution increases, errors typically decay at an exponential rate rather than at the polynomial rates characteristic of finite difference approximations [27]. Relatively coarse grids are sufficient for most accuracy requirements and allow for efficient algorithms. Consequently, we turn to spectral methods and investigate whether they can be employed to discretize the spatial derivatives while preserving the underlying multi-symplectic structure.

In this chapter we show that, in fact, spectral discretizations do provide another class of multi-symplectic integrators which have a corresponding discrete spectral multi-symplectic conservation law. In the first section we introduce multi-symplectic PDEs in Fourier space [13]. In section 2 we show how to obtain a multi-symplectic discretization by truncating the Fourier expansion. This produces a system of Hamiltonian ODEs which can be discretized in time with symplectic methods. In section 3 we apply this to the NLS equation to obtain a new multi-symplectic spectral discretization. Not surprisingly, we show for the NLS equation that the MS spectral method outperforms the multi-symplectic discretization based on finite differences. In section 4 we examine how well the phase space geometry is preserved by MS spectral methods for the sine-Gordon equation. We implement both MS and non-symplectic spectral methods and use the associated nonlinear spectrum of the SG equation as a basis for comparing the effectiveness of the integrators. The relevant quantities to monitor are the periodic/anti periodic eigenvalues of the associated spectral problem. These eigenvalues are the spectral representation of the action variables and are directly related to the geometry of the SG phase space. Significantly, we show that the MS spectral methods provide an improved resolution of phase space structures, as measured by the nonlinear spectrum, when compared with non-symplectic spectral integrators. This is the first examination of the implications, in terms of preservation of the nonlinear spectrum

and phase space structure, of preserving the MS structure under discretization.

V.1 MULTI-SYMPLECTIC PDES IN FOURIER SPACE

We consider the space $L_2(I)$ of L-periodic, square integrable functions in $I = [-L/2, L/2]$ and the space l_2 of square summable complex sequences. Let

$$U = \boldsymbol{F}u \in l_2$$

denote the discrete Fourier transform of $u \in L_2(I)$. Here

$$\boldsymbol{F} : L_2 \to l_2$$

denotes the Fourier operator which gives the complex-valued Fourier coefficients

$$U_k \in \mathbb{C},\ k = -\infty, \ldots, -1, 0, 1, \ldots, \infty$$

which we collect in the infinite-dimensional vector

$$U = (\ldots, U_{-1}, U_0, U_1, \ldots) \in l_2.$$

Denote the L_2 inner product by (u, v) and the l_2 inner product by $\langle U, V \rangle$. Then the inverse Fourier operator

$$\boldsymbol{F}^{-1} : l_2 \to L_2$$

is defined by

$$\langle V, \boldsymbol{F}u \rangle = (\boldsymbol{F}^{-1}V, u).$$

Furthermore, partial differentiation with respect to $x \in I$ simply reduces to

$$\partial_x u = \boldsymbol{F}^{-1}\Theta U$$

where $\Theta : l_2 \to l_2$ is the diagonal spectral operator

$$\Theta = \begin{pmatrix} \ddots & & & & \\ & \ddots & & & \\ & & \theta_k & & \\ & & & \ddots & \\ & & & & \ddots \end{pmatrix}$$

with entries

$$\theta_k = \frac{2\pi i}{L} k. \tag{63}$$

These definitions can be generalized to vector-valued functions $z = (z_1, \ldots, z_d)^T \in L_2^d(I)$. Let $\hat{F} : L_2^d(I) \to l_2^d$ be defined such that

$$Z = \hat{F}z = \begin{pmatrix} Fz^1 \\ \vdots \\ Fz^d \end{pmatrix} = \begin{pmatrix} Z^1 \\ \vdots \\ Z^d \end{pmatrix}.$$

It is useful to see different representations of Z such as

$$Z = \begin{pmatrix} \ldots, Z_{-1}^1, Z_0^1, Z_1^1, \ldots \\ \vdots \\ \ldots, Z_{-1}^d, Z_0^d, Z_1^d, \ldots \end{pmatrix} = (\ldots, Z_{-1}, Z_0, Z_1, \ldots)$$

Now let us apply these ideas to multi-symplectic PDEs. Let ϕ_k be an orthonormal basis for $L_2(I)$ given by the functions

$$\phi_k(x) = \frac{1}{\sqrt{L}} e^{\theta_k x},$$

with θ_k defined as in (63). Then the discrete Fourier transform and its inverse are given by

$$\begin{aligned} Z_k &= F(z) = \int_{-L/2}^{L/2} z(x,t)\phi_{-k}(x)\,dx \\ z &= F^{-1}(Z) = \sum_{k=-\infty}^{\infty} Z_k \phi_k. \end{aligned} \tag{64}$$

Substituting (64) into the multi-symplectic PDE (13) we obtain

$$M\left(\sum_{k=-\infty}^{\infty} Z_k\phi_k\right)_t + K\left(\sum_{k=-\infty}^{\infty} Z_k\phi_k\right)_x = \nabla_z S\left(\sum_{k=-\infty}^{\infty} Z_k\phi_k\right).$$

Multiplying by ϕ_{-l} and integrating we get

$$\begin{aligned} M\partial_t Z_l + K\theta_l Z_l &= \int_{-L/2}^{L/2} \nabla_z S\left(\sum_{k=-\infty}^{\infty} Z_k\phi_k\right)\phi_{-l}\,dx \\ &= \int_{-L/2}^{L/2} \nabla_z S\left(\sum_{k=-\infty}^{\infty} Z_k\phi_k\right)\phi_l\,dx \\ &= \int_{-L/2}^{L/2} \nabla_z S\left(\sum_{k=-\infty}^{\infty} Z_k\phi_k\right)\frac{\partial z}{\partial Z_l}\,dx \\ &= \int_{-L/2}^{L/2} \nabla_{Z_l} S\left(\sum_{k=-\infty}^{\infty} Z_k\phi_k\right)dx \\ &= \nabla_{Z_l}\bar{S}(Z), \end{aligned}$$

where

$$\bar{S}(Z) = \int_{-L/2}^{L/2} S\left(\sum_{k=-\infty}^{\infty} Z_k \phi_k\right) dx.$$

Collecting these equations into a single equation we obtain the infinite dimensional system of ODEs

$$MZ_t + K\Theta Z = \nabla_Z \bar{S}(Z). \tag{65}$$

This equation can appropriately be called a multi-symplectic spectral PDE and associated with it we have a multi-symplectic conservation law and local energy conservation law in Fourier space.

The multi-symplectic conservation law can be obtained by introducing the Fourier transforms

$$\mathcal{W} = F\omega, \quad \mathcal{K} = F\kappa.$$

Then from the multi-symplectic conservation law (15) we obtain the following conservation laws of symplecticity in Fourier space:

$$\mathcal{W}_t + \Theta\mathcal{K} = 0.$$

Similarly, by introducing the transforms

$$\mathcal{E} = FE, \quad \mathcal{F} = FF,$$

the local energy conservation law (16) becomes the spectral energy conservation law

$$\mathcal{E}_t + \Theta\mathcal{F} = 0.$$

Here ω, κ, E, and F are defined in equations (14), (17), and (18).

V.2 A MULTI-SYMPLECTIC SPECTRAL DISCRETIZATION

As examined for the Zakharov-Kutsnesov equations [13], we can show that upon truncating the discrete Fourier transform, the discretization described above turns out to be multi-symplectic. To show this, we need to write the discretization of the x-derivative in terms of a differentiation matrix.

Let u_l, $l = 0, 1, \ldots, N-1$, denote a finite number of values for u. For these N u-values, the discrete Fourier transform can be defined as

$$U_k = \frac{1}{N} \sum_{l=0}^{N-1} u_l \, e^{-\theta_k l \Delta x}, \quad k = 0, 1, \ldots, N-1, \tag{66}$$

with $\Delta x = L/N$, producing N complex Fourier coefficients U_k. The inverse discrete Fourier transform

$$u_l = \sum_{k=0}^{N-1} U_k \, e^{\theta_k l \Delta x}, \quad j = 0, 1, \ldots, N-1, \tag{67}$$

recovers the original values u_l. To discretize the derivative we proceed as follows.

First notice that the form of (66) allows for the following interpretation. Any multiple of N added to k does not change the exponentials, or the sum in (66). Therefore we have

$$U_{N-k} = U_{-k}, \quad k = 1, 2, \ldots, N/2 - 1$$

and the mode $U_{N/2}$ (the *Nyquist* or *reflection* frequency) can be viewed as containing equal contributions from modes $N/2$ and $-N/2$. From now on we write it as $U_{\pm N/2}$.

With the modes $k = 0, 1, \ldots, N-1$ interpreted as modes $k = 0, 1, \ldots, N/2 - 1, \pm N/2, -N/2+1, \ldots, -1$, we then have that for all values of l

$$\begin{aligned} u_l &= \sum_{k=-N/2+1}^{N/2-1} U_k \, e^{\theta_k l \Delta x} + U_{\pm N/2} \left(\frac{e^{\theta_{N/2} l \Delta x} + e^{\theta_{-N/2} l \Delta x}}{2} \right) \\ &= \sum_{k=-N/2+1}^{N/2-1} U_k \, e^{\theta_k l \Delta x} + U_{\pm N/2} \left(\frac{e^{\pi i l} + e^{-\pi i l}}{2} \right) \\ &= \sum_{k=-N/2+1}^{N/2-1} U_k \, e^{\theta_k l \Delta x} + U_{\pm N/2} \cos \pi l. \end{aligned}$$

Second, considering the continuous interpolating trigonometric polynomial and requiring it to take the values u_l at locations $x_l = -L/2 + l\Delta x$, $l = 0, 1, \ldots, N-1$, leads to the following closed form

$$u(x) = \sum_{k=-N/2+1}^{N/2-1} U_k \, e^{\theta_k (x + L/2)} + U_{\pm N/2} \cos \frac{\pi N}{L} \left(x + \frac{L}{2} \right).$$

Thus, the first and second derivatives are given by

$$\begin{aligned} u'(x) &= \sum_{k=-N/2+1}^{N/2-1} \theta_k \, U_k \, e^{\theta_k (x + L/2)} - \frac{\pi N}{L} U_{\pm N/2} \sin \frac{\pi N}{L} \left(x + \frac{L}{2} \right), \\ u''(x) &= \sum_{k=-N/2+1}^{N/2-1} \theta_k^2 \, U_k \, e^{\theta_k (x + L/2)} - \left(\frac{\pi N}{L} \right)^2 U_{\pm N/2} \cos \frac{\pi N}{L} \left(x + \frac{L}{2} \right), \end{aligned}$$

At the gridpoints x_l, while the 0 and $\pm N/2$ modes do not contribute to the first derivative, the $\pm N/2$ mode does contribute to the second derivative. Therefore, the first and second partial derivatives with respect to x can be discretized as follows

$$\partial_x u = \boldsymbol{F}^{-1}\bar{\Theta}\boldsymbol{F}u, \tag{68}$$

$$\partial_{xx} u = \boldsymbol{F}^{-1}\Theta^2\boldsymbol{F}u, \tag{69}$$

where the diagonal matrix $\bar{\Theta}$ has the entries $\bar{\theta}_k$ defined by

$$\bar{\theta}_k = \begin{cases} \theta_k & \text{for } k = 0, \ldots, N/2-1, \\ 0 & \text{for } k = N/2, \\ -\theta_{N-k} & \text{for } k = N/2+1, \ldots, N-1, \end{cases} \tag{70}$$

where θ_k is given by (63).

The spectral differentiation matrices

In order to show that the spectral discretization is multi-symplectic, we need to write the spectral discretizations (68)-(69) in a suitable matrix form.

The first derivative

First, the inverse discrete Fourier transform given by equation (67), in matrix form, becomes

$$\begin{pmatrix} u_0 \\ u_1 \\ u_2 \\ \vdots \\ \vdots \\ u_{N-1} \end{pmatrix} = \begin{pmatrix} 1 & 1 & 1 & 1 & \ldots & 1 \\ 1 & \lambda & \lambda^2 & \lambda^3 & \ldots & \lambda^{N-1} \\ 1 & \lambda^2 & \lambda^4 & \lambda^6 & \ldots & \lambda^{2(N-1)} \\ \vdots & \vdots & & & & \\ \vdots & \vdots & & & & \\ 1 & \lambda^{N-1} & \ldots & \ldots & \ldots & \lambda^{(N-1)^2} \end{pmatrix} \begin{pmatrix} U_0 \\ U_1 \\ U_2 \\ \vdots \\ \vdots \\ U_{N-1} \end{pmatrix}$$

where $\lambda = e^{2\pi i/N}$. The x-derivative is approximated by

$$\begin{pmatrix} u_{x0} \\ u_{x1} \\ u_{x2} \\ \vdots \\ \vdots \\ u_{xN-1} \end{pmatrix} = \begin{pmatrix} 1 & 1 & 1 & 1 & \ldots & 1 \\ 1 & \lambda & \lambda^2 & \lambda^3 & \ldots & \lambda^{N-1} \\ 1 & \lambda^2 & \lambda^4 & \lambda^6 & \ldots & \lambda^{2(N-1)} \\ \vdots & \vdots & & & & \\ \vdots & \vdots & & & & \\ 1 & \lambda^{N-1} & \ldots & \ldots & \ldots & \lambda^{(N-1)^2} \end{pmatrix} \begin{pmatrix} \bar{\theta}_0 U_0 \\ \bar{\theta}_1 U_1 \\ \bar{\theta}_2 U_2 \\ \vdots \\ \vdots \\ \bar{\theta}_{N-1} U_{N-1} \end{pmatrix}$$

or using the definition of $\bar{\Theta}$ (70)

$$\begin{pmatrix} u_{x0} \\ u_{x1} \\ u_{x2} \\ \vdots \\ \vdots \\ u_{xN-1} \end{pmatrix} = \begin{pmatrix} 1 & 1 & 1 & 1 & \dots & 1 \\ 1 & \lambda & \lambda^2 & \lambda^3 & \dots & \lambda^{N-1} \\ 1 & \lambda^2 & \lambda^4 & \lambda^6 & \dots & \lambda^{2(N-1)} \\ \vdots & \vdots & & & & \\ \vdots & \vdots & & & & \\ 1 & \lambda^{N-1} & \dots & \dots & \dots & \lambda^{(N-1)^2} \end{pmatrix} \begin{pmatrix} 0 \\ \theta_1 U_1 \\ \theta_2 U_2 \\ \vdots \\ -\theta_2 U_{N-2} \\ -\theta_1 U_{N-1} \end{pmatrix}$$

$$= \begin{pmatrix} 0 & \theta_1 & \theta_2 & \dots & -\theta_2 & -\theta_1 \\ 0 & \lambda\theta_1 & \lambda^2\theta_2 & \dots & -\lambda^{N-2}\theta_2 & -\lambda^{N-1}\theta_1 \\ 0 & \lambda^2\theta_1 & \lambda^4\theta_2 & \dots & -\lambda^{2(N-2)}\theta_2 & -\lambda^{2(N-1)}\theta_1 \\ \vdots & \vdots & & & & \\ \vdots & \vdots & & & & \\ 0 & \lambda^{N-1}\theta_1 & \lambda^{2(N-1)}\theta_2 & \dots & -\lambda^{(N-2)(N-1)}\theta_2 & -\lambda^{(N-1)^2}\theta_1 \end{pmatrix} \begin{pmatrix} U_0 \\ U_1 \\ U_2 \\ \vdots \\ U_{N-2} \\ U_{N-1} \end{pmatrix}$$

Using the fact that $\lambda^N = 1$, a typical row, r_l, of this matrix can be written as

$$r_l = \left(0,\ \lambda^l\theta_1, \dots, \lambda^{(N/2-1)l}\theta_{N/2-1},\ 0,\ -\lambda^{-(N/2-1)l}\theta_{N/2-1}, \dots, -\lambda^{-2l}\theta_2,\ -\lambda^{-l}\theta_1\right). \tag{71}$$

Next we note that the discrete Fourier transform, in matrix form, is given by

$$\begin{pmatrix} U_0 \\ U_1 \\ U_2 \\ \vdots \\ \vdots \\ U_{N-1} \end{pmatrix} = \frac{1}{N} \begin{pmatrix} 1 & 1 & 1 & 1 & \dots & 1 \\ 1 & \lambda^{-1} & \lambda^{-2} & \lambda^{-3} & \dots & \lambda^{-(N-1)} \\ 1 & \lambda^{-2} & \lambda^{-4} & \lambda^{-6} & \dots & \lambda^{-2(N-1)} \\ \vdots & \vdots & & & & \\ \vdots & \vdots & & & & \\ 1 & \lambda^{-N-1} & \dots & \dots & \dots & \lambda^{-(N-1)^2} \end{pmatrix} \begin{pmatrix} u_0 \\ u_1 \\ u_2 \\ \vdots \\ \vdots \\ u_{N-1} \end{pmatrix}.$$

This matrix has typical columns, c_k, given by

$$c_k = \left(1,\ \lambda^{-k},\ \lambda^{-2k},\ \dots,\ \lambda^{-(N/2-1)k},\ \lambda^{-N/2k},\ \lambda^{(N/2-1)k},\ \dots,\ \lambda^{2k},\ \lambda^{k}\right)^T. \tag{72}$$

Finally, by multiplying these matrices we obtain the differentiation matrix, $\boldsymbol{D_1}$, whose entries are given by the product of r_l and c_k given by (71) and (72). The product yields

$$\begin{aligned} (D_1)_{lk} &= \frac{1}{N} r_l c_k \\ &= \frac{1}{N}\left[\left(\alpha - \alpha^{-1}\right)\theta_1 + \left(\alpha^2 - \alpha^{-2}\right)\theta_2 + \cdots \left(\alpha^{N/2-1} - \alpha^{-(N/2-1)}\right)\theta_{N/2-1}\right], \end{aligned}$$

where $\alpha = \lambda^{l-k}$. The entries $(D_1)_{lk}$ can be simplified as follows:

For $l = k$, $\alpha = 1$ and the diagonal entries, $(D_1)_{ll} = 0$.

For $l \neq k$, setting $\mu = 2\pi/L$, we see that $(D_1)_{lk}$ has the representation

$$(D_1)_{lk} = i\,\frac{\mu}{N}\left[S^+ - S^-\right], \tag{73}$$

where

$$S^{\pm} = \alpha^{\pm} + 2\,\alpha^{\pm 2} + \cdots + m\,\alpha^{\pm m}$$

with $m = N/2 - 1$. To calculate these sums, let $\beta = \alpha^{\pm}$ and notice that

$$\begin{aligned} S &= \beta\left(1 + 2\,\beta + \cdots + m\,\beta^{m-1}\right) = \beta\frac{d}{d\beta}\left(\beta + \beta^2 + \cdots + \beta^m\right) \\ &= \beta\frac{d}{d\beta}\left(\frac{\beta^{m+1} - 1}{\beta - 1} - 1\right) = \beta\frac{(m+1)\,\beta^m(\beta - 1) - \beta^{m+1}}{(\beta - 1)^2}, \end{aligned}$$

or

$$S = \frac{\beta^{m+1}(m\,\beta - (m+1))}{(\beta - 1)^2}.$$

Applying this with $\beta = \pm\alpha$, $(D_1)_{lk}$ simplifies to

$$\begin{aligned} (D_1)_{lk} &= \frac{\mu}{N}\left[\frac{\alpha^{N/2}((N/2-1)\alpha - N/2)}{(\alpha-1)^2} - \frac{\alpha^{-N/2}((N/2-1)\alpha^{-1} - N/2)}{(\alpha^{-1}-1)^2}\right] \\ &= \frac{\mu}{N}\left[\frac{\alpha^{N/2}((N/2-1)\alpha - N/2) - \alpha^{-N/2}((N/2-1)\alpha - N/2\alpha^2)}{(\alpha-1)^2}\right]. \end{aligned}$$

This expression can be simplified using the relation

$$\alpha^{\pm N/2} = \left(\lambda^{l-k}\right)^{\pm N/2} = \left(e^{2\pi i/N}\right)^{\pm(l-k)N/2} = \left(e^{\pm\pi i}\right)^{l-k} = (-1)^{l-k}.$$

As a consequence,

$$\begin{aligned} (D_1)_{lk} &= i(-1)^{l-k}\,\frac{\mu}{2}\,\frac{\alpha^2 - 1}{(\alpha-1)^2} \\ &= i(-1)^{l-k}\,\frac{\mu}{2}\,\frac{\alpha+1}{\alpha-1} \\ &= i(-1)^{l-k}\,\frac{\mu}{2}\,\frac{\lambda^{l-k}+1}{\lambda^{l-k}-1} \\ &= i(-1)^{l-k}\,\frac{\mu}{2}\,\frac{e^{2\pi i(l-k)/L}+1}{e^{2\pi i(l-k)/L}-1} \\ &= (-1)^{l-k}\,\frac{\mu}{2}\,\cot\frac{\mu}{2}(x_l - x_k). \end{aligned}$$

Finally, the differentiation matrix $\boldsymbol{D_1}$ is given by

$$(D_1)_{lk} = \begin{cases} (-1)^{l-k}\,\frac{\mu}{2}\,\cot\frac{\mu}{2}(x_l - x_k) & \text{if } l \neq k, \\ 0 & \text{if } l = k. \end{cases} \tag{74}$$

In terms of the differentiation matrix $\boldsymbol{D_1}$, we find that the spectral discretization of the x-derivative, equation (68), can be written as

$$u_x = \boldsymbol{D_1} u. \tag{75}$$

An important property of $\boldsymbol{D_1}$ is that it is a skew-symmetric matrix. This will allow us to show that the spectral discretization is a multi-symplectic discretization.

The second derivative

Taking identical steps we arrive at the following expression for the spectral discretization of the second derivative

$$(D_2)_{lk} = \frac{1}{N}\left[\left(\alpha+\alpha^{-1}\right)\theta_1^2 + \cdots + \left(\alpha^{N/2-1}+\alpha^{-(N/2-1)}\right)\theta_{N/2-1}^2 + \alpha^{N/2}\theta_{N/2}^2\right],$$

where, as before, $\alpha = \lambda^{l-k}$, $\lambda = e^{2\pi i/N}$ and $\theta_k = 2\pi i/Lk = \mu k i$.

For $l = k$, $\alpha = 1$ and the diagonal entries are given by

$$\begin{aligned}(D_2)_{lk} &= -\frac{2\mu^2}{N}\left(1 + 2^2 + \cdots + \left(\frac{N}{2}-1\right)^2 + \tfrac{1}{2}\left(\frac{N}{2}\right)^2\right)\\ &= -\frac{\mu^2}{12}\left(N^2+2\right)\end{aligned}$$

For $l \neq k$, we can write the off-diagonal entries as

$$(D_2)_{lk} = -\frac{\mu^2}{N}\alpha\frac{d}{d\alpha}\left(S^+ - S^-\right), \tag{76}$$

where $S^{\pm}$ are as in equation (73). Expressing α in terms of μ,

$$\alpha = e^{i\mu(l-k)L/N},$$

we find that

$$\alpha\frac{d}{d\alpha} = \frac{N}{i(l-k)L}\frac{d}{d\mu}. \tag{77}$$

Substituting equations (73) and (74) into equation(76) and using relation (77), we find that

$$\begin{aligned}(D_2)_{lk} &= -\frac{\mu^2}{N}\frac{N}{i(l-k)L}\frac{d}{d\mu}\left[-i\frac{N}{\mu}(D_1)_{lk}\right]\\ &= -\frac{\mu^2}{N}\frac{N}{i(l-k)L}\frac{d}{d\mu}\left[-i\frac{N}{\mu}(-1)^{l-k}\,\frac{\mu}{2}\,\cot\frac{\mu}{2}(x_l-x_k)\right]\\ &= (-1)^{l-k}\,\frac{N\mu^2}{2(l-k)L}\left[-\csc^2\frac{\mu}{2}(x_l-x_k)\right]\frac{(x_l-x_k)}{2}\\ &= (-1)^{l-k+1}\,\frac{\mu^2}{4}\csc^2\frac{\mu}{2}(x_l-x_k).\end{aligned}$$

In summary, the spectral approximation to the second partial derivative with respect to x is given by the matrix $\boldsymbol{D_2}$

$$(D_2)_{lk} = \begin{cases} (-1)^{l-k+1} \frac{\mu^2}{4} \csc^2 \frac{\mu}{2}(x_l - x_k) & \text{if } l \neq k, \\ -\frac{\mu^2(N^2+2)}{12} & \text{if } l = k. \end{cases} \tag{78}$$

Notice that $\boldsymbol{D_2} \neq \boldsymbol{D_1}^2$. Therefore, u_{xx} is given by

$$u_{xx} = \boldsymbol{D_2} u. \tag{79}$$

The spectral multi-symplectic discretization

Now it is straightforward to prove that a discretization based on the discrete Fourier transform is multi-symplectic. Using the discretization (75) for the x-derivative, the multi-symplectic equation (65) becomes

$$\boldsymbol{M} z_t + \boldsymbol{K}\boldsymbol{D_1} z = \nabla_z S(z).$$

The associated variational system of equations is

$$\boldsymbol{M} dz_t + \boldsymbol{K}\boldsymbol{D_1} dz = \boldsymbol{S_{zz}}(z)\, dz.$$

Then, taking the wedge product with dz and using the fact that

$$dz \wedge \boldsymbol{S_{zz}}(z)\, dz = \boldsymbol{S_{zz}}(z)\, dz \wedge dz = 0,$$

we obtain

$$\begin{aligned} 0 &= dz \wedge \boldsymbol{M} dz_t + dz \wedge \boldsymbol{K}\boldsymbol{D_1} dz \\ &= (dz \wedge \boldsymbol{M} dz)_t - dz_t \wedge \boldsymbol{M} dz - \boldsymbol{K} dz \wedge \boldsymbol{D_1} dz \\ &= (dz \wedge \boldsymbol{M} dz)_t + \boldsymbol{M} dz_t \wedge dz - \boldsymbol{K} dz \wedge \boldsymbol{D_1} dz \\ &= (dz \wedge \boldsymbol{M} dz)_t - dz \wedge \boldsymbol{M} dz_t - \boldsymbol{K} dz \wedge \boldsymbol{D_1} dz \\ &= (dz \wedge \boldsymbol{M} dz)_t + dz \wedge \boldsymbol{K}\boldsymbol{D_1} dz + \boldsymbol{D_1} dz \wedge \boldsymbol{K} dz \end{aligned}$$

or

$$(dz \wedge \boldsymbol{M} dz)_t + \boldsymbol{D_1} dz \wedge \boldsymbol{K} dz + dz \wedge \boldsymbol{K}\boldsymbol{D_1} dz = 0. \tag{80}$$

This is a spectral discretization of the multi-symplectic conservation law (15)

$$(dz \wedge \boldsymbol{M} dz)_t + (dz \wedge \boldsymbol{K} dz)_x = (dz \wedge \boldsymbol{M} dz)_t + dz_x \wedge \boldsymbol{K} + dz \wedge \boldsymbol{K} dz_x = 0.$$

This shows that the discrete Fourier transform preserves the multi-symplectic structure, i.e., the spectral discretization is multi-symplectic.

Conservation of total symplecticity

A different way to express the multi-symplectic conservation law (80) is as follows. We can think that in Fourier space there exists a family of discrete multi-symplectic conservation laws. Let ω_l and κ_{lk} be the 2-forms, defined by

$$\omega_l = \frac{1}{2}\, dz_l \wedge \boldsymbol{M} dz_l \qquad \text{and} \qquad \kappa_{lk} = \frac{1}{2}\,(dz_l \wedge \boldsymbol{K} dz_k + dz_k \wedge \boldsymbol{K} dz_l).$$

Then, in terms of ω_l and κ_{lk}, one finds that the discrete conservation law of symplecticity is given by

$$\partial_t \omega_l + \sum_{k=0}^{N-1} (D_1)_{lk} \kappa_{lk} = 0,$$

where

$$\boldsymbol{D_1} = \boldsymbol{F}^{-1} \bar{\Theta} \boldsymbol{F}$$

is the spectral differentiation matrix.

We arrive at the following remarkable result. Since $(D_1)_{lk} = -(D_1)_{kl}$ and $\kappa_{lk} = \kappa_{kl}$, summing over the spatial index, we obtain

$$\partial_t \sum_{l=0}^{N-1} \omega_l = 0.$$

This implies that in addition to conservation of local symplecticity, we also have conservation of *total* symplecticity in time. This observation helps to explain the remarkable performance of the multi-symplectic spectral discretizations in the numerical experiments.

V.3 EXAMPLE: THE NONLINEAR SCHRÖDINGER EQUATION

The multi-symplectic spectral discretization

As before we consider the focusing one dimensional nonlinear Schrödinger (NLS) equation,

$$iu_t + u_{xx} + 2|u|^2 u = 0. \tag{81}$$

The NLS equation can be written in multi-symplectic form by letting $u = p + iq$ and introducing the new variables $v = p_x$, $w = q_x$. Separating (81) into real and imaginary parts, we get the system

$$q_t - v_x \;=\; 2\left(p^2 + q^2\right) p$$

$$\begin{aligned} -p_t - w_x &= 2\left(p^2+q^2\right)q \\ p_x &= v \\ q_x &= w. \end{aligned} \tag{82}$$

Applying the truncated discrete Fourier transform yields the system

$$\begin{aligned} \partial_t Q_k - \bar{\theta}_k V_k &= \partial_{P_k}\bar{S}(U) \\ -\partial_t P_k - \bar{\theta}_k W_k &= \partial_{Q_k}\bar{S}(U) \\ \bar{\theta}_k P_k &= V_k \\ \bar{\theta}_k Q_k &= W_k, \end{aligned} \tag{83}$$

or in terms of the differentiation matrix

$$\begin{aligned} q_t - \boldsymbol{D_1} v &= 2\left(p^2+q^2\right)p \\ -p_t - \boldsymbol{D_1} w &= 2\left(p^2+q^2\right)q \\ \boldsymbol{D_1} p &= v \\ \boldsymbol{D_1} q &= w. \end{aligned} \tag{84}$$

Associated with it we have the the following discrete ECL

$$E_t + \boldsymbol{D_1} F = 0,$$

where E and F are given by

$$\begin{aligned} E &= \frac{1}{2}\left(\left(p^2+q^2\right)^2 - v^2 - w^2\right), \\ F &= vp_t + wq_t. \end{aligned}$$

We discretize (84) using the symplectic implicit midpoint rule. Let u^0 be the current value and u^1 the new values which is to be found. Then applying the midpoint rule yields

$$\begin{aligned} \frac{q^1-q^0}{\Delta t} - \boldsymbol{D_1} v^{1/2} &= 2\left((p^{1/2})^2 + (q^{1/2})^2\right)p^{1/2} \\ -\frac{p^1-p^0}{\Delta t} - \boldsymbol{D_1} w^{1/2} &= 2\left((p^{1/2})^2 + (q^{1/2})^2\right)q^{1/2} \\ \boldsymbol{D_1} p^{1/2} &= v^{1/2} \\ \boldsymbol{D_1} q^{1/2} &= w^{1/2} \end{aligned} \tag{85}$$

where

$$p^{1/2} = 1/2(p^1 + p^0),$$

etc. This multi-symplectic spectral scheme for the NLS, (85) will be denoted as MS-S in the numerical experiments.

Associated with this discrete system we have the residual ECL, R_i, given by

$$R_i = \frac{E_i^1 - E_i^0}{\Delta t} + \left(\boldsymbol{D}_1 F^{1/2}\right)_i \tag{86}$$

where

$$\begin{aligned} E_i^j &= \frac{1}{2}\left(\left((p_i^j)^2 + (q_i^j)^2\right)^2 - (v_i^j)^2 - (w_i^j)^2\right) \\ F^{1/2} &= v^{1/2}\frac{p^1 - p^0}{\Delta t} + w^{1/2}\frac{q^1 - q^0}{\Delta t}. \end{aligned}$$

We solve (85) with an iteration scheme and substitute the solution into R_i to obtain the residual ECL. The residual ECL, R_i, is monitored in the numerical simulations.

Standard Fourier discretization

By setting $U_k = P_k + iQ_k$, the truncated Fourier system, (83), can be recombined into

$$i\partial_t U_k + \theta_k^2 U_k = -\nabla_{U_k}\bar{S}(U),$$

or using the differentiation matrix for the second derivative (79)

$$iu_t + \boldsymbol{D_2}u = -2|u|^2 u.$$

This recovers the standard Fourier discretization which is relatively easy to implement and adds to the general appeal of MS spectral integrators. The multi-symplectic perspective provides a framework that allows: 1) a local description in space-time through the local conservation laws and 2) a deeper understanding of why MS spectral discretizations (i.e., the spectral discretization implemented with a symplectic integrator in time) more accurately resolve solutions (as we demonstrate in the numerical experiments).

Numerical experiments for the nonlinear Schrödinger equation

In this section we show that within the class of multi-symplectic integrators performance can vary, i.e., we show that the MS-S discretization (85) for the nonlinear Schrödinger equation outperforms the MS-CC discretization (43). As in chapter 3, to test the numerical scheme we consider initial conditions of the form

$$u_0(x) = a(1 + \epsilon \cos \mu x) \tag{87}$$

for both the one ($a = 0.5$, $L = 2\sqrt{2}\pi$) and two ($a = 0.5$, $L = 4\sqrt{2}\pi$) unstable mode regimes.

We begin with initial data (87) for the one unstable mode regime given by the parameters $a = 0.5$, $\epsilon = 0.1$, $\mu = 2\pi/L$, $L = 2\sqrt{2}\pi$. Figure 8(a-b) shows the residual ECL, R, equation (86), using the centered-cell and the spectral discretizations, MS-CC and MS-S, respectively, with $N = 64$, $\Delta t = 2.5 \times 10^{-3}$, $T = 450 - 500$. The errors in the local ECL (86) and in the corresponding global energy obtained using MS-S are found to be several orders of magnitude smaller than the errors obtained with MS-CC. In fact the error in the local ECL is $\mathcal{O}(10^{-6})$ using the MS-CC scheme whereas it is $\mathcal{O}(10^{-10})$ using the MS-S discretization. The oscillations in the error in the global energy are bounded since the multi-symplectic schemes are also globally symplectic in time (as proven in propositions 3 and 4). The surface of the wave profile in the one-mode case obtained with MS-S is essentially identical to the surface obtained with MS-CC (Figure 1) and is not repeated. Similar results are obtained for the errors in the local MCL. However, since the global momentum and norm are quadratic invariants, they are conserved exactly by both schemes (up to the error criterion of 10^{-14} in the implementation of the schemes).

Figure 9 shows the surfaces $|u(x,t)|$ of the waveform obtained using the MS-S and MS-CC discretizations, respectively, for initial data (87) in the two unstable mode regime. The discretization parameters are $N = 64$, $\Delta t = 5 \times 10^{-3}$, $T = 0-50$. Here we are interested in whether the schemes provide the correct qualitative behavior. The MS-S scheme correctly resolves the quasi-periodic motion. However, using the MS-CC integrator, the onset of numerically induced temporal chaos is observed at approximately $t = 25$. In this scenario temporal chaos is characterized by a random switching in time of the location of the spatial excitations in the waveform, see Figure 9 bottom. As mentioned, the correct quasi-periodic motion is captured using the MS-S scheme and switching in the spatial excitations *does*

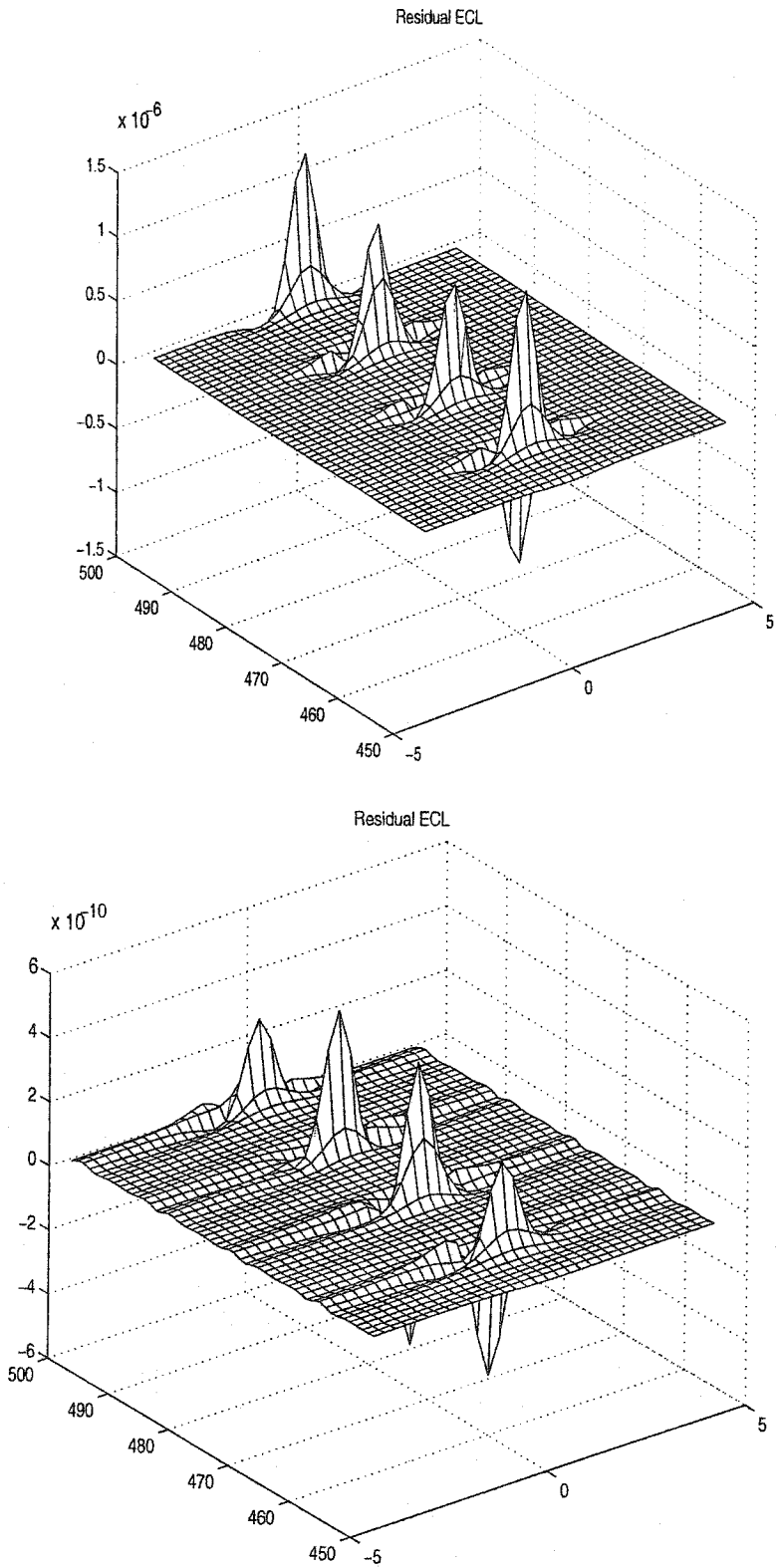

FIG. 8: MS-CC and MS-S local ECL R.

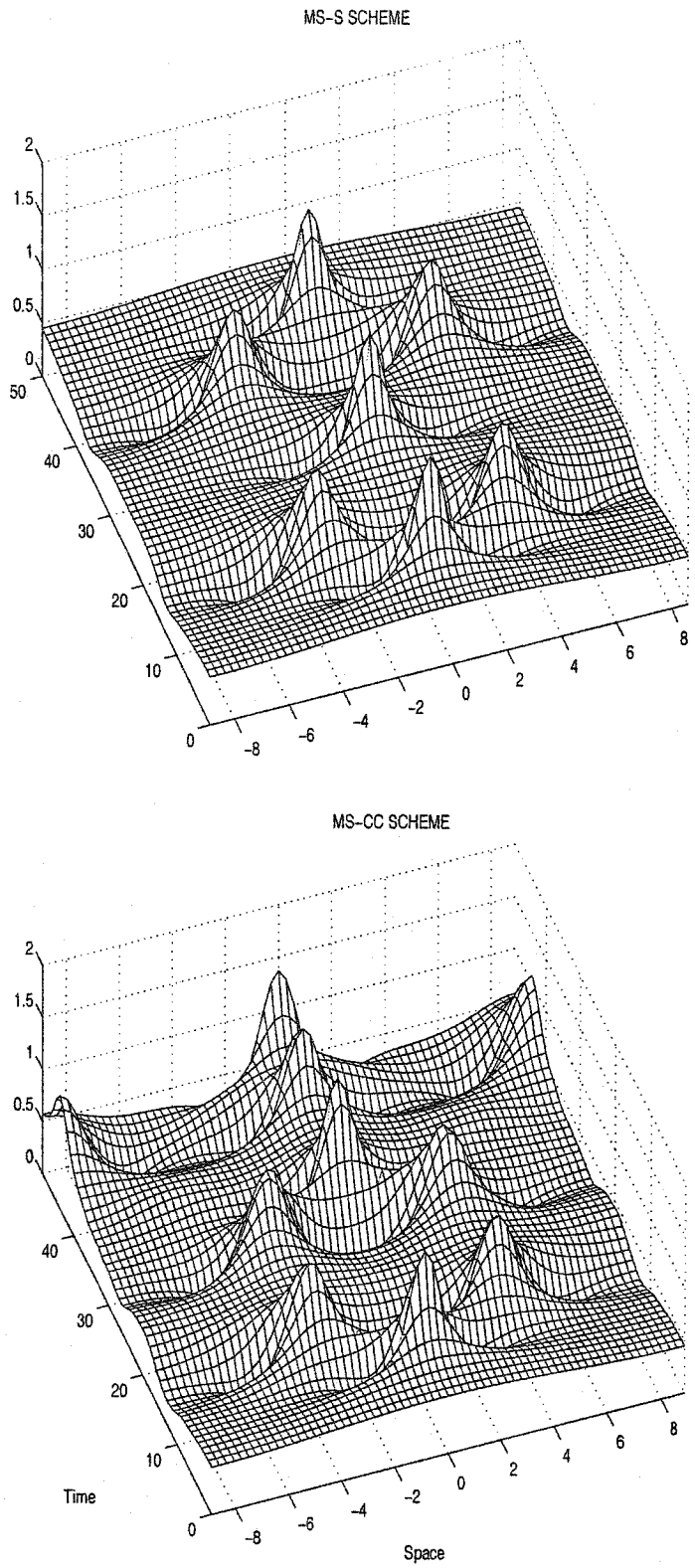

FIG. 9: MS-CC and MS-S two-mode multi-phase surfaces.

not occur for the duration of the simulation, $0 < t < 500$. The global momentum and norm are preserved within roundoff by both schemes. As in the one mode case, the ECL and MCL are preserved several orders of magnitude better by the MS-S scheme.

The local conservation laws appear to provide more insight into the qualitative behavior of the numerical solution than the global invariants. Since a significant improvement in the resolution of the qualitative features of the solution is obtained with the MS-S scheme in 1-D, multi-symplectic spectral schemes should prove to be a valuable tool in integrating multi-dimensional PDEs.

V.4 EXAMPLE: THE SINE-GORDON EQUATION

A multi-symplectic spectral discretization for the sine-Gordon equation

Another example is provided by the sine-Gordon equation which is given by

$$u_{tt} - u_{xx} + \sin u = 0. \tag{88}$$

The SG equation can be cast in multi-symplectic form by introducing the variables $v = u_t$ and $w = u_x$. Then (88) can be written as the system of equations

$$\begin{aligned} -v_t \;+\; w_x &= \sin u \\ u_t \qquad\;\; &= v \\ -\; u_x &= -w. \end{aligned} \tag{89}$$

Using the discrete Fourier transform, system (89) becomes in Fourier space

$$\begin{aligned} -\partial_t V_k \;+\; \bar{\theta}_k W_k &= \boldsymbol{F}_k(\sin u) \\ \partial_t U_k \qquad\;\; &= V_k \\ -\; \bar{\theta}_k U_k &= -W_k, \end{aligned} \tag{90}$$

or in terms of the differentiation matrix $\boldsymbol{D_1}$,

$$\begin{aligned} -v_t \;+\; \boldsymbol{D_1} w &= \sin u \\ u_t \qquad\;\; &= v \\ -\; \boldsymbol{D_1} u &= -w. \end{aligned} \tag{91}$$

Standard Fourier discretization

As with the NLS equation, this system of equations can be recombined into a single equation. In Fourier space we have that (90) becomes

$$\ddot{U}_k = -\theta^2 U_k - (\boldsymbol{F} \sin u)_k \,, \tag{92}$$

where

$$(\boldsymbol{F} \sin u)_k = \frac{1}{N} \sum_{l=0}^{N-1} \sin u_l \, e^{-\theta_k l \Delta x},$$

and the discrete Hamiltonian is given by

$$H = \tfrac{1}{2} \sum_{l=0}^{N-1} \left[|\dot{U}_l|^2 + \mu_l^2 |U_l|^2 \right] - \frac{1}{N} \sum_{l=0}^{N-1} \cos u_l. \tag{93}$$

In physical space equation (92) becomes

$$u_{tt} = -\boldsymbol{D_2} u - \sin u.$$

To discretize (92) in time we note that the Hamiltonian (93) is separable which allows one to use explicit symplectic integrators. A general form of explicit higher order symplectic schemes is given by [60]

$$\begin{aligned} p_{i+1} &= p_i - C_i \, k \, V'(q_i) \\ q_{i+1} &= q_i + D_i \, k \, T'(p_{i+1}), \end{aligned}$$

where $i = 1, \ldots, m$ and the coefficients C_i and D_i are determined in order for the scheme to be symplectic and of $O(k^m)$. Here p_1 and q_1 are the numerical approximation at the time t and p_{m+1} and q_{m+1} are the approximations at the next time level, $t + k$. For example, first order scheme is given by $m = 1$ and

$$C_1 = 1, \;\; D_1 = 1.$$

Similarly a second order scheme is given by $m = 2$ and,

$$C_1 = 0, \;\; C_2 = 1, \;\; D_1 = \tfrac{1}{2} = D_2,$$

etc.

Numerical experiments for the sine-Gordon equation

The multi-symplectic property can be lost in a discretization by using either a non-symplectic discretization in space or in time. Here we compare the loss of multi-symplecticity due to the time discretization. We compare the performance of the spatial spectral discretization implemented with second and fourth order symplectic methods in time (and thus multi-symplectic) with the spatial spectral discretization implemented with non-symplectic Runge-Kutta methods in time of the same order. We are interested in the following questions: i) Does the multi-symplectic integrator preserve the structure of the sine-Gordon phase space appreciably better than the non-symplectic methods? and ii) Does the relative performance of symplectic integrators improve during very long time integrations?

As derived using the inverse scattering theory and discussed in the Appendix, the sine-Gordon equation has an infinite number of local conservation laws and global invariants. In this example, rather than monitor the local energy and momentum conservation laws, we choose to examine the preservation of the nonlinear spectrum (which incorporates all of the global invariants).

Under the sine-Gordon flow, the spectrum remains invariant. However, due to perturbations induced by the numerical discretization, the spectrum evolves in time. We now attempt to answer the above questions by examining the nonlinear spectral of the initial data and monitoring its evolution under the different schemes. The spectral method is exponentially accurate in space which allows for a very accurate initial approximation of the spectral configuration. The evolution of the spectrum under the numerical flow is primarily due to the time integrators.

For the numerical experiments in the unstable regime, the following initial data is used:

$$u(x,0) = \pi + 0.1\cos(\mu x), \quad u_t(x,0) = 0, \tag{94}$$

with parameters $\mu = 2\pi/L$ and $L = 2\sqrt{2}\pi$. This initial data is in the "effectively" chaotic regime as the zeroth double point remains closed, i.e. the initial data is on the level set containing the homoclinic manifold. (Closed double points cannot be preserved by the numerical schemes and in the following experiments one observes that the zeroth mode is immediately split into a gap state by the numerical scheme.)

To interpret the evolution of spectrum plots, recall that under perturbations the complex double points can split in two ways – either into a gap along an arc

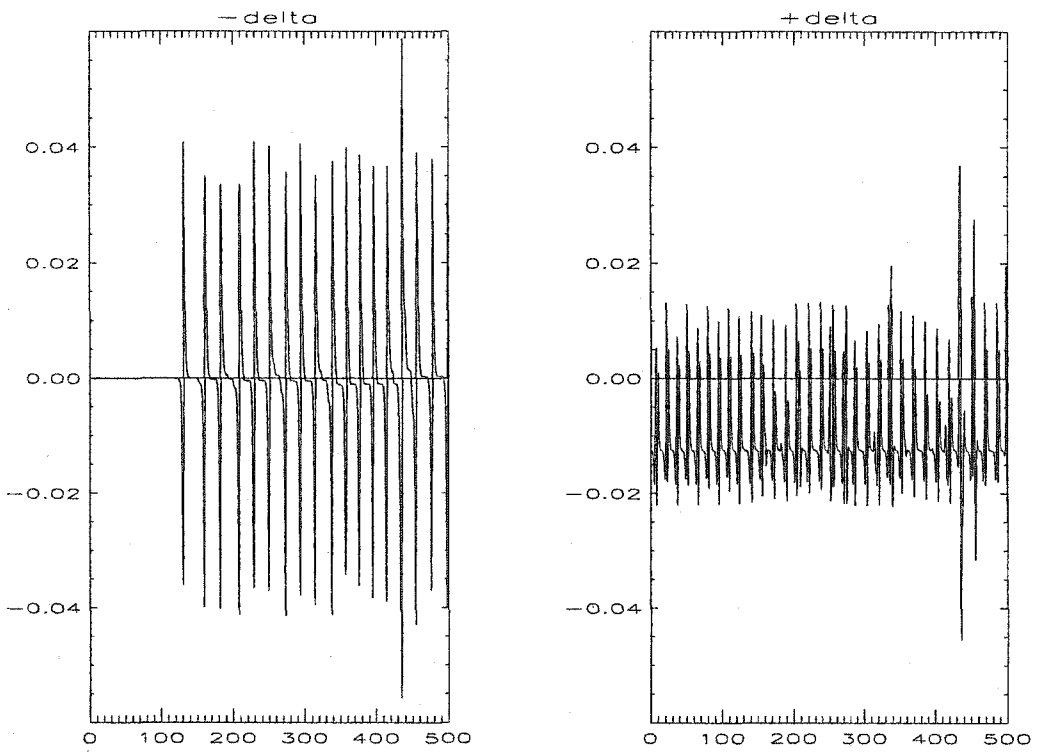

FIG. 10: S-1SY: $u(x,0) = \pi + 0.1\cos\mu x$, $u_t(x,0) = 0$, $N = 32$, $t = 0 - 500$.

of the circle, or into a cross along the radius (cf. Figure 20). For each set of experiments, we show a signed measure of the splitting distance for each complex double point as a function of time. Positive and negative values represent gap and cross states, respectively. When the splitting distance passes through zero, the double points coalesce and homoclinic crossings occur.

We consider the exponentially accurate spectral scheme (91) implemented with non-symplectic Runge-Kutta (2nd and 4th order) and with symplectic (1st, 2nd and 4th order) time-integrators. These integrators will be denoted by S-2RK, S-4RK and S-1SY, S-2SY, S-4SY. In the spectral experiments we use $N = 32$ Fourier modes and a fixed time step $\Delta t = L/512$. For initial data (94), the deviations in the spectrum corresponding to the first two nonlinear modes under the S-1SY, S-2RK, S-2SY, S-4RK, S-4SY flows are given in Figures 10-12.

The splitting distance for both modes obtained with S-1SY (Figure 10) is $O(10^{-2})$. Even with the first order symplectic, *bounded* oscillations are observed. Using S-2RK and S-2SY (Figure 11), the spectrum for the first mode does not

execute any homoclinic crossings for $0 < t < 500$ and so the torus component is accurately preserved. The zeroth mode still displays homoclinic crossings which occur earlier than with the lower order S-1SY. Since the initial data is chosen on the homoclinic manifold, it is to be expected that there will be an earlier onset and higher density of homoclinic crossings when a more accurate scheme is used. Refinement can accentuate the frequency of homoclinic crossings as the numerical trajectory is trapped in a narrower band about the homoclinic manifold.

The main observation is that with the non-symplectic S-2RK there is a $O(10^{-3})$ linear drift in the error in the nonlinear spectrum. The error in the nonlinear spectrum is smaller with S-2SY and further, it doesn't drift. The drift in the nonlinear spectrum obtained with S-2RK can be eliminated on the time-scale $0 < t < 500$ by increasing the accuracy of the integrator and using S-4RK. In this case the nonlinear spectral deviations are $O(10^{-4})$ for S-4RK and S-4SY (Figure 12). There does not seem to be an appreciable difference.

In long time studies of low dimensional Hamiltonian systems, symplectic integrators have been reported as superior in capturing global phase space structures since standard integrators may allow the actions to drift [50]. We continue the integration to $t = 10,000$ and examine the time slice $10,000 \leq t \leq 10,500$. For S-4RK (Figure 13) a drift has occurred. The deviations in the actions associated with the zeroth mode oscillates about 1.2×10^{-4} whereas for S-4SY (Figure 13) it oscillates about 5×10^{-5}. Although the drift observed with non-symplectic schemes can be reduced by using a higher order integrator, it can never be eliminated. This problem is avoided using the multi-symplectic integrator.

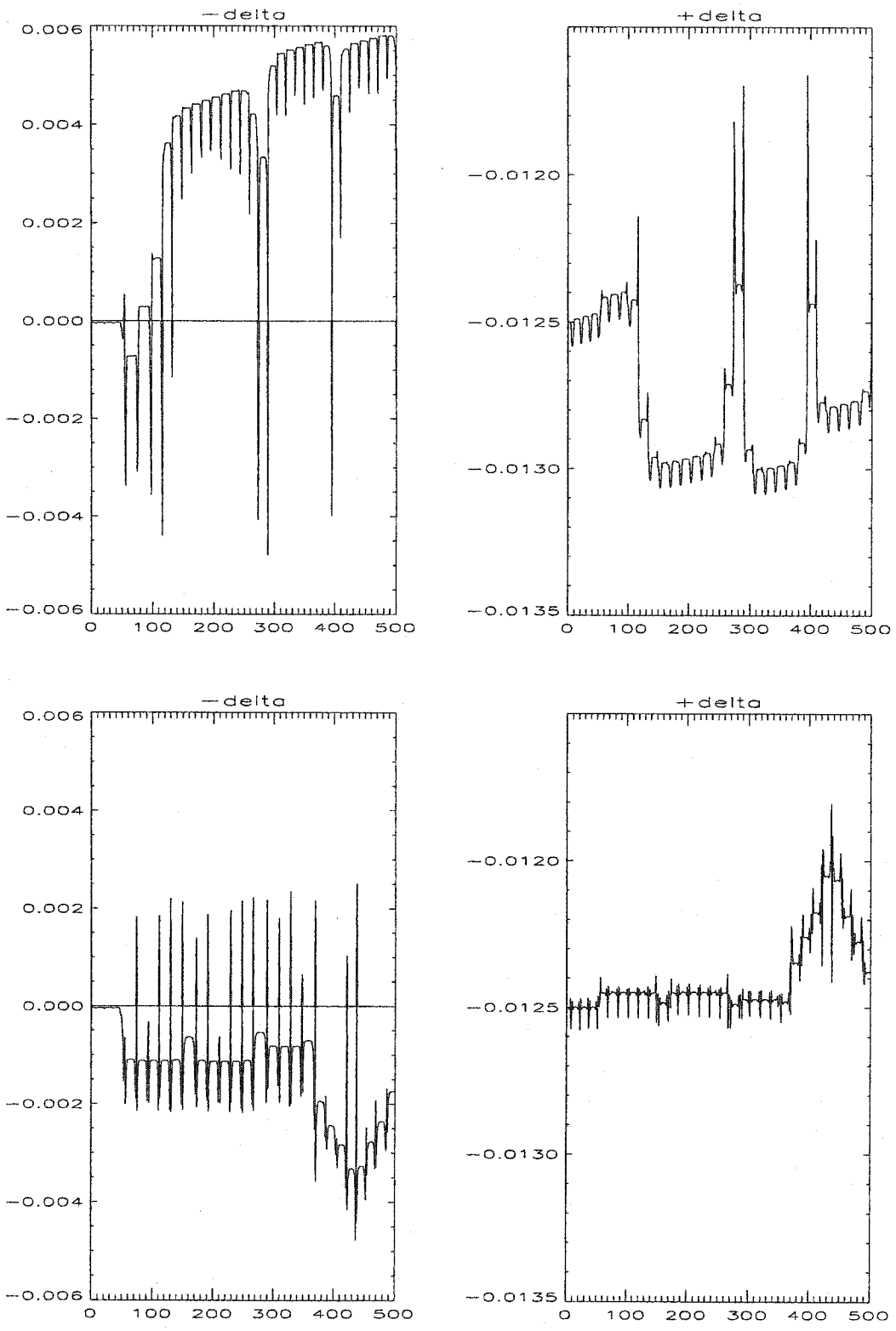

FIG. 11: S-2RK (top) and S-2SY: $t = 0 - 500$.

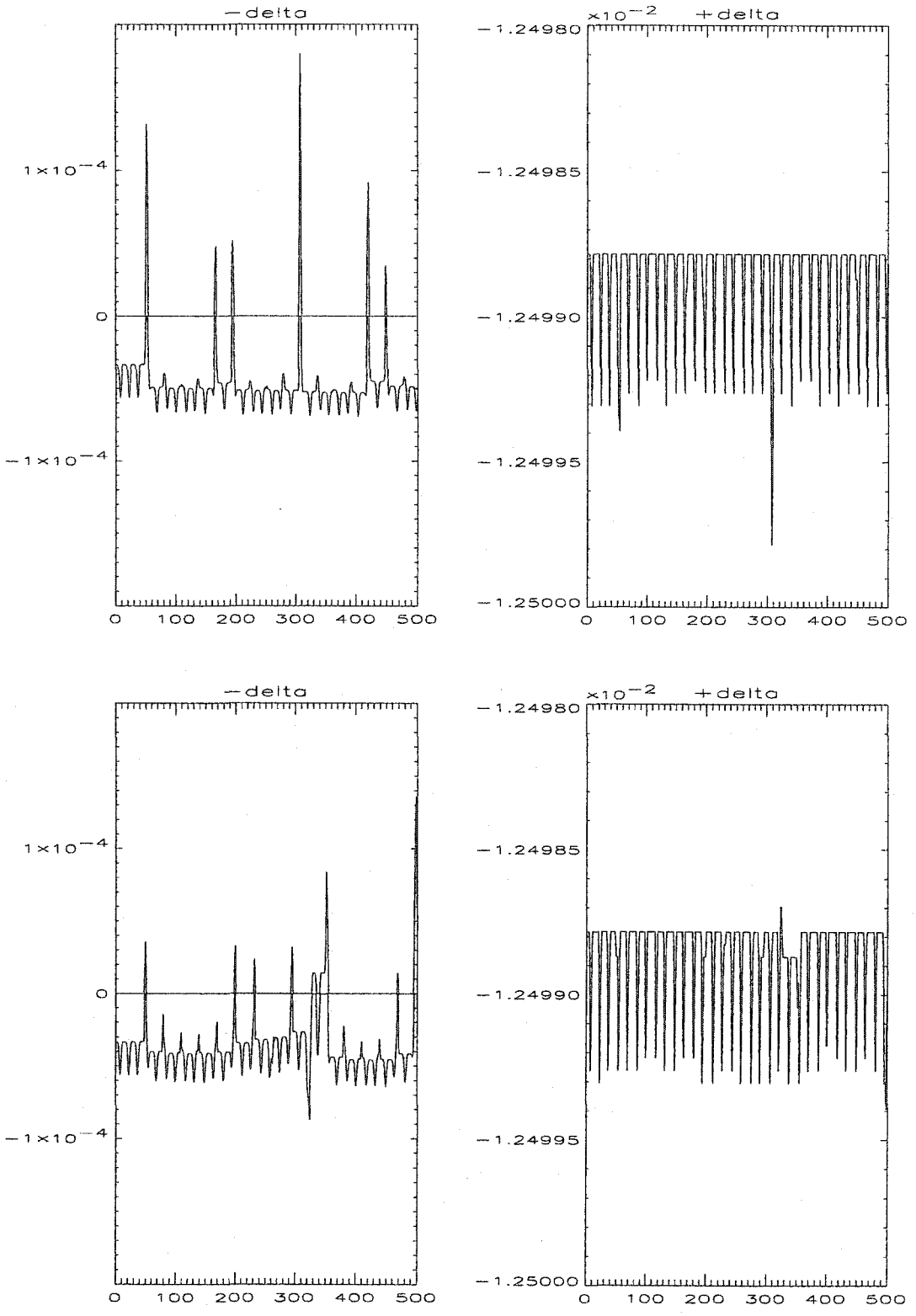

FIG. 12: S-4RK (top) and S-4SY: $t = 0 - 500$.

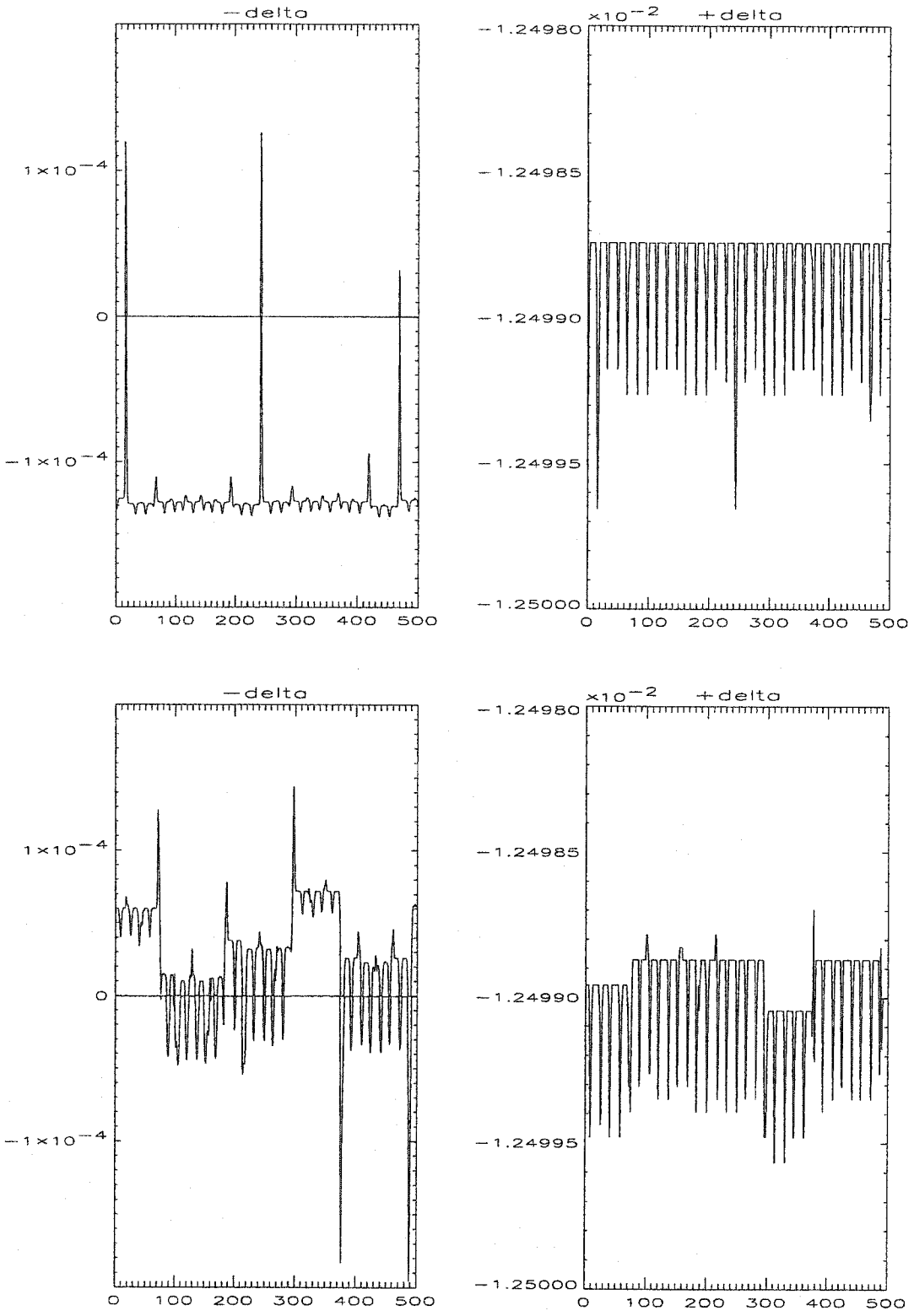

FIG. 13: S-4RK (top) and S-4SY: $t = 10000 - 10500$.

CHAPTER VI

MS INTEGRATORS IN D SPACE DIMENSIONS

The concept of multi-symplecticity can easily be generalized to several space dimensions. A Hamiltonian PDE with D space dimensions is said to be *multi-symplectic* if it can be written as

$$M z_t + \sum_{i=1}^{D} K_i z_{x_i} = \nabla_z S(z) \tag{95}$$

where

$$-\frac{L_i}{2} < x_i < \frac{L_i}{2}, \qquad L_i > 0, \qquad i = 1, \ldots, D,$$

and with periodic boundary conditions in each x_i, $i = 1, \ldots, D$ [13]. Here $M, K_1, \ldots, K_D \in \mathbb{R}^{d \times d}$ are skew-symmetric matrices, $z \in \mathbb{R}^d$, and $S : \mathbb{R}^d \to \mathbb{R}$ is a smooth function of z [13].

System (95) has an associated multi-symplectic conservation law as well as local energy and momentum conservation laws. These are straightforward generalizations of those given before and can be derived as follows. The variational system of equations associated with (95) is given by

$$M dz_t + \sum_{i=1}^{D} K_i dz_{x_i} = S_{zz}(z) dz. \tag{96}$$

Also the $D + 1$ 2-forms

$$\omega = \frac{1}{2} dz \wedge M dz, \qquad \kappa_i = \frac{1}{2} dz \wedge K_i dz, \quad i = 1, \ldots, D$$

determine a multi-symplectic structure associated with time and the D space directions x_i, $i = 1, \ldots, D$, respectively. The multi-symplectic conservation law can be obtained as before by taking the exterior product of (96) with dz and simplifying. This gives

$$\partial_t \omega + \sum_{i=1}^{D} \partial_{x_i} \kappa_i = 0.$$

The generalization of the local energy and momentum conservation laws is also easily obtained. For example, when the Hamiltonian $S(z)$ is independent of t, the PDE has a local energy conservation law (LECL)

$$\frac{\partial E}{\partial t} + \sum_{i=1}^{D} \frac{\partial F_i}{\partial x_i} = 0, \quad E = S(z) - \frac{1}{2} z^T \sum_{i=1}^{D} K_i z_{x_i}, \quad F_i = \frac{1}{2} z^T K_i z_t,$$

while when $S(z)$ is independent of x_i, $i = 1, \ldots, D$, the PDE has a local momentum conservation law (LMCL)

$$\sum_{i=1}^{D} \frac{\partial I_i}{\partial t} + \sum_{i=1}^{D} \frac{\partial G}{\partial x_i} = 0, \quad G = S(z) - \frac{1}{2} z^T M \, z_t, \quad I_i = \frac{1}{2} z^T M \, z_{x_i}.$$

When the local conservation laws are integrated we obtain global conservation of the total energy and total momentum.

In this chapter we develop a multi-symplectic spectral integrator for a generalized (variable coefficient) NLS equation in two space dimensions. The NLS equation in two space dimensions with an external potential is used to model the mean-field dynamics of a dilute-gas Bose Einstein condensate (BEC) [19]. In this case the equation is referred to as the Gross-Pitaevskii (GP) equation and, although it has the additional novel feature of variable coefficients, we show in section 1 that it has a multi-symplectic formulation [34]. In section 2 we develop a MS spectral integrator for the GP equation and in section 3 we test the MS integrator on quasi-periodic solutions (in both x and y).

Systems with spatial dimension $D \geq 2$ are particularly important, as they provide an important test for the applicability and scalability of the properties of multi-symplectic integrators. We choose a spectral method since, overall, the MS-S method exhibited improved resolution of complicated phase space structures, local conservation laws and global invariants. We find that the multi-symplectic spectral method scales well to several spatial dimensions and is, in fact, the method of choice for the variable coefficient GP equation.

VI.1 THE GROSS-PITAEVSKII EQUATION

After rescaling the physical variables, the GP equation is given by

$$iu_t = -\frac{1}{2}(u_{xx} + u_{yy}) + \alpha|u|^2 u + V(x,y)u, \tag{97}$$

where $u(x,y,t)$ is the macroscopic wave function of the condensate and $V(x,y)$ is an experimentally generated macroscopic potential. The GP equation has the form of a generalized NLS equation with a variable coefficient. The parameter α determines whether (97) is repulsive ($\alpha = 1$, defocusing nonlinearity), or attractive ($\alpha = -1$, focusing nonlinearity). Although in BEC applications both signs of α

are relevant, here we will concentrate on (97) with repulsive nonlinearity. Numerical experiments with the GP equation are used to provide insight into the BEC stability properties.

As in [19], we consider the family of periodic lattice potentials given by

$$V(x,y) = -\left(A_1 \operatorname{sn}_1^2 + B_1\right)\left(A_2 \operatorname{sn}_2^2 + B_2\right) + \left(m_1 k_1 \operatorname{sn}_1\right)^2 + \left(m_2 k_2 \operatorname{sn}_2\right)^2, \qquad (98)$$

where $\operatorname{sn}_i = \operatorname{sn}(m_i x,\, k_i)$ denotes the Jacobian elliptic sine functions, with elliptic moduli k_i. An important feature of potential (98) is that closed form solutions of (97) exist which can be used for comparative purposes.

The GP equation can be reformulated as a multi-symplectic PDE by letting $u = p + iq$ and $v_1 = p_x$, $v_2 = p_y$, $w_1 = q_x$, $w_2 = q_y$. Then, with the state vector $z = (p, q, v_1, w_1, v_2, w_2)$, the GP equation in two dimensions can be cast into the multi-symplectic form

$$\boldsymbol{M} z_t + \boldsymbol{K_1} z_x + \boldsymbol{K_2} z_y = \nabla_z S(z),$$

where the skew-symmetric matrices are given by

$$\boldsymbol{M} = \begin{pmatrix} 0 & 1 & 0 & 0 & 0 & 0 \\ -1 & 0 & 0 & 0 & 0 & 0 \\ 0 & 0 & 0 & 0 & 0 & 0 \\ 0 & 0 & 0 & 0 & 0 & 0 \\ 0 & 0 & 0 & 0 & 0 & 0 \\ 0 & 0 & 0 & 0 & 0 & 0 \end{pmatrix},$$

$$\boldsymbol{K_1} = \begin{pmatrix} 0 & 0 & -1/2 & 0 & 0 & 0 \\ 0 & 0 & 0 & -1/2 & 0 & 0 \\ 1/2 & 0 & 0 & 0 & 0 & 0 \\ 0 & 1/2 & 0 & 0 & 0 & 0 \\ 0 & 0 & 0 & 0 & 0 & 0 \\ 0 & 0 & 0 & 0 & 0 & 0 \end{pmatrix},$$

$$\boldsymbol{K_2} = \begin{pmatrix} 0 & 0 & 0 & 0 & -1/2 & 0 \\ 0 & 0 & 0 & 0 & 0 & -1/2 \\ 0 & 0 & 0 & 0 & 0 & 0 \\ 0 & 0 & 0 & 0 & 0 & 0 \\ 1/2 & 0 & 0 & 0 & 0 & 0 \\ 0 & 1/2 & 0 & 0 & 0 & 0 \end{pmatrix},$$

and the Hamiltonian $S(z)$ is given by

$$S(z) = -\frac{1}{4}\left[\left(p^2+q^2\right)^2 + 2V\left(p^2+q^2\right) - \left(v_1^2+w_1^2+v_2^2+w_2^2\right)\right].$$

The multi-symplectic law is given by

$$\partial_t \omega + \partial_x \kappa_1 + \partial_y \kappa_2 = 0,$$

with

$$\omega = dp \wedge dq, \quad \kappa_1 = dv_1 \wedge dp + dw_1 \wedge dq, \quad \text{and} \quad \kappa_2 = dv_2 \wedge dp + dw_2 \wedge dq,$$

Similarly, the energy conservation law is given by

$$\frac{\partial E}{\partial t} + \frac{\partial F_1}{\partial x} + \frac{\partial F_2}{\partial y} = 0,$$

with

$$\begin{aligned}
E &= -\frac{1}{4}\left[\left(p^2+q^2\right)^2 + 2V\left(p^2+q^2\right) - \left(p\,v_{1x} + q\,w_{1x} + p\,v_{2y} + q\,w_{2y}\right)\right], \\
F_1 &= -\frac{1}{4}\left(p\,v_{1t} + q\,w_{1t} - p_t\,v_1 - q_t\,w_1\right), \\
F_2 &= -\frac{1}{4}\left(p\,v_{2t} + q\,w_{2t} - p_t\,v_2 - q_t\,w_2\right),
\end{aligned}$$

which can be simplified to

$$\begin{aligned}
\left[\left(p^2+q^2\right)^2 + 2V\left(p^2+q^2\right) + \left(v_1^2+w_1^2+v_2^2+w_2^2\right)\right]_t & \\
-2\left[\left(p_t\,v_1 + q_t\,w_1\right)_x + \left(p_t\,v_2 + q_t\,w_2\right)_y\right] &= 0.
\end{aligned}$$

VI.2 A MULTI-SYMPLECTIC SPECTRAL SCHEME FOR THE GP EQUATION

We consider a spectral discretization of multi-symplectic PDEs in two dimensions with periodic boundary conditions over the domain

$$(x,y) \in \left[-\frac{L}{2}, \frac{L}{2}\right] \times \left[-\frac{L}{2}, \frac{L}{2}\right],$$

for some period L. The transformation of the multi-symplectic PDE (95) into Fourier space follows as in Chapter V.3. Here we present its implementation in two spatial variables.

Let $\Delta x = \Delta y = L/N$ and consider the one-dimensional Fourier transform $\boldsymbol{F} = \mathbb{R}^N \to \mathbb{C}^N$. The discretized state variable over the rectangular mesh is denoted by

$$z_{ij}(t) = z(t, i\Delta x, j\Delta y)$$

and its Fourier coefficients are given by

$$Z_{kl} = \frac{1}{N^2} \sum_{i,j=0}^{N-1} z_{ij}\, e^{-\theta_k i\Delta x}\, e^{-\theta_l j\Delta y}, \quad k, l = 0, 1, \ldots, N-1.$$

Then the multi-symplectic discretized PDE becomes

$$\boldsymbol{M}\partial_t Z_{kl} + \boldsymbol{K_1}\bar{\theta}_k Z_{kl} + \boldsymbol{K_2}\bar{\theta}_l Z_{kl} = \nabla_{Z_{kl}} \bar{S}(Z),$$

where Z is the matrix $\{Z_{kl}\}$ and

$$\bar{S}(Z) = \sum_{i,j=0}^{N-1} S\left(\frac{1}{N^2} \sum_{k,l=0}^{N-1} Z_{kl}\, e^{\theta_k i\Delta x}\, e^{\theta_l j\Delta y}\right).$$

The frequencies θ_k and $\bar{\theta}_k$ are defined as in Chapter V.3, equations (63) and (70).

In physical space this equation becomes

$$i\boldsymbol{u}_t + \tfrac{1}{2}\left(\boldsymbol{D}^2\boldsymbol{u} + \boldsymbol{u}\boldsymbol{D}^2\right) + \boldsymbol{C} = 0, \tag{99}$$

where the matrices $\boldsymbol{u}$ and $\boldsymbol{C}$ are given by

$$\boldsymbol{u} = \{u_{ij}\}, \qquad \boldsymbol{C}_{ij} = -|u_{ij}|^2 u_{ij} - V(x_i, y_j)u_{ij},$$

and $\boldsymbol{D}$ is the differentiation matrix defined in Chapter 5, equation (74).

VI.3 NUMERICAL EXPERIMENTS FOR THE GP EQUATION

We are interested in simulating multi-phase quasi-periodic solutions to the GP equation under periodic boundary conditions (in both x and y). In the following experiments periodic boundary conditions in x and y are imposed and we use a fixed $N \times N$ spatial lattice with $N = 32$. We are interested in determining if the main features of the solution can be recovered with this relatively crude lattice. The time step used throughout is $\Delta t = 2 \times 10^{-3}$. We begin by considering the GP equation (97) with an elliptic function potential (98) that has the following choice

of constants: $k_1 = k_2 = 1/2$, $m_1 = m_2 = 1$, $A_1 = A_2 = -1$, $B_1 = B_2 = -A_1/k_1^2$ and the initial condition

$$u_0(x, y) = \sqrt{B_1}\sqrt{B_2}\,\mathrm{dn}(m_1 x,\, k_1)\,\mathrm{dn}(m_2 x,\, k_2), \tag{100}$$

where $\mathrm{dn}(x, k)$ denotes the third Jacobian elliptic function. This is initial data for a linearly stable stationary solution of the GP equation.

The evolution of the solution obtained using the GP-MS scheme (99) is shown in Figures (14)–(15). The plots are at $t = 0$ and $t = 60$, top and bottom figures respectively. As analytically determined in [19], this solution is stable. In further numerical simulations (not shown) for $0 < t < 1000$, the solution obtained with GP-MS (99) remains stable with no growth in the Fourier modes. The ECL is preserved on the order of 10^{-3} and the error in the global energy oscillates in a bounded fashion as is typical of the behavior of a symplectic integrator.

Next, we examine the solution obtained using the elliptic function potential (98) with the values of the constants now specified to be $k_1 = k_2 = 1/2$, $m_1 = m_2 = 1$, $A_1 = A_2 = 1$, $B_1 = B_2 = -A_1$ and the initial condition

$$u_0(x, y) = \sqrt{B_1}\sqrt{B_2}\,\mathrm{cn}(m_1 x,\, k_1)\mathrm{cn}(m_2 x,\, k_2), \tag{101}$$

where $\mathrm{cn}(x, k)$ denotes the Jacobian elliptic cosine function. Figure (16) shows the surface of the waveform $|u(x, y, t)|$ obtained using the GP-MS scheme (99) at $t = 0$ and $t = 60$, in the same order as before. Figure (17) shows the fourier spectrum. Clearly these figures show that this solution is unstable, as reported in [19]. The onset of the instability occurs between $t = 15$ and $t = 20$ and by $t = 60$ a significant number of additional Fourier modes have become excited. The ECL, as well as the global invariants are well preserved by the GP-MS discretization. Although a coarse lattice has been used, we are able to reproduce the main qualitative features of the solution, which makes multi-symplectic methods to be very promising.

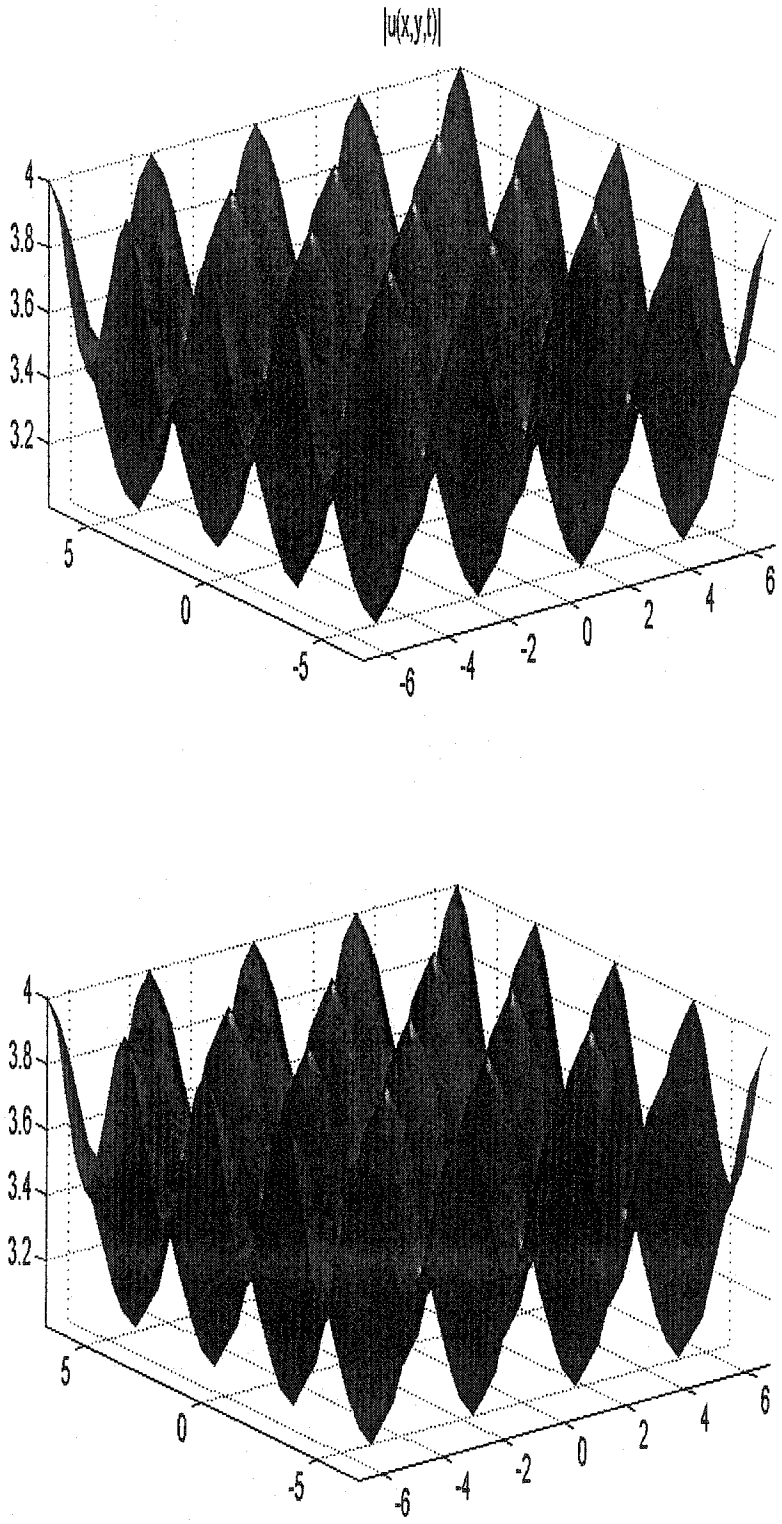

FIG. 14: Surface at $T = 0$ and $T = 60$ for stable IC (100).

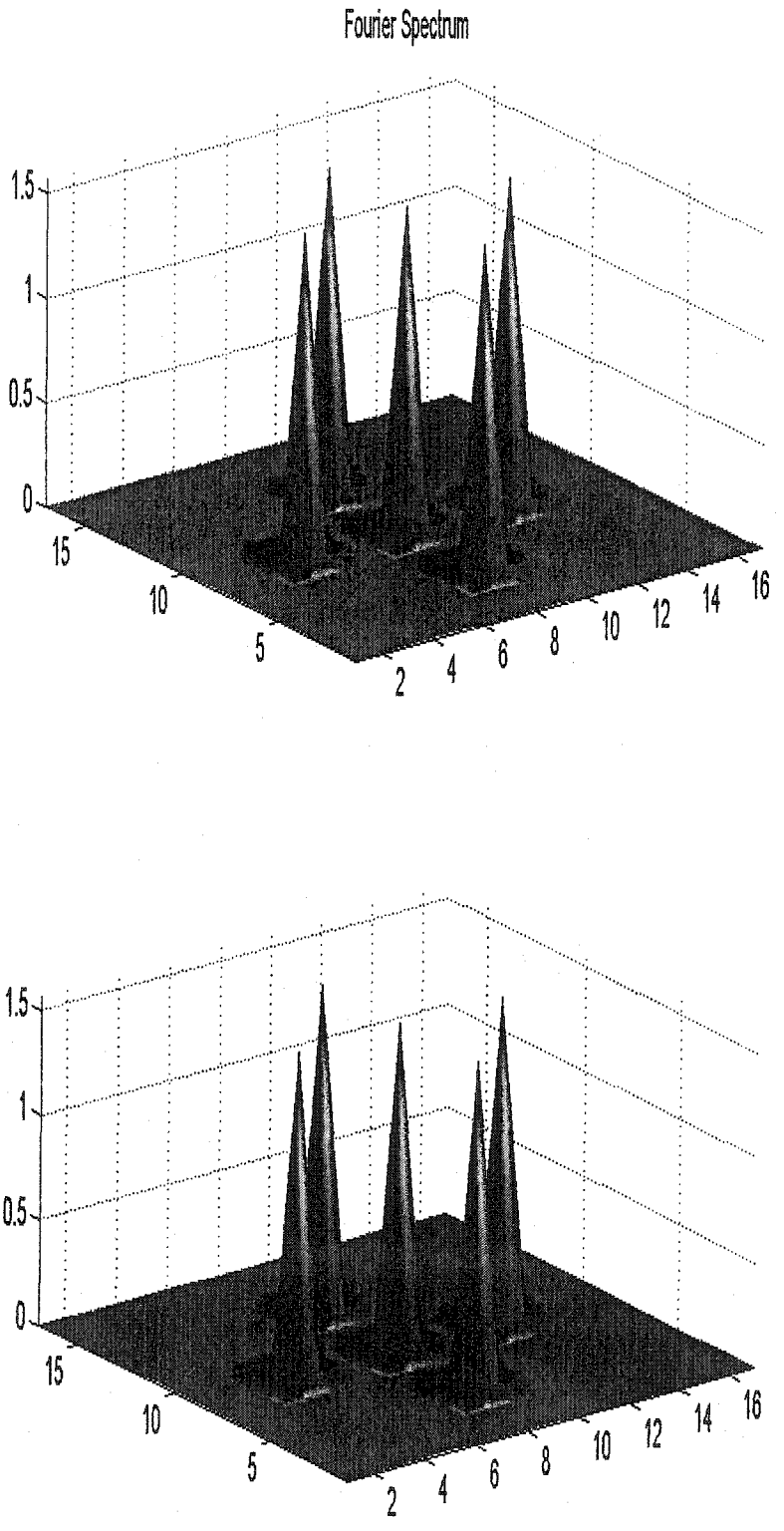

FIG. 15: Spectrum at $T = 0$ and $T = 60$ for stable IC (100).

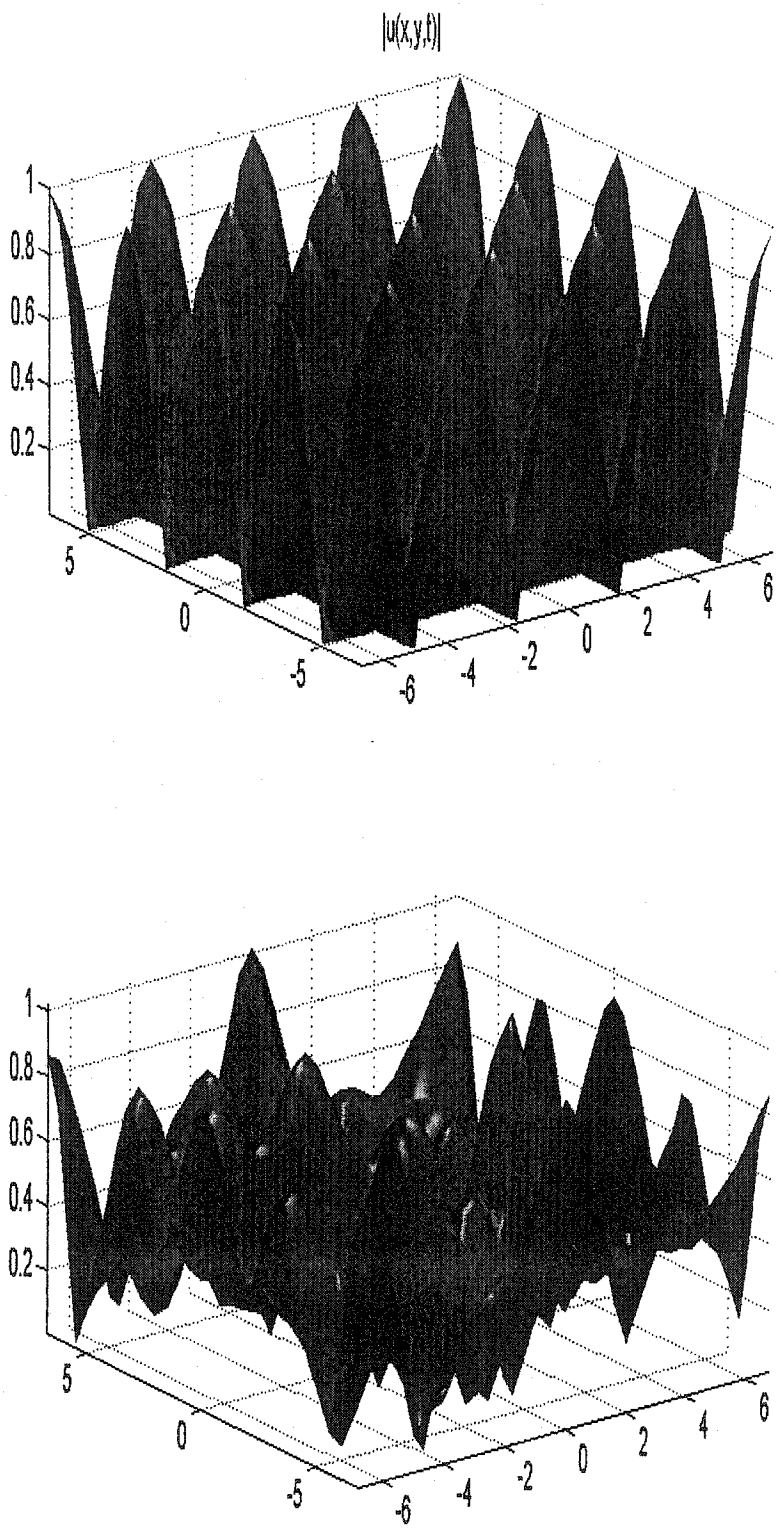

FIG. 16: Surface at $T = 0$ and $T = 60$ for unstable IC (101).

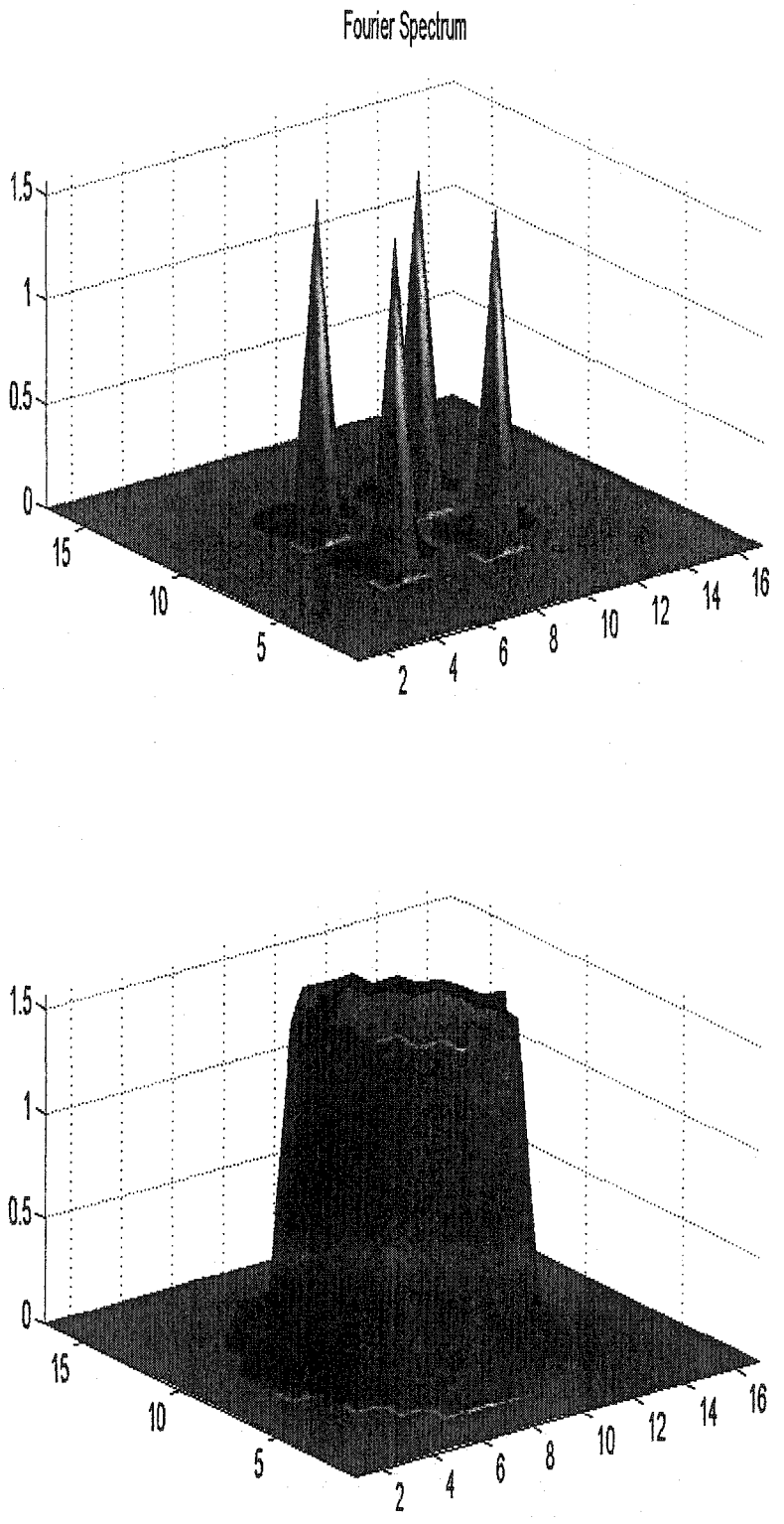

FIG. 17: Spectrum at $T = 0$ and $T = 60$ for unstable IC (101).

CHAPTER VII

CONCLUSIONS

The multi-symplectic formulation of Hamiltonian PDEs is a recent theoretical development which involves a local concept of symplecticity. In this formulation space and time are treated equally which reveals an underlying space-time symplectic structure characterized by a local multi-symplectic conservation law. Multi-symplectic integrators are discretizations of the PDE which preserve exactly a discrete version of the MS conservation law and can be constructed by applying symplectic discretizations both in space and time. An advantage of the new MS formulation is that it provides a systematic approach to handling the spatial discretization, an issue which was not successfully addressed previously. In this thesis we developed two classes of multi-symplectic integrators (finite difference and spectral) for our model equations and investigated their local and global properties.

By applying a pair of s- and r- stage symplectic Runge-Kutta schemes in space and time we derived a new class of MS finite difference discretizations for the NLS equation. We numerically implemented the second-order member of this family of integrators for the NLS equation (the centered-cell discretization) and examined the preservation of the local conservation laws and global invariants. Our numerical experiments demonstrated that multi-symplectic methods have remarkable preservation properties. For instance, we showed that the local and global energy are preserved far better than expected, given the order of the scheme. In addition, other global invariants, the norm and momentum, are preserved within roundoff.

MS integrators have been designed to preserve the MS structure, but not necessarily other quantities such as the local energy and momentum, or the global invariants such as the nonlinear spectrum. The question that arises then is, in practice, to what extent are these other invariants preserved? The numerical experiments on the NLS and SG equations have shown that in addition to preserving the discrete MS conservation law exactly, MS schemes preserve these other invariants very well (although not exactly) over long times. We carried out a backward error analysis of the MS finite difference discretization of the NLS equation and showed that the numerical solution can be interpreted as the exact solution of a

perturbed PDE which is again multi-symplectic. This perturbed MS PDE and it's associated modified conservation laws are approximated by the MS scheme to higher order. Our numerical experiments verified that the modified conservation laws are preserved to higher order by the numerical solution. This helps explain the improved resolution of the local conservation laws observed in the original numerical experiments and provides further justification for applying MS integrators to Hamiltonian PDEs in long time numerical simulations.

The numerical experiments for the NLS equation in the unstable regime demonstrated that MS finite difference schemes can have difficulty in resolving spatial structures in very sensitive regimes. On the other hand, spectral methods have proven to be highly effective methods for solving evolution equations with simple boundary conditions. As the number N of space grid points increases, errors typically decay at an exponential rate rather than at the polynomial rates obtained with finite difference approximations. We proved that spectral discretizations provide another class of multi-symplectic integrators and derived MS spectral discretizations for the NLS and SG equations. For the NLS equation we showed that a significant improvement in the resolution of the qualitative features of the solution is obtained with a MS spectral method. To ensure adequate spatial resolution in sensitive regimes the MS spectral method is the method of choice.

For the Sine-Gordon equation, we addressed the question of how well the phase space geometry of the system is preserved by MS spectral methods. We implemented both MS and nonsymplectic spectral methods and used the associated nonlinear spectrum of the SG equation as a basis for comparing the effectiveness of the integrators. The relevant quantities to monitor are the periodic/antiperiodic eigenvalues of the associated spectral problem. These eigenvalues are the spectral representation of the action variables and are directly related to the geometry of the SG phase space. Significantly, we showed that the MS spectral methods provide an improved resolution of the phase space geometry, as measured by the nonlinear spectrum, when compared with non-symplectic spectral integrators. This is the first examination of the implications, in terms of preservation of the nonlinear spectrum and phase space structure, of preserving the MS structure under discretization. In sum, the benefits of multi-symplectic integrators include improved resolution of the global invariants, local conservation laws as well as complicated phase space structures.

Finally, we showed that the concept of multi-symplecticity can easily be generalized to several space dimensions. We developed a MS formulation for a generalized (variable coefficient) NLS equation in two space dimensions known as the Gross-Pitaevskii (GP) equation. We derived a MS spectral integrator for the GP equation and tested it on both stable and unstable regimes. Again, we find that multi-symplectic spectral discretizations provide very efficient geometric integrators at reasonable computational costs.

Future work includes the development of other classes of MS integrators and of higher order methods, as well as applications to systems of physical interest. We plan to continue numerically investigating the local and global properties of MS discretizations of systems with spatial dimension $D > 2$ as well as establishing error bounds on the approximate preservation of local conservation laws and validity regions for such estimates.

BIBLIOGRAPHY

[1] M. J. Ablowitz, B. M. Herbst and C. M. Schober, On the numerical solution of the sine-Gordon equation I. Integrable discretizations and homoclinic manifolds, *J. Comput. Phys.* **126**, 299 (1996).

[2] M. J. Ablowitz, B. M. Herbst and C. M. Schober, On the numerical solution of the sine-Gordon equation II. Performance of numerical schemes, *J. Comput. Phys.* **131**, 354 (1997).

[3] M. J. Ablowitz, B. M. Herbst and C. M. Schober, Discretizations, integrable systems and computation, *J. Phys. A* **34**, 10671 (2001).

[4] M. J. Ablowitz, D. J. Kaup, A. C. Newell and H. Segur, The inverse scattering transform - Fourier analysis for nonlinear problems, *Stud. Appl. Math.* **53**, 249 (1974).

[5] M. J. Ablowitz and J. F. Ladik, A nonlinear difference scheme and inverse scattering, *Stud. Appl. Math.* **55**, 213 (1976).

[6] M. J. Ablowitz and C. M. Schober, Effective chaos in the nonlinear Schrödinger equation, *Contemp. Math.* **172**, 253 (1994).

[7] M. J. Ablowitz and H. Segur, *Solitons and the inverse scattering transform* (SIAM Studies in Applied Math., SIAM, Philadelphia, 1981).

[8] V. Arnold, *Mathematical methods of classical mechanics* (Springer-Verlag, New York, 1978).

[9] E. D. Belokolos, A. I. Bobenko, V. Z. Enol'skii, A. R. Its, and V. B. Matveev, *Algebro-geometric approach to nonlinear integrable problems* (Springer Series in Nonlinear Dynamics, Springer-Verlag, Berlin, 1994).

[10] G. Benettin and A. Giorgilli, On the Hamiltonian interpolation of near-to-the identity symplectic mappings with application to symplectic integration algorithms, *J. Stat. Phys.* **74**, 1117 (1994).

[11] T. Bridges, Multi-symplectic structures and wave propagation, *Math. Proc. Cambridge Philos. Soc.* **121**, 147 (1997).

[12] T. J. Bridges and S. Reich, Multi-symplectic integrators: numerical schemes for Hamiltonian PDEs that conserve symplecticity, *Phys. Lett. A* **284**, 184 (2001).

[13] T. J. Bridges and S. Reich, Multi-symplectic spectral discretizations for the Zakharov-Kuznetsov and shallow water equations, *Physica D* **152**, 491 (2001).

[14] M. P. Calvo and E. Hairer, Accurate long-time integration of dyamical systems, *Appl. Numer. Math.* **18**, 95 (1995).

[15] M. P. Calvo, A. Murura and J. M. Sanz-Serna, Modified equations for ODEs, *Contemp. Math.* **172**, 63 (1994).

[16] J. Candy and W. Rozmus, A symplectic integration algorithm for separable Hamiltonian functions, *J. Comput. Phys.* **92**, 230 (1991).

[17] P. J. Channell and C. Scovel, Symplectic integration of Hamiltonian systems, *Nonlinearity* **3**, 231 (1990).

[18] P. J. Channell and C. Scovel, Integrators for Lie-Poisson dynamical systems, *Physica D* **50**, 80 (1991).

[19] B. F. Deconinck, B. A. Frigyik, and J. Kutz, Stability of exact solutions of the defocusing nonlinear Schrödinger equation with periodic potential in two dimensions, *Phys. Lett. A* **283**, 177 (2001).

[20] D. B. Duncan, Symplectic finite difference approximations of the nonlinear Klein-Gordon equation, *SIAM J. Numer. Anal.* **34**, 1742 (1997).

[21] K. B. Dysthe, Note on modification to the nonlinear Schrödinger equation for application to deep water waves, *Proc. Roy. Soc. Lond. A* **369**, 105 (1979).

[22] T. Eirola and J. M. Sanz-Serna, Conservation of integrals and symplectic structure of differential equations by multistep methods, *Numer. Math.* **61**, 281 (1992).

[23] N. Ercolani, M. G. Forest and D. W. McLaughlin. Geometry of the modulational instability III: Homoclinic orbits for the periodic sine-Gordon equation, *Physica D* **43**, 349 (1990).

[24] K. Feng, On difference schemes and symplectic geometry, in *Proceedings of the 1984 Beijing Symposium on Differential Geometry and Differential Equations, 42*, edited by K. Feng (Science Press, Beijing, 1985).

[25] K. Feng, Difference schemes for Hamiltonian formalism and symplectic geometry, *J. Comput. Math.* **4**, 279 (1986).

[26] L. D. Faddeev, and L. A. Takhtajan, *Hamiltonian methods in the theory of solitons* (Springer, Berlin, 1987).

[27] B. Fornberg, *A practical guide to pseudospectral methods* (Cambridge University Press 1998).

[28] E. Hairer, Backward error analysis of numerical integrators and symplectic methods, *Annals of Num. Math.* **1**, 107 (1994).

[29] E. Hairer and Ch. Lubich, The lifespan of backward error analysis for numerical integrators, *Numer. Math.* **76**, 441 (1997).

[30] E. Hairer, S. P. Norsett and G. Wanner, *Solving ordinary differential equations I. Non-stiff problems* (Springer-Verlag, Berlin, 1993).

[31] B. M. Herbst, F. Varadi and M. J. Ablowitz, Symplectic methods for the nonlinear Schrödinger equation, *Math. Comput. Sim.* **37**, 353 (1994).

[32] A. Iserles, *Numerical analysis of differential equations* (Cambridge University Press, Cambridge, 1996).

[33] A. L. Islas, D. A. Karpeev and C. M. Schober, Geometric integrators for the nonlinear Schrödinger equation, *J. Comput. Phys.* **173**, 116 (2001).

[34] A. L. Islas and C. M. Schober, Multi-symplectic spectral methods for the Gross-Pitaevski equation, *Lect. Notes Comp. Sci.* **2331**, 486 (2002).

[35] F. M. Lasagni, Canonical Runge-Kutta methods, *J. Appl. Math. Phys.* **39**, 952 (1998).

[36] J. E. Marsden, G. P. Patrick and S. Shkoller, Multisymplectic geometry, variational integrators, and nonlinear PDEs, *Comm. in Math. Phys.* **199**, 351 (1999).

[37] J. E. Marsden and S. Shkoller, Multisymplectic geometry, covariant Hamiltonians and water waves, *Math. Proc. Camb. Phil. Soc.* **125**, 553 (1999).

[38] R. I. McLachlan, Symplectic integration of Hamiltonian wave equations, *Numer. Math.* **66**, 465 (1994).

[39] R. I. McLachlan, On the numerical integration of ordinary differential equations by symmetric composition methods, *SIAM J. Sci. Comput.* **16**, 151 (1995).

[40] K. R. Meyer and G. R. Hall, *Introduction to Hamiltonian dynamical systems and the N-body problem* (Springer-Verlag, New York, 1991).

[41] P. D. Miller, *Macroscopic lattice dynamics* (Ph.D. Thesis, University of Arizona, 1994).

[42] D. Okunbor and R. D. Skeel, An explicit Runga-Kutta-Nyström method is canonical if and only if its adjoint is explicit, *SIAM J. Numer. Anal.* **20**, 521 (1992).

[43] S. Reich, Backward error analysis for numerical integrators, *SIAM J. Numer. Anal.* **36**, 1549 (1997).

[44] S. Reich, Multi-symplectic Runge-Kutta collocation methods for Hamiltonian wave equations, *J. Comput. Phys.* **157**, 473 (2000).

[45] R. D. Ruth, A canonical integration technique, *IEEE Transactions on Nuclear Science* **30**, 2669 (1983).

[46] J. M. Sanz-Serna, An explicit finite difference scheme with exact conservation properties, *J. Comput. Phys.* **47**, 199 (1982).

[47] J. M. Sanz-Serna, Studies in numerical nonlinear instability I. Why do leapfrog schemes go unstable?, *SIAM J. Sci. Stat. Comput.* **6**, 923 (1985).

[48] J. M. Sanz-Serna, Runge-Kutta schemes for Hamiltonian systems, *BIT* **28**, 877 (1988).

[49] J. M. Sanz-Serna, Symplectic integrators for Hamiltonian problems: an overview, *Acta Numérica* **1**, 243 (1992).

[50] J. M. Sanz-Serna, and M. Calvo, *Numerical Hamiltonian problems* (Chapman and Hall, London 1994).

[51] C. M. Schober, Symplectic integrators for the Ablowitz-Ladik discrete nonlinear Schrödinger equation, *Phys. Lett. A* **259**, 140 (1999).

[52] M. Schreiber, *Differential forms: A heuristic introduction* (Springer-Verlag, New York 1977).

[53] C. Scovel, Symplectic numerical integration of Hamiltonian systems, in *The geometry of Hamiltonian systems, 463* (Springer, 1989).

[54] R. D. Skeel, Variable step size destabilizes the Störmer-Leapfrog-Verlet method, *BIT* **33**, 172 (1992).

[55] R. D. Skeel, G. Zhang and T. Schlick, A family of symplectic integrators: stability, accuracy and molecular dynamics applications, *SIAM J. Sci. Comp.* **18**, 203 (1997).

[56] A. M. Stuart and A. R. Humphries, *Dynamical systems and numerical analysis* (Camb. Monographs in Appl. and Comp. Math. No. 2, Cambridge University Press, Cambridge, 1996).

[57] Y. B. Suris, On the preservation of the symplectic structure in the course of numerical integration of Hamiltonian systems, in *Numerical solutions of ODEs, 148*, edited by S. S. Filippov (USSR Academy of Sciences, Moscow 1988).

[58] Y. F. Tang, V. M. Pérez-García and L. Vázquez, Symplectic methods for the Ablowitz-Ladik model, *Appl. Math. Comput.* **82**, 17 (1997).

[59] H. Yoshida, Recent progress in the theory and application of symplectic integrators, *Cel. Mech. Dyn. Astr.* **56**, 27 (1993).

[60] H. Yoshida, Construction of higher order symplectic integrators, *Phys. Lett. A* **150**, 262 (1990).

[61] V. E. Zakharov and A. B. Shabat, Exact theory of two-dimensional self-focusing and one-dimensional self-modulation of waves in nonlinear media, *Soviet Phys. JETP* **34**, 62 (1972).

[62] G. Zhong and J. E. Marsden, Lie-Poisson Hamilton-Jacobi theory and Lie-Poisson integrators, *Phys. Lett. A* **133**, 134 (1998).

APPENDIX A

BACKGROUND: THE AKNS EQUATIONS

In this appendix we explain the context in which our benchmark equations, the nonlinear Schrödinger (NLS), sine-Gordon (SG) and complex modified Korteweg-de-Vries (CMKDV) equations are related. The NLS, SG and CMKDV equations can be derived from first principles in many branches of physics and have myriad applications (e.g., for applications in plasma physics, water waves, optics, see [7, 26]). Even so, we show how these nonlinear wave equations can all be obtained from an eigenvalue problem introduced by Ablowitz, Kaup, Newel and Segur (AKNS) (1974) [4] as a generalization of a scattering problem of Zakharov and Shabat (1972) [61].

We briefly review some of the common properties of the AKNS hierarchy equations. We focus on those elements of the integrable theory which are relevant for interpreting the ability of the symplectic and multi-symplectic numerical schemes that we develop to preserve phase space structures. In the first section we show how to obtain the global invariants and local conservation laws using the inverse scattering theory. In the second section we present rudiments of the nonlinear spectral theory. Thorough treatments of integrable equations and the inverse scattering theory are provided in [7, 26] and of the inverse spectral theory in [9, 23].

A.1 DERIVATION OF THE NLS, CMKDV AND SG EQUATIONS

The AKNS linear eigenvalue problem is given by

$$\begin{cases} V_{1x} + i\zeta V_1 = \quad qV_2, \\ V_{2x} - i\zeta V_1 = \quad -q^* V_1, \end{cases} \tag{102}$$

where the most general linear time dependence of these functions is
where the most general linear time dependence of these functions is

$$\begin{cases} V_{1t} = AV_1 + BV_2, \\ V_{2t} = CV_1 + DV_2. \end{cases} \tag{103}$$

Here A, B, C and D are scalar functions of x and t [7]. These two systems of equations are known as a *Lax pair*, and can be written in the form

$$\begin{cases} \mathcal{L}V = \quad \zeta V, \\ V_t = \quad \mathcal{M}V, \end{cases}$$

where

$$\mathcal{L} = i \begin{pmatrix} -\frac{\partial}{\partial x} & q \\ r & \frac{\partial}{\partial x} \end{pmatrix},$$

and

$$\mathcal{M} = i \begin{pmatrix} A & B \\ C & D \end{pmatrix},$$

and

$$V = \begin{pmatrix} V_1 \\ V_2 \end{pmatrix}.$$

The compatibility of (102) and (103) requires that

$$V_{xt} = V_{tx}, \tag{104}$$

which implies that

$$\mathcal{L}_t + [\mathcal{L}, \mathcal{M}] = 0.$$

This imposes the following conditions on A, B, C, D:

$$\begin{aligned} A_x &= qC - rB, \\ B_x + 2i\zeta B &= q_t - (A - D)q, \\ C_x - 2i\zeta C &= r_t + (A - D)r, \\ -D_x &= qC - rB. \end{aligned}$$

Without loss of generality we can take $D = -A$. Then the compatibility condition requires

$$\begin{aligned} A_x &= qC - rB, \\ B_x + 2i\zeta B &= q_t - 2Aq, \\ C_x - 2i\zeta C &= r_t + 2Ar. \end{aligned} \tag{105}$$

To solve these equations we assume polynomial expansions in ζ for A, B and C. This can be done up to any power of ζ, and this generates the different evolution equations which form the AKNS hierarchy. For example, to obtain the NLS equation, to second order, let

$$\begin{aligned} A &= A_0 + A_1\zeta + A_2\zeta^2, \\ B &= B_0 + B_1\zeta + B_2\zeta^2, \\ C &= C_0 + C_1\zeta + C_2\zeta^2. \end{aligned} \tag{106}$$

Then by substituting (106) into (105) and equating powers of ζ, beginning with the highest power, it is found that

$$\begin{aligned} B_2 &= C_2 = 0, \\ A_1 &= a_1 = \text{constant}, \\ A_2 &= a_2 = \text{constant}, \\ B_1 &= ia_2 q, \\ C_1 &= ia_2 \gamma. \end{aligned}$$

Taking $a_1 = 0$ gives

$$\begin{aligned} A_0 &= -\frac{a_2}{2} qr + a_0, \\ B_0 &= -\frac{a_2}{2} q_x, \\ C_0 &= -\frac{a_2}{2} r_x, \end{aligned}$$

where a_0 and a_2 are arbitrary constants. For simplicity, let $a_0 = 0$. Then, the ζ^0 equation gives the evolution equations

$$\begin{aligned} -\frac{1}{2} a_2 q_{xx} &= q_t - a_2 q^2 r, \\ \frac{1}{2} a_2 r_{xx} &= r_t - a_2 q r^2. \end{aligned}$$

If we let

$$a_2 = 2i, \qquad r = \mp q^*,$$

we derive the nonlinear Schrödinger equation,

$$iq_t = q_{xx} \pm 2|q|^2 q.$$

Physically, the $\pm 2|q|^2 q$ term corresponds to a focusing/defocusing nonlinearity [7].

To obtain the CMKdV equation one expands in ζ up to order 3:

$$\begin{aligned} A &= A_0 + A_1 \zeta + A_2 \zeta^2 + A_3 \zeta^3, \\ B &= B_0 + B_1 \zeta + B_2 \zeta^2 + B_3 \zeta^3, \\ C &= C_0 + C_1 \zeta + C_2 \zeta^2 + C_3 \zeta^3. \end{aligned}$$

Substituting these expansions into (105) and equating powers of ζ, we then find

$$\begin{aligned} A &= a_3 \zeta^3 + a_2 \zeta^2 + \frac{1}{2} (a_3 qr + a_1) \zeta + \frac{1}{2} a_2 qr - \frac{i}{4} a_3 (qr_x - q_x r) + a_0, \\ B &= ia_3 q \zeta^2 + \left(ia_2 q - \frac{1}{2} a_3 q_x \right) \zeta + \left(ia_1 q + \frac{i}{2} a_3 q^2 r - \frac{1}{2} a_2 q_x - \frac{i}{4} a_3 q_{xx} \right), \\ C &= ia_3 r \zeta^2 + \left(ia_2 r - \frac{1}{2} a_3 r_x \right) \zeta + \left(ia_1 r + \frac{i}{2} a_3 q r^2 - \frac{1}{2} a_2 r_x - \frac{i}{4} a_3 r_{xx} \right), \end{aligned}$$

which correspond to the two evolution equations

$$\begin{aligned} q_t + i\frac{1}{4}a_3\left(q_{xxx} - 6qrq_x\right) + \frac{1}{2}a_2\left(q_{xx} - 2q^2r\right) - ia_1q_x - 2a_0q &= 0, \\ r_t + i\frac{1}{4}a_3\left(r_{xxx} - 6qrr_x\right) - \frac{1}{2}a_2\left(r_{xx} - 2q^2r\right) - ia_1r_x - 2a_0r &= 0, \end{aligned}$$

where a_0, a_1, a_2 and a_3 are arbitrary constants. Letting

$$a_0 = a_1 = a_2 = 0, \quad a_3 = -4i, \quad r = -1,$$

one obtains the KdV equation

$$q_t \pm 6qq_x + q_{xxx} = 0,$$

while taking

$$a_0 = a_1 = a_2 = 0, \quad a_3 = -4i, \quad r = \mp q,$$

one obtains the CMKdV equation

$$q_t \pm 6|q|^2q_x + q_{xxx} = 0.$$

Note that if we take

$$a_0 = a_1 = a_3 = 0, \quad a_2 = -2i, \quad r = \mp q,$$

we obtain the NLS equation again.

In the same way that evolution equations are found corresponding to the expansions of A, B, C in positive powers of ζ, it is also possible to find equations corresponding to expansions in inverse powers of ζ (or both). For example, taking

$$A = \frac{a(x,t)}{\zeta}, \quad B = \frac{b(x,t)}{\zeta}, \quad C = \frac{c(x,t)}{\zeta}$$

yields

$$a_x = \frac{1}{2}(qr)_t, \quad q_{xt} = -4iaq, \quad r_{xt} = -4iar.$$

A special case is

$$a = \left(\frac{i}{4}\right)\cos u, \quad b = c = \left(\frac{i}{4}\right)\sin u, \quad q = -r = -\frac{u_x}{2},$$

which produces the sine-Gordon equation

$$u_{xt} = \sin u.$$

Transforming the underlying coordinate system, the sine-Gordon can also be written as

$$u_{tt} - u_{xx} + \sin u = 0.$$

The above equations are only a few of the evolution equations obtainable by this expansion procedure.

Some common properties of the AKNS hierarchy equations

All the equations in this hierarchy have an infinite number of conserved quantities and are therefore integrable. It is important to keep this in mind when one looks for discretizations which reflect the properties of the continuous problems. To obtain the conservation laws for these equations on the infinite line we start with the eigenvalue system of equations (102). Define two pairs of linearly independent eigenfunctions ϕ, $\bar{\phi}$ and ψ, $\bar{\psi}$ with the following boundary conditions ($\zeta = \xi + i\eta$)

$$\begin{aligned}
\phi &\approx \begin{pmatrix} 1 \\ 0 \end{pmatrix} e^{-i\xi x} \quad \text{as } x \to -\infty, \\
\bar{\phi} &\approx \begin{pmatrix} 0 \\ -1 \end{pmatrix} e^{i\xi x} \quad \text{as } x \to -\infty, \\
\psi &\approx \begin{pmatrix} 0 \\ 1 \end{pmatrix} e^{i\xi x} \quad \text{as } x \to +\infty, \\
\bar{\psi} &\approx \begin{pmatrix} 1 \\ 0 \end{pmatrix} e^{-i\xi x} \quad \text{as } x \to +\infty.
\end{aligned}$$

By linear independence

$$\phi = a(\zeta)\bar{\psi} + b(\zeta)\psi.$$

Then if

$$\phi = \begin{pmatrix} \phi_1 \\ \phi_2 \end{pmatrix},$$

the boundary conditions imply

$$\phi_1 \to a(\zeta)e^{-i\xi x} \quad \text{as } x \to +\infty,$$

and thus

$$a(\zeta) = \lim_{x\to\infty} \phi_1 e^{i\zeta x}.$$

Let ϕ_1 and ϕ_2 be solutions of the eigenvalue problem (102). Then we can solve for ϕ_2 in terms of ϕ_1 to obtain the following equation for ϕ_1:

$$\phi_{1xx} = \phi_1 \left(qr - \zeta^2\right) + \frac{q_x}{q}\left(\phi_{1x} + i\zeta\phi_1\right).$$

To solve this equation let

$$\phi_1 = e^{-i\zeta x + \alpha}. \tag{107}$$

Then α satisfies the equation

$$\alpha_{xx} - 2i\zeta\alpha_x + \alpha_x^2 = qr + \frac{q_x}{q}\alpha_x.$$

Letting

$$\mu = \alpha_x, \tag{108}$$

μ satisfies the Riccati equation

$$2i\zeta\mu = \mu^2 - qr + q\left(\frac{\mu}{q}\right).$$

To find the solution to this equation, let

$$\mu = \sum_{n=0}^{\infty} \frac{\mu_n}{(2i\zeta)^{n+1}}.$$

By equating the coefficients of $(2i\zeta)^{-1}$ one obtains a recursion relation for μ_n:

$$\mu_0 = -qr, \quad \mu_1 = -qr_x, \quad \mu_{n+1} = q\left(\frac{\mu_n}{q}\right)_x + \sum_{k=0}^{n-1} \mu_k\mu_{n-k-1}, \quad n \geq 1 \tag{109}$$

Now let us return to the beginning and note that

$$a(\zeta) = \lim_{x\to\infty} \phi_1 e^{i\xi x} = \lim_{x\to\infty} e^{\alpha},$$

or

$$\log a(\zeta) = \lim_{x\to\infty} \alpha.$$

That is,

$$\log a(\zeta) = \alpha(x = +\infty).$$

Since

$$\alpha_x = \mu = \sum_{n=0}^{\infty} \frac{\mu_n(x,t)}{(2i\zeta)^{n+1}},$$

we then have that

$$\alpha = \sum_{n=0}^{\infty} \frac{1}{(2i\zeta)^{n+1}} \int_{-\infty}^{x} \mu_n(y,t)\, dy.$$

Thus

$$\log a(\zeta) = \alpha(x = +\infty) = \sum_{n=0}^{\infty} \frac{C_n}{(2i\zeta)^{n+1}}$$

where

$$C_n = \int_{-\infty}^{x} \mu_n(y)\, dy.$$

Now, $\log a(\zeta)$ is time independent. Hence C_n is time independent. This provides the global constants of motion. The first few are:

$$\begin{aligned} C_0 &= \int_{-\infty}^{\infty} (-qr)dx, \\ C_1 &= \int_{-\infty}^{\infty} (-qr_x)dx, \\ C_2 &= \int_{-\infty}^{\infty} \left[-qr_{xx} + (qr)^2\right] dx, \\ C_3 &= \int_{-\infty}^{\infty} \left[4q^2 r r_x + q q_x r^2 - q r_{xxx}\right] dx. \end{aligned} \tag{110}$$

It is well known that the global conservation laws for the case when the potentials are periodic are exactly the same with the integration being over one period.

We now obtain the local conservation laws. Equations (103) imply

$$\begin{aligned} \phi_t &= A\phi_1 + B\phi_2 \\ &= A\phi_1 + \frac{B}{q}\left(\phi_{1x} + i\zeta\phi_1\right). \end{aligned}$$

Using relation (107), this becomes

$$\alpha_t = A + \frac{B}{q}\alpha_x,$$

which combined with the definition of μ (108) and the compatibility condition yields

$$\partial_t \mu = \partial_x \left(A + \frac{B}{q}\mu\right).$$

The local conservation laws can be obtained from the expansion of μ

$$\frac{\partial}{\partial t}\left(\sum_{n=0}^{\infty} \frac{\mu_n}{(2i\zeta)^{n+1}}\right) = \frac{\partial}{\partial x}\left(A + \frac{B}{q}\sum_{n=0}^{\infty} \frac{\mu_n}{(2i\zeta)^{n+1}}\right). \tag{111}$$

Particular evolution equations can be obtained by specifying A and B appropriately. Their corresponding conservation laws follow from expansion (111), by equating coefficients of $(2i\zeta)^{-n}$, and using (109).

For example, if

$$r = \mp q^*, \quad A = -2i\zeta^2 \pm i|q|^2, \quad B = 2\zeta q + iq_x,$$

the evolution equation is the nonlinear Schrödinger equation

$$iq_t + q_{xx} \pm 2|q|^2 q = 0$$

and (111) becomes

$$\frac{\partial}{\partial t}\left\{\sum_{n=0}^{\infty}\frac{\mu_n}{(2i\zeta)^{n+1}}\right\}+i\frac{\partial}{\partial x}\left\{2\zeta^2\mp|q|^2+\left(2i\zeta-\frac{q_x}{q}\right)\sum_{n=0}^{\infty}\frac{\mu_n}{(2i\zeta)^{n+1}}\right\}=0.$$

Equating coefficients of $(2i\zeta)^{-n}$ we obtain

$$\begin{aligned}
n=0,\quad & \frac{\partial}{\partial t}\left(|q|^2\right)+i\frac{\partial}{\partial x}\left(qq_x^*-q^*q_x\right)=0,\\
n=1,\quad & \frac{\partial}{\partial t}\left(-qq_x^*\right)+i\frac{\partial}{\partial x}\left(|q_x|^2-qq_{xx}^*\pm|q|^4\right)=0,\\
n=2,\quad & \frac{\partial}{\partial t}\left(|q|^2\right)+i\frac{\partial}{\partial x}\left(qq_x^*-q^*q_x\right)=0,
\end{aligned}\tag{112}$$

etc. When $n=0$, $n=1$ and $n=2$ we obtain the local norm, momentum and energy conservation laws respectively. Integrating the local conservation laws with respect to the spatial domain yields the global invariants C_0, C_1, C_2 ..., given previously in equation (110). In Chapter III, we develop an alternate derivation of these local conservation laws and investigate how well they are preserved by the multi-symplectic numerical schemes.

A.2 INTEGRABLE STRUCTURE OF THE SINE-GORDON EQUATION.

In this section we review certain features of the integrable structure of the sine-Gordon equation. In the following treatment, although the Hamiltonian functional and the Lax pair are different for the NLS and CMKDV equations, the description of the phase space geometry using the associated inverse spectral theory is qualitatively the same. We single out the sine-Gordon equation from the AKNS hierarchy since we examine the preservation of the SG nonlinear spectrum by multi-symplectic spectral schemes in Chapter V.3.

The sine-Gordon equation can be viewed as an infinite-dimensional Hamiltonian system,

$$q_t=\frac{\delta H}{\delta p},\quad p_t=-\frac{\delta H}{\delta q}$$

with

$$H(p,q)=\int_0^L\left[\tfrac{1}{2}p^2+\tfrac{1}{2}(q_x)^2+1-\cos q\right]dx$$

and where $q=u$ and $p=u_t$ are the conjugate variables and δ denotes the variational derivative.

The Poisson bracket of any two functionals F and G is defined to be

$$\{F,G\} = \int_0^L \left[\frac{\delta F}{\delta q}\frac{\delta G}{\delta p} - \frac{\delta F}{\delta p}\frac{\delta G}{\delta q}\right] dx, \tag{113}$$

and the evolution of any functional F under the sine-Gordon flow is governed by

$$\frac{dF}{dt} = \{F,H\}.$$

The Hamiltonian H is conserved by the sine-Gordon flow. In addition, for the AKNS equations such as sine-Gordon, there exists an infinite family of conserved functionals, in involution with respect to the Poisson bracket (113). Thus the sine-Gordon equation is a completely integrable system and can be solved with the inverse scattering transform.

In general the integrability is lost by numerical discretizations. In the case of infinite dimensional problems, this may have severe adverse effects on the quality of the numerical solutions, in particular in the vicinity of sensitive structures such as homoclinic orbits. However, it is not obvious how to determine the proximity to homoclinic manifolds from the global constants of motion; another representation is called for. We now proceed to show how the geometric structure of the infinite-dimensional phase space may be described in terms of the Floquet discriminant. The discriminant implicitly defines the homoclinic orbits and allows one to measure the width of the chaotic layer which appears about the homoclinic orbits when the system is perturbed.

Spectral Theory

The phase space of the sine-Gordon equation with periodic boundary conditions can be described in terms of the Floquet spectrum of the following linear operator (the spatial part of the associated Lax pair; for a detailed description see [23]):

$$\mathcal{L}(u,\lambda) = \left[\boldsymbol{A}\frac{d}{dx} + \frac{i}{4}\boldsymbol{B}(u_x + u_t) + \frac{1}{16\lambda}\boldsymbol{C} - \lambda\boldsymbol{I}\right], \tag{114}$$

where

$$\boldsymbol{A} = \begin{pmatrix} 0 & -1 \\ 1 & 0 \end{pmatrix}, \qquad \boldsymbol{B} = \begin{pmatrix} 0 & 1 \\ 1 & 0 \end{pmatrix}$$

$$\boldsymbol{C} = \begin{pmatrix} e^{iu} & 0 \\ 0 & e^{-iu} \end{pmatrix}, \qquad \boldsymbol{I} = \begin{pmatrix} 1 & 0 \\ 0 & 1 \end{pmatrix},$$

$u = u(x,t)$ is the potential and $\lambda \in \mathbb{C}$ denotes the spectral parameter.

The spectrum of $\mathcal{L}^{(x)}$ is defined as

$$\sigma(\mathcal{L}) := \left\{ \lambda \in \mathbb{C} | \mathcal{L}^{(x)} v = 0, |v| \text{ bounded } \forall x \right\}.$$

Since the potential u solves the sine-Gordon equation, and is of spatial period L, the spectrum is obtained using Floquet theory. The fundamental matrix, $M(x, x_0; u, \lambda)$, of the spectral operator (114) is defined by

$$\mathcal{L}(u,\lambda)M = 0, \quad M(x_0, x_0; u, \lambda) = \begin{pmatrix} 1 & 0 \\ 0 & 1 \end{pmatrix}$$

and the Floquet discriminant by

$$\Delta(u,\lambda) := \mathrm{tr} M(x_0 + L, x_0; u, \lambda).$$

The spectrum of $\mathcal{L}(u,\lambda)$ is given by the following condition on Δ:

$$\sigma(\mathcal{L}^{(x)}) = \{ \lambda \in \mathbb{C} | \Delta(u,\lambda) \text{ is real and } -2 \leq \Delta(u,\lambda) \leq 2 \}.$$

The discriminant is analytic in both its arguments. Moreover, for a fixed λ, Δ is invariant along solutions of the sine-Gordon equation:

$$\frac{d}{dt}\Delta(u(t),\lambda) = 0.$$

Since Δ is invariant and the functionals $\Delta(u,\lambda)$, $\Delta(u,\lambda')$ are pairwise in involution, Δ provides an infinite number of commuting invariants for the sine-Gordon equation.

When discussing the numerical experiments, we monitor the following elements of the spectrum which determine the nonlinear mode content of solutions of the sine-Gordon equation and the dynamical stability of these modes:

(i) Simple periodic/anti-periodic spectrum

$$\sigma^s = \{ \lambda_j^s | \Delta(\lambda, u) = \pm 2, \, d\Delta/d\lambda \neq 0 \}.$$

(ii) Double points of the periodic/anti-periodic spectrum

$$\sigma^d = \{ \lambda_j^d | \Delta(\lambda, u) = \pm 2, \, d\Delta/d\lambda = 0, \, d^2\Delta/d\lambda^2 \neq 0 \}.$$

The periodic/anti-periodic spectrum provides the actions in an action-angle description of the system. The values of these actions fix a particular level set. Let λ denote the spectrum associated with the potential u. The level set defined by u is then given by,

$$\mathcal{M}_u \equiv \{v \in \mathcal{F} | \Delta(v,\lambda) = \Delta(u,\lambda), \lambda \in \mathbb{C}\}.$$

Typically, $\mathcal{M}_u$ is an infinite-dimensional stable torus. However, the sine-Gordon phase space also contains degenerate tori that may be unstable. If a torus is unstable, its invariant level set consists of the torus and an orbit homoclinic to the torus. These invariant level sets, consisting of an unstable component, are represented in general by complex double points in the spectrum. A complete and detailed description of the sine-Gordon phase space structure is provided in [23]; we illustrate the main ideas by means of a simple example.

Consider the solution, $u(x,t) = (\pi, 0)$. This solution is modulationally unstable: assuming that

$$u(x,t) = \pi + \epsilon(x,t), \quad |\epsilon(x,t)| << 1,$$

with

$$\epsilon(x,t) = \hat{\epsilon}_n(t)e^{i\mu_n x} + \hat{\epsilon}_n^*(t)e^{-i\mu_n x}, \quad \mu_n = 2\pi n/L,$$

n an arbitrary integer, it follows that

$$\frac{d^2}{dt^2}\hat{\epsilon}_n + \omega_n^2 \hat{\epsilon}_n = 0,$$

(and similarly for $\hat{\epsilon}_n^*(t)$) where $\omega_n^2 = \mu_n^2 - 1$. The n-th mode grows exponentially, if $0 \leq \mu_n^2 < 1$. For this solution, the Floquet discriminant is given by

$$\Lambda(u,\lambda) = 2\cos\left(\lambda + \frac{1}{16\lambda}\right) L$$

and the spectrum by

$$\sigma(\mathcal{L}) = \mathbb{R} \bigcup (|\lambda|^2 = 1/16).$$

The periodic spectrum is located at

$$\lambda_j = \tfrac{1}{2}\left[\frac{j\pi}{L} \pm \sqrt{\frac{j^2\pi^2}{L^2} - \frac{1}{4}}\right], \quad j \text{ integer}.$$

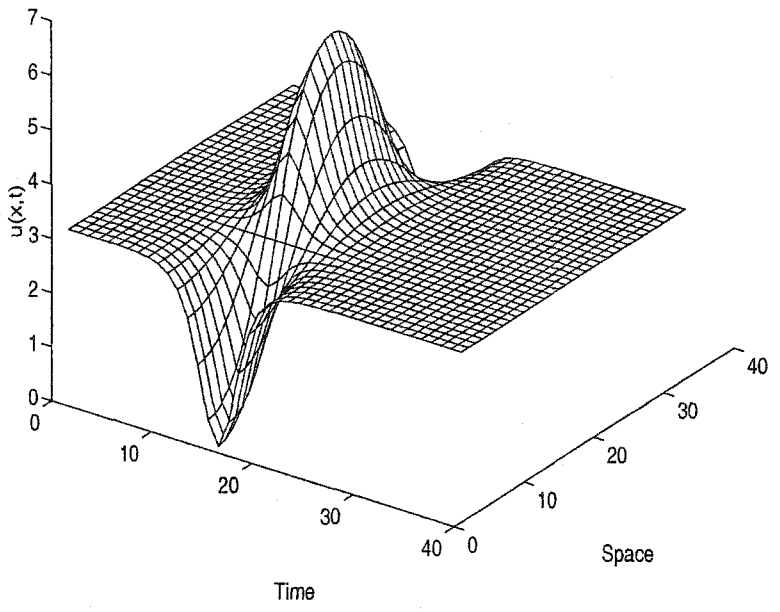

FIG. 18: The homoclinic orbit.

Each of these points is a double point embedded in the continuous spectrum and becomes complex if

$$0 \leq \left(\frac{2\pi j}{L}\right)^2 < 1.$$

Note that the condition for complex double points is exactly the same as the condition for unstable modes.

The initial data used in the numerical experiments are small perturbations of $u(x,t) = (\pi, 0)$. We begin by considering the case of two unstable modes. Figures 18 and 19 show three possible nearby states. Figure 18 is obtained using the initial value,

$$\begin{aligned} u(x,0) &= \pi + 0.1\cos(\mu x) \\ u_t(x,0) &= 0.1\sqrt{1-\mu^2}\cos(\mu x), \end{aligned}$$

where $L = 2\sqrt{2}\pi$ and $\mu = 2\pi/L$. It shows a solution homoclinic to $u_0(x,t) = \pi$.

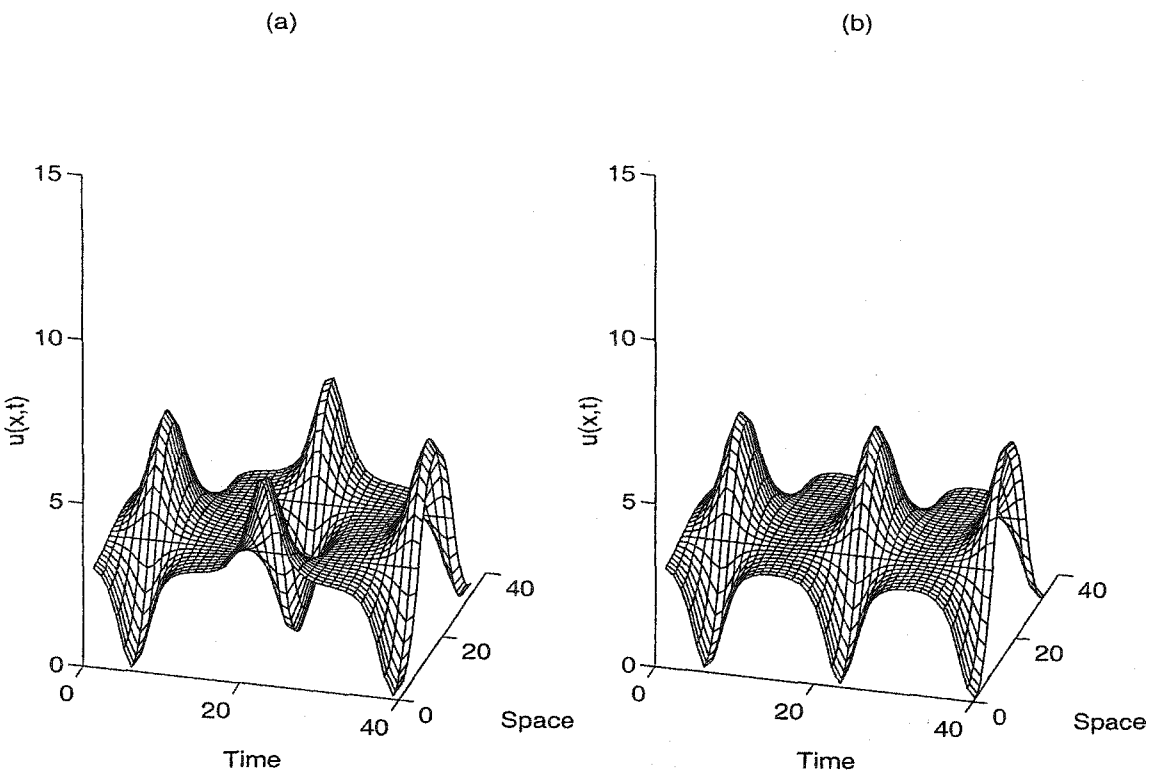

FIG. 19: (a) Outside and (b) inside the homoclinic orbit.

Figures 19(a) and (b) show solutions obtained using the initial values,

$$\begin{aligned} u(x,0) &= \pi + 0.1\sqrt{1-\mu^2}\cos(\mu x) \\ u_t(x,0) &= (0.1 \pm 0.01)\sqrt{1-\mu^2}\cos(\mu x). \end{aligned}$$

Despite a small difference in the initial values, the subsequent behavior is quite different – the period shown in Figure 19(a) is about twice that of Figure 19(b). We refer to these solutions as being "outside" and "inside" the homoclinic orbit, respectively. These differences are also reflected in the associated nonlinear spectrum shown in Figure 20. Figure 20(a) corresponds to the homoclinic orbit of Figure 18 and shows that both eigenvalues are double. Figures 20(b) and (c), which are the spectral representations of the waveforms shown in Figures 19(a) and (b), respectively, show how the complex double point at 45° has split into two simple points; it has opened either into a "gap" in the spectrum (Figure 20(b)) or has formed a "cross state" in the spectrum (Figure 20(c)). These results were obtained analytically in [1] with a perturbation analysis.

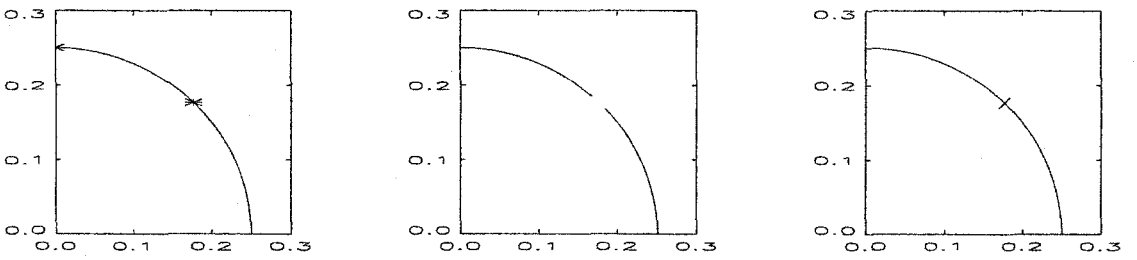

FIG. 20: The nonlinear spectrum.

APPENDIX B

GENERATING FUNCTIONS

B.1 THE ABLOWITZ-LADIK DISCRETE NLS

The Ablowitz-Ladik discrete NLS system

$$\begin{aligned} i\frac{d}{dt}q_n + \frac{q_{n-1}+q_{n+1}-2q_n}{h^2} + p_n q_n (q_{n-1}+q_{n+1}) &= 0, \\ -i\frac{d}{dt}p_n + \frac{p_{n-1}+p_{n+1}-2p_n}{h^2} + p_n q_n (p_{n-1}+p_{n+1}) &= 0, \end{aligned} \tag{115}$$

has a non-canonical Hamiltonian form

$$\dot{z} = \boldsymbol{P}(z)\nabla H(z), \tag{116}$$

where $z = (p,q)^T = (p_1,...,p_N,q_1,...,q_N)^T$ and $p = u^*$, $q = u$ are the conjugate variables. The Hamiltonian is given by

$$H = \frac{i}{h^3}\sum_{n=1}^{N}\left[h^2 p_n(q_{n-1}+q_{n+1}) - 2\ln(1+h^2 q_n p_n)\right], \tag{117}$$

and $\boldsymbol{P}(z)$ is a $2N \times 2N$ skew-symmetric matrix -

$$\boldsymbol{P}(z) = \begin{pmatrix} 0 & -\boldsymbol{R} \\ \boldsymbol{R} & 0 \end{pmatrix}, \qquad \boldsymbol{R} = diag[r_1,\ldots,r_N], \quad r_n = \frac{1+h^2 q_n p_n}{h},$$

so that the fundamental Poisson brackets are given in coordinates (p,q) by

$$\{p_m, q_n\} = -r_n\delta_{m,n}, \quad \{p_m, p_n\} = \{q_m, q_n\} = 0.$$

The phase space of any Hamiltonian system with a non-degenerate bracket carries a natural symplectic structure. For the AL system (115) the symplectic 2-form is given by

$$\omega(p,q) = \sum_{n=1}^{N}\frac{h}{1+h^2 q_n p_n}\,dp_n \wedge dq_n. \tag{118}$$

In the continuum limit $h \to 0$ with $p_n = q_n^*$ the Hamiltonian H and the nonstandard Poisson bracket $\{,\}$ for the AL system approach the Hamiltonian and the standard Poisson bracket, respectively, for the NLS PDE, and the 2-form (118) reduces to the continuous form. The AL system inherits all the properties of the original PDE system and it is possible to derive the N-soliton solution for rapidly decreasing

whole-line boundary conditions, as well as quasi-periodic Riemann theta function solutions for periodic boundary conditions [5, 41].

As mentioned above, the AL system carries on its phase space a non-canonical symplectic structure, for which standard symplectic integrators are not immediately applicable. For example, symplectic implicit Runge-Kutta schemes for AL (116) do not exist. We explore several methods for obtaining symplectic schemes for the discrete AL system: 1) we introduce a time dependent coordinate transformation which yields a non-canonical Hamiltonian for which splitting methods can be applied 2) using an additional transformation we reduce the symplectic structure to canonical form and apply standard symplectic schemes and 3) via the generating function method, we develop integrators that preserve the original non-canonical structure (118).

A separable form of the Ablowitz-Ladik System

Under the time-dependent unitary transformation

$$u_n \mapsto (a_n + ib_n)e^{-2it/h^2}$$

the AL system is transformed into another non-canonical Hamiltonian system in *real* coordinates (a, b) [58]. Letting

$$w_n(t) = u_n(t)e^{2it/h^2},$$

then the new equations of motion are

$$\dot{w}_n = i\left(w_{n-1} + w_{n+1}\right)\left(\frac{1}{h^2} + |w_n|^2\right).$$

We remark that the equations of motion in this form do not have a well-defined limit as $h \to 0$ since the phase of the right-hand side is then undefined. Scaling of time is necessary to regularize the limit, which is equivalent to a transformation to a system of the original AL form.

Separating $w_n = a_n + ib_n$ into real and imaginary parts, we obtain the following equations of motion in the new real coordinates

$$\dot{a}_n = -c_n(b_{n+1} + b_{n-1}), \quad \dot{b}_n = c_n(a_{n+1} + a_{n-1}), \quad c_n = 1 + h^2(a_n^2 + b_n^2). \tag{119}$$

These can be cast as a non-canonical Hamiltonian system

$$\dot{Z} = \boldsymbol{K}(Z)\,\nabla H(Z), \tag{120}$$

where $Z = (a_1, \ldots, a_N, b_1, \ldots, b_N)^T$,

$$K(Z) = \begin{pmatrix} 0 & -S \\ S & 0 \end{pmatrix}, \qquad S = diag[s_1, \ldots, s_N], \quad s_n = 1 + h^2(a_n^2 + b_n^2)$$

and

$$H = \frac{1}{h^2} \sum_{n=1}^{N} \left[a_n a_{n+1} + b_n b_{n+1} \right].$$

Denoting the right-hand side of (120) by the vector field $V(Z)$ we write the system in the form

$$\dot{Z} = V(Z). \tag{121}$$

A symplectic method for the integration of (121) can be obtained based on the following splitting of V: the vector field V separates into the sum of the A-field

$$\dot{a}_n = -\left[1 + h^2\left(a_n^2 + b_n^2\right)\right](b_{n+1} + b_{n-1}), \quad \dot{b}_n = 0, \tag{122}$$

and the B-field

$$\dot{a}_n = 0, \quad \dot{b}_n = \left[1 + h^2\left(a_n^2 + b_n^2\right)\right](a_{n+1} + a_{n-1}). \tag{123}$$

Both systems are Hamiltonian with respect to the same Poisson bracket as (120) and the corresponding Hamiltonians are given by

$$\begin{aligned} H_A(Z) &= \frac{1}{h^2} \sum_{n=1}^{N} a_n a_{n+1}, \\ H_B(Z) &= \frac{1}{h^2} \sum_{n=1}^{N} b_n b_{n+1}. \end{aligned}$$

Both systems can be trivially integrated. We consider the A-system (122) first and let

$$\overline{B}_n = b_{n-1} + b_{n+1}, \qquad B_n^2 = (\frac{1}{h^2} + b_n^2), \qquad A_n = a_n.$$

Then

$$\frac{dA_n}{dt} = -\overline{B}_n(B_n^2 + A_n^2), \qquad \overline{B}_n = \text{const}, \quad B_n = \text{const},$$

which is easily integrated in the form

$$A_n(t) = B_n \frac{\frac{A_n(0)}{B_n} - \tan(B_n \overline{B}_n t)}{1 + \frac{A_n(0)}{B_n} \tan(B_n \overline{B}_n t)}.$$

The B-system (123) is similarly integrated as (with the obvious changes in notation)

$$B_n(t) = A_n \frac{\frac{B_n(0)}{A_n} + \tan(A_n \overline{A}_n t)}{1 - \frac{B_n(0)}{A_n} \tan(A_n \overline{A}_n t)}.$$

We denote the corresponding *symplectic* flows by e^{At} and e^{Bt}. To approximate the flow corresponding to V we can use the Baker-Campbell-Hausdorff formula to expand $e^{(tA+tB)}$ in terms of compositions of e^{tA} and e^{tB}, and match the terms up to the given order in t. Additional constraints have to be placed on the expansion coefficients to ensure that the compounded flow is symplectic as well. This is done systematically in [39]; we use a well-known second order symplectic *leapfrog method* that defines a symplectic approximation $\tilde{Z}(t)$ to e^{tV} as

$$\tilde{Z}(t) = (e^{\frac{1}{2}tA})(e^{tB})(e^{\frac{1}{2}tA}). \tag{124}$$

We denote this integrator by LF.

The Ablowitz-Ladik System in Canonical Form

In general, any non-degenerate symplectic form can be reduced to the canonical one using a suitable local coordinate transformation. These transformations are not unique since any Darboux transform followed by a symplectic map reduces the system to canonical form. In particular, we consider such transformations for the AL system and upon reduction apply standard symplectic integrators.

We begin with the transformed non-canonical Hamiltonian system (120). Next, standardization of the symplectic structure is accomplished using the Darboux transformation $(a, b) \mapsto (c, d)$ given by

$$\begin{aligned} a_n &= \frac{1}{h}\sqrt{1 + h^2 d_n^2}\, \tan\left(h\sqrt{1 + h^2 d_n^2}\, c_n\right) \\ b_n &= d_n. \end{aligned}$$

The AL system can then be rewritten in the canonical form (denoted by the c-AL system)

$$\dot{Y} = J^{-1}\, \nabla H(Y),$$

where $Y = (c_1, \ldots, c_N, d_1, \ldots, d_N)^T$,

$$J = \begin{pmatrix} 0 & I \\ -I & 0 \end{pmatrix},$$

with I being the identity matrix and

$$H(c,d) = \frac{1}{h^2}\sum_{n=1}^{N}\left[\frac{1}{h}\sqrt{1+h^2d_n^2}\,\tan\left(h\sqrt{1+h^2d_n^2}\,c_n\right)\right.$$
$$\left.\times\ \frac{1}{h}\sqrt{1+h^2d_{n+1}^2}\,\tan\left(h\sqrt{1+h^2d_{n+1}^2}\,c_{n+1}\right)+d_nd_{n+1}\right]$$

The c-AL system can then be discretized in time using standard symplectic schemes such as the second order implicit midpoint rule (see section II.2) and we denote this integrator as CS2.

Symplectic Schemes for the Non-canonical AL System

An alternate approach to standardization of the symplectic structure is to construct integrators that directly preserve the non-canonical form (118). Since the form (118) is not of potential type, Hamilton-Jacobi theory does not apply. Thus, the most appropriate approach to deriving symplectic integrators for the AL system is based on generating functions [31, 51]. In this section, the method is generalized to generate symplectic integrators of arbitrary order for general non-canonical systems carrying a symplectic structure of the AL type.

We consider symplectic structures given by 2-forms of the type

$$\omega(p,q) = \sum_{n=1}^{N}\omega_n(p_n,\,q_n)\,dp_n\wedge dq_n,$$

where $\omega_n(p_n,\,q_n)$ is a function of $(p_n,\,q_n)$ only. This is perhaps the simplest form of a non-canonical symplectic structure; the standard form is recovered from this expression by setting $\omega_n\equiv 1$. For the AL system $\omega_n = r_n^{-1}$. The Poisson bracket dual to ω has the fundamental brackets

$$\{p_m,\,q_n\} = -r_n\,\delta_{m,n} = -\omega_n^{-1}\,\delta_{m,n},\quad \{p_m,\,p_n\} = \{q_m,\,q_n\} = 0,$$

and the equations of motion generated by a Hamiltonian function $H(p,q)$ relative to this bracket have the form

$$\dot{p}_n = -r_n\frac{\partial H}{\partial q_n},\quad \dot{q}_n = r_n\frac{\partial H}{\partial p_n}. \tag{125}$$

A transformation $(p,q)\to(P,Q)$ is called symplectic with respect to ω if

$$\omega(p,q) = \omega(P,Q). \tag{126}$$

Since ω is closed, it is exact, at least locally, and there exists a local primitive 1-form θ such that $\omega = d\theta$. The primitive is not unique since for any smooth function F the form $\theta' = \theta + dF$ is also a (local) primitive for ω. One such θ can be obtained by integrating ω with respect to p along any path in a simply-connected neighborhood of (p, q) as follows

$$\theta(p,q) = f^T dq = \sum_{n=1}^{N} f_n(p_n,\, q_n) dq_n, \quad f_n(P_n,\, Q_n) = \int_{p_n}^{P_n} \omega_n(\xi,\, Q_n) d\xi.$$

Likewise, integrating with respect to q obtains another primitive

$$\theta'(p,q) = -g^T dp = -\sum_{n=1}^{N} g_n(p_n,\, q_n) dp_n, \quad g_n(P_n,\, Q_n) = \int_{q_n}^{Q_n} \omega_n(P_n,\, \xi) d\xi.$$

Given *any* two primitives θ and θ' we can write (126) as

$$d\theta(p,q) - d\theta'(P,Q) = 0,$$

which means that $\theta(p,q) - \theta'(P,Q)$ is also closed and thus locally exact. Therefore

$$\theta(p,q) - \theta'(P,Q) = dG \tag{127}$$

for some smooth function G. In general, (127) characterizes any symplectic map $(p,q) \to (P,Q)$ and the function G is called the *generating function* of the transformation [8]. Equations (127) can be solved for (P,Q) in the vicinity of the point (p,q) to obtain an explicit local representation of the transformation. In particular, since the phase flow generated by the equations of motion (125) is a symplectic map for any value of the time parameter, for sufficiently small t we can obtain an explicit representation of the flow in local coordinates P, Q. We follow Channell & Scovel's approach [17], which uses the transformation equations with a certain generating function $\tilde{G}$ to define the approximate flow so that it is exactly symplectic. The function $\tilde{G}$ is specified by an asymptotic power expansion in t obtained from the equations of motion to ensure the prescribed accuracy of the method. All of the following constructions are local, taking place in a neighborhood of some point (p,q) where the form ω is assumed non-degenerate and all functions are sufficiently smooth.

Taking the primitives $\theta = f^T dq$ and $\theta' = -g^T dp$ obtained above, the transformation equations (127) become

$$f^T\, dq + g^T\, dP = dG,$$

or in the component form

$$\frac{\partial G}{\partial q_n} = f_n(p_n, q_n), \quad \frac{\partial G}{\partial P_n} = g_n(P_n, Q_n). \tag{128}$$

Note that G is a generating function of the second kind, i.e., such that $\dfrac{\partial^2 G}{\partial P \partial q}$ is non-degenerate, so we can take (P, q) to be the local coordinates in the neighborhood of (p, q). Let $(P(t), Q(t))$ be the solution of the system (125) with the initial data (p, q) and for sufficiently small t. The right-hand side of the equations of motion

$$\dot{P}_n = -R_n \frac{\partial H}{\partial Q_n}(P, Q), \quad \dot{Q}_n = R_n \frac{\partial H}{\partial P_n}(P, Q), \qquad R_n = r_n(P_n, Q_n), \tag{129}$$

is smooth in a neighborhood of (p, q), which justifies asymptotic power expansions in t for $Q_n(t)$ at the point (P, q). Likewise, smoothness of f_n and g_n and the relations (128) imply the existence of a similar expansion for $G(t)$. Thus we have asymptotic expressions

$$Q_n(t) = q_n + \underbrace{\sum_{m=1}^{\infty} \frac{t^m}{m!} Q_{m,n}(P, q)}_{\Delta q_n}, \quad G(t) = \sum_{m=0}^{\infty} \frac{t^m}{m!} G_m(P, q)$$

holding in the vicinity of (P, q). Now we can solve for G in terms of $Q_{m,n}$. To do so, write the second part of the transformation equations as an asymptotic series in t at (P, q) by expanding g_n in a Taylor series about q with Δq defined above:

$$\begin{aligned} \sum_{m=0}^{\infty} \frac{t^m}{m!} G_m(P, q) &= \sum_{k=0}^{\infty} \frac{1}{k!} \left(\Delta q_n \frac{\partial}{\partial q_n} \right)^k g_n(P_n, q_n) \\ &= \sum_{k=0}^{\infty} \frac{1}{k!} \left(\sum_{s=1}^{\infty} \frac{t^s}{s!} Q_{s,n} \frac{\partial}{\partial q_n} \right)^k g_n(P_n, q_n). \end{aligned}$$

Expanding the double series obtains an asymptotic series for g_n

$$\begin{aligned} &\sum_{k=0}^{\infty} \frac{1}{k!} \left(\sum_{s=1}^{\infty} \frac{t^s}{s!} Q_{s,n} \frac{\partial}{\partial q_n} \right)^k g_n(P_n, q_n) = \\ &\sum_{m=0}^{\infty} t^m \underbrace{\sum_{k=0}^{m} \frac{\partial^k g_n}{\partial q_n^k}(P_n, q_n) \sum_{\substack{l_i, \ldots, l_k \geq 0 \\ \sum l_i = m \\ \sum i l_i = k}} \frac{1}{l_1! \ldots l_k!} \left(\frac{Q_{1,n}}{1!} \right)^{l_1} \cdots \left(\frac{Q_{m,n}}{s!} \right)^{l_k}}_{g_{m,n}} \end{aligned}$$

Equating powers of t yields the following relation between the coefficients G_m and $Q_{m,n}$

$$\frac{\partial G_m}{\partial P_n}(P,q) = m! \sum_{k=0}^{m} \frac{\partial^k g_n}{\partial q_n^k}(P_n,\, q_n) \sum_{\substack{l_i,\ldots,l_m \geq 0 \\ \sum l_i = k \\ \sum i l_i = m}} \frac{1}{l_1! \ldots l_m!} \left(\frac{Q_{1,n}}{1!}\right)^{l_1} \cdots \left(\frac{Q_{m,n}}{s!}\right)^{l_m} \tag{130}$$

If the $Q_{m,n}$ were known, the G_m could be easily determined by integration. The $Q_{m,n}$ are calculated using the equations of motion as follows. The full time derivative of Q_n is

$$\dot{Q}_n = \frac{\partial Q_n}{\partial t} + \sum_{j=1}^{N} \frac{\partial Q_n}{\partial P_j} \dot{P}_j,$$

and using (129), this is written

$$\frac{\partial Q_n}{\partial t} = R_n \frac{\partial H}{\partial P_n} + \sum_{j=1}^{N} \frac{\partial Q_n}{\partial P_j} R_j \frac{\partial H}{\partial Q_j}. \tag{131}$$

Next, we obtain asymptotic expansions for R_n and the derivatives of H in the same way as was done for g_n above:

$$\frac{\partial H}{\partial P_n} = \sum_{s=0}^{\infty} t^s \underbrace{\sum_{k=0}^{s} \sum_{j_1,\ldots,j_k=1}^{N} \frac{\partial^{k+1} H}{\partial P_n \partial q_{j_1} \ldots \partial q_{j_k}} \sum_{\substack{l_i,\ldots,l_s \geq 0 \\ \sum l_i = k \\ \sum i l_i = s}} \frac{1}{l_1! \ldots l_s!} \left(\frac{Q_{1,j_1}}{1!}\right)^{l_1} \cdots \left(\frac{Q_{s,j_k}}{s!}\right)^{l_s}}_{H_{s,P_n}}.$$

Likewise,

$$\frac{\partial H}{\partial Q_n} = \sum_{s=0}^{\infty} t^s \underbrace{\sum_{k=0}^{s} \sum_{j_1,\ldots,j_k=1}^{N} \frac{\partial^{k+1} H}{\partial q_n \partial q_{j_1} \ldots \partial q_{j_k}} \sum_{\substack{l_i,\ldots,l_s \geq 0 \\ \sum l_i = k \\ \sum i l_i = s}} \frac{1}{l_1! \ldots l_s!} \left(\frac{Q_{1,j_1}}{1!}\right)^{l_1} \cdots \left(\frac{Q_{s,j_k}}{s!}\right)^{l_s}}_{H_{s,Q_n}},$$

and

$$R_n(P_n,\, Q_n) = \sum_{m=0}^{\infty} t^m \underbrace{\sum_{k=0}^{m} \frac{\partial^k R_n}{\partial Q_n^k}(P_n,\, q_n) \sum_{\substack{l_i,\ldots,l_k \geq 0 \\ \sum l_i = m \\ \sum i l_i = k}} \frac{1}{l_1! \ldots l_k!} \left(\frac{Q_{1,n}}{1!}\right)^{l_1} \cdots \left(\frac{Q_{m,n}}{s!}\right)^{l_k}}_{R_{m,n}}.$$

Upon substituting these series into (131), $Q_{m,n}$ can be solved for recursively since a coupling exists among $Q_{m,n}$ such that all the terms appearing on the right-hand

side have lower m-indices than that on the left, i.e.,

$$Q_{m+1,n} = m! \left(\sum_{\substack{s+k=m \\ s,k\geq 0}} R_{s,n}\, H_{k,P_n} + \sum_{\substack{s+k+l=m \\ s\geq 1,\ k,l\geq 0}} \frac{1}{s!} \sum_{j=1}^{N} \frac{\partial Q_{s,n}}{\partial P_j} R_{k,j}\, H_{l,Q_j} \right).$$

Once $Q_{m,n}$ are obtained and substituted into (130), expressions for G_m are integrated and the generating function G is specified in the form

$$G(P,q) = \sum_{m=0}^{\infty} \frac{t^m}{m!} G_m(P,q).$$

It can be calculated to any prescribed accuracy using *any* finite expansion

$$\tilde{G}(t) = \sum_{m=0}^{r} \frac{t^m}{m!} G_m(P,q), \tag{132}$$

as long as t is sufficiently small. Thus, the truncated function $\tilde{G}(P,q)$ generates the transformation equations

$$f_n(p,q) = \frac{\partial \tilde{G}}{\partial q_n}(\tilde{P},q), \quad g_n(\tilde{P},\tilde{Q}) = \frac{\partial \tilde{G}}{\partial \tilde{P}_n}(\tilde{P},q), \tag{133}$$

which can be solved for $(\tilde{P},\tilde{Q})$ to define a symplectic transformation $(p,q) \to (\tilde{P},\tilde{Q})$ that agrees with the exact flow $(p,q) \to (P,Q)$ to r-th order. We state this fact as follows:

Proposition 5 *Transformation equations (133) obtained from a truncated generating function (132) can be solved uniquely for sufficiently small t to produce $(\tilde{P},\tilde{Q})$ such that*

$$(\tilde{P},\tilde{Q}) = (P,Q) + \mathcal{O}(t^{r+1}),$$

where (P,Q) are the solution of the transformation equations with the exact generating function G corresponding to the Hamiltonian flow of the system (129).

Proof: Observe that $\tilde{G}(t) = G(t) + \mathcal{O}(t^{r+1})$ and therefore

$$\begin{aligned} f_n(p_n,\, q_n) &= \frac{\partial G}{\partial q_n}(\tilde{\mathbf{P}},\, \mathbf{q}) + \mathcal{O}(t^{r+1}) \\ g_n(\tilde{P}_n,\, \tilde{Q}_n) &= \frac{\partial G}{\partial P_n}(\tilde{\mathbf{P}},\, \mathbf{q}) + \mathcal{O}(t^{r+1}). \end{aligned} \tag{134}$$

The function $G(P,q)$ generates the transformation equations

$$f_n(p,q) = \frac{\partial G}{\partial q_n}(P,q), \quad g_n(P,Q) = \frac{\partial G}{\partial P_n}(P,q). \tag{135}$$

From the second equation of (135) we calculate the derivative matrix

$$\boldsymbol{J}^1(t) = \left\{ \frac{\partial^2 G}{\partial P_n \partial q_m} \right\} = \left\{ \sum_{j=1}^{N} \frac{\partial g_n}{\partial Q_j} \frac{\partial Q_j}{\partial q_m} \right\}.$$

Using the expansion $Q = q + \mathcal{O}(t)$ to calculate $\dfrac{\partial Q}{\partial q}$ and setting $t = 0$ yields

$$J^1_{n,m}(0) = \sum_{j=1}^{N} \frac{\partial g_n}{\partial Q_j}(P, Q)\delta_{j,m} = \frac{\partial g_n}{\partial q_m}(p, q) = \delta_{m,n}\omega_n(p_n,\, q_n).$$

Since ω is non-degenerate at (p, q) by assumption, $\boldsymbol{J}^1(t)$ is non-singular for $t = 0$ and for sufficiently small non-zero t the same holds by continuity. Since $\tilde{G}(t) = G(t) + \mathcal{O}(t^{r+1})$, $\tilde{\boldsymbol{J}}^1 = \dfrac{\partial^2 G}{\partial \tilde{P} \partial q}$ is non-singular for small t as well. Taking the smaller of the two values for t we ensure that the first equations of both systems (133) and (135) are solvable for P. (Incidentally, this argument establishes that G and $\tilde{G}$ obtained by this technique are indeed generating functions of the second kind). Next, we substitute the obtained P and $\tilde{P}$ into the second equations of (133) and (135) and solve for Q and $\tilde{Q}$ respectively. This is possible since the appropriate Jacobi matrix is

$$\boldsymbol{J}^2(t) = \left\{ \frac{\partial g_n}{\partial Q_m}(P, Q) \right\} = \left\{ \delta_{m,n}\omega_n(P_n,\, Q_n) \right\},$$

and it is non-degenerate for the chosen values of t by construction.

Having obtained (P, Q) and $(\tilde{P}, \tilde{Q})$ we compare their Taylor expansions at $t = 0$. For that, we differentiate equations (133) and (135) with respect to t to k-th order and solve for $\dfrac{d^k}{dt^k}(P, Q)\big|_{t=0}$ and $\dfrac{d^k}{dt^k}(\tilde{P}, \tilde{Q})\Big|_{t=0}$, respectively. By virtue of (134), upon setting $t = 0$, the differentiated equations reduce to the same system as long as $k \leq r$, and by non-degeneracy of $\boldsymbol{J}^1(0)$ and $\boldsymbol{J}^2(0)$, the solution is unique so that

$$\frac{d^k}{dt^k}(P, Q)\big|_{t=0} = \frac{d^k}{dt^k}(\tilde{P}, \tilde{Q})\Big|_{t=0}, \quad k = 0, \ldots, r$$

and therefore

$$(P, Q) = (\tilde{P}, \tilde{Q}) + \mathcal{O}(t^{r+1})$$

for all t as determined above.

We use this result to derive a second-order symplectic discretization of the AL system.

In the case of the AL system,

$$f_n(p_n,\, q_n) = \frac{1}{hq_n}\ln(1+h^2p_nq_n), \quad g_n(P_n,\, Q_n) = \frac{1}{hP_n}\ln(1+h^2P_nQ_n),$$

and using the well-known Taylor series for $\ln(1+x)$ yields an expression of $\dfrac{\partial G_m}{\partial P_n}$ as obtained from (130)

$$\begin{aligned}
\frac{\partial G_0}{\partial P_n} &= \frac{1}{hP_n}\ln(1+h^2P_nq_n), \\
\frac{\partial G_m}{\partial P_n} &= \frac{m!}{hP_n}\sum_{k=1}^{m}(-1)^{k-1}(k-1)!\Big(\frac{h^2P_n}{1+h^2P_nq_n}\Big)^k \\
&\quad\times \sum_{\substack{l_i,\ldots,l_m\geq 0 \\ \sum l_i=k \\ \sum il_i=m}} \frac{1}{l_1!\ldots l_m!}\Big(\frac{Q_{1,n}}{1!}\Big)^{l_1}\cdots\Big(\frac{Q_{m,n}}{s!}\Big)^{l_m}. \qquad (136)
\end{aligned}$$

Next, using the expression for the Hamiltonian and

$$R_n = \frac{1+h^2P_nQ_n}{h}$$

along with the formulae for their expansion coefficients, we solve for $Q_{m,n}$ with $m = 1, 2$ and substitute into (136). Except for $m = 0$, these expressions are identified as total derivatives and trivially integrated to yield

$$\begin{aligned}
G_0(P,q) &= \sum_{n=1}^{N}\int^{q_n}\frac{1}{hP_n}\ln(1+h^2P_n\xi)d\xi = \sum_{n=1}^{N}\int^{P_n}\frac{1}{hq_n}\ln(1+h^2\xi q_n)d\xi, \\
G_1(P,q) &= H, \\
G_2(P,q) &= \sum_j\frac{1}{h}(1+h^2P_jq_j)\frac{\partial H}{\partial P_j}\frac{\partial H}{\partial q_j}.
\end{aligned}$$

Substituting the truncated generating function

$$\tilde{G} = G_0 + tG_1 + \frac{t^2}{2}G_2$$

into (133) and solving for $\tilde{P}_n$ and $\tilde{Q}_n$, the following second order symplectic scheme is obtained

$$\begin{aligned}
\tilde{P}_n &= \frac{1}{h^2q_n}\left[\left(1+h^2q_np_n\right)e^{-hq_n\frac{\partial E}{\partial q_n}} - 1\right], \qquad E = tG_1 + \frac{t^2}{2}G_2 \\
\tilde{Q}_n &= \frac{1}{h^2\tilde{P}_n}\left[\left(1+h^2q_n\tilde{P}_n\right)e^{h\tilde{P}_n\frac{\partial E}{\partial \tilde{P}_n}} - 1\right], \qquad (137)
\end{aligned}$$

which we denote by S2. Note that G_0 generates the identity transformation and its exact expression is not needed.

As the scheme is implicit, to advance one time step from (p, q) to $(\tilde{P}, \tilde{Q})$ the system (137) has to be solved using some type of nonlinear solver. We choose to use a simple fixed-point iteration procedure (FPI), which converges rapidly with a good initial guess given by (p, q) for all values of t that we used in our numerical experiments.

Standard Schemes

Standard time integrators are also used in the numerical study below for comparison with the geometric integrators just derived as well as in the implementation of AL in canonical form. Specifically, we use the explicit second order Runge-Kutta and the implicit midpoint schemes defined below. Given a dynamical system

$$\dot{z} = F(z)$$

and initial data z we compute an approximation $\tilde{Z}$ at the time t by the explicit second order Runge-Kutta scheme

$$\tilde{Z} = z + tF\left(z + \frac{t}{2}F(z)\right) \tag{138}$$

and by the implicit midpoint scheme

$$\tilde{Z} = z + tF\left(\frac{1}{2}(z + \tilde{Z})\right). \tag{139}$$

We denote (138) and (139) by R2 and CS2 respectively. The implicit midpoint rule, CS2, is the lowest order member of the Gauss-Legendre family of implicit Runge-Kutta methods which are symplectic schemes for canonical Hamiltonian systems [32, 50]. Thus CS2 defines a symplectic transformation when applied to the canonical AL system. As CS2 is implicit, we use the same nonlinear solver (FPI) as with S2 to obtain $\tilde{Z}$ at each time step.

B.2 NUMERICAL EXPERIMENTS

In this section we examine the performance of the symplectic and multi-symplectic methods in solving the NLS equation under periodic boundary conditions $q(x + L, t) = q(x, t)$ over the time interval $[0, T]$ with $T = 500$. For consistency, all the

discretizations of the PDE examined are second-order in space and time with a fixed time step used throughout the integration. We are interested in simulating multi-phase quasi-periodic (in time) solutions. Initial data can be obtained by perturbing the plane wave solution $q_0(x,t) = ae^{2i|a|^2t}$. In the experiments we use initial data of the following form:

$$q_n(0) = p_n^*(0) = 0.5(1 + \epsilon\cos(\mu x_n)) \tag{140}$$

for $x_n = -L/2 + (n-1)h$, $h = L/N$, $n = 1, 2, ..., N+1$, where $\epsilon = 10^{-2}$, $\mu = 2\pi/L$ and L is either (140a) $L = 2\sqrt{2}\pi$ or (140b) $L = 4\sqrt{2}\pi$. The plane wave solution is modulationally unstable and for a fixed amplitude, as the period L is increased, the number of unstable modes increases. Thus initial data (140a) and (140b) correspond to multi-phase solutions, near the plane wave, which are characterized by either one or two excited modes, respectively. For brevity, we will refer to these cases as the one mode and two mode case. In almost all the experiments initial data (140a) is used. It is only in the final comparison between the generating function symplectic scheme and the multi-symplectic scheme that we consider initial data (140b).

The non-canonical AL system: symplectic vs non-symplectic integrators

We begin by comparing the performance of the generating function symplectic scheme S2 (137) and the explicit Runge-Kutta scheme R2 (138), applied to the non-canonical AL system (115) for the one mode case (140a). The numerical schemes are evaluated by monitoring the Hamiltonian H (117), the norm I defined as

$$I(p,q) = \sum_{n=1}^{N} \left[p_n(q_{n-1} + q_{n+1})\right],$$

as well as the amplitude of the waveform of the solution.

Figures 21a-b show the error in the Hamiltonian obtained using S2 and R2 for (a) $N = 4$ with $t = 10^{-2}$ and for (b) $N = 32$ with $t = 10^{-3}$. The symplectic scheme S2 preserves the Hamiltonian extremely well during long time integrations as the error in the Hamiltonian oscillates in a bounded fashion and does not exhibit a linear drift as it does with R2. However, the linear error growth in H which occurs using the non-symplectic method becomes less significant as the time step t decreases and the dimension of the system N increases (compare Figure 21a-b).

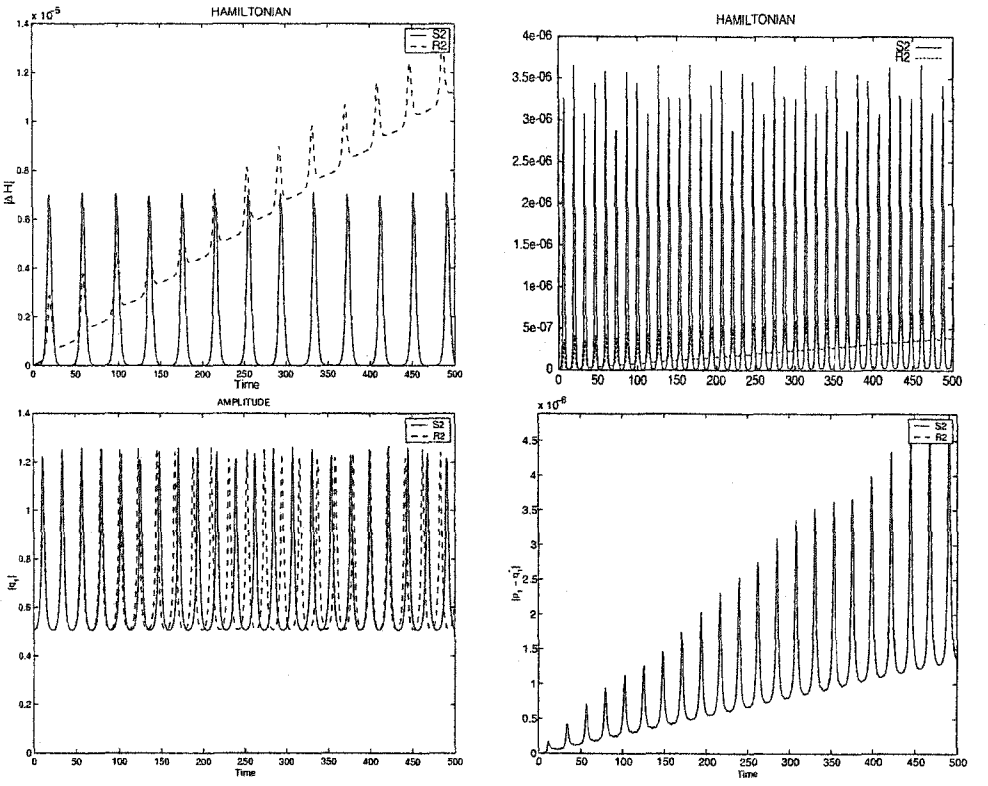

FIG. 21: Comparison of integrators S2 and R2 for the AL system.

This behavior is summarized in Table II which provides the maximum error in H of the AL system as a function of N and t using schemes S2 and R2, i.e., for mesh sizes $N = 16,\ 32$ and 64, each for two time steps. The preservation of the second invariant I is not presented as it is qualitatively similar to H. The experiments with different time steps t indicate that the error in the Hamiltonian is bounded by $\gamma_{S2}t^2$ for the method S2, whereas it behaves like $\alpha_{R_2}t^2 + \beta_{R_2}Tt^3$ for the method R2. The dependence of the constants $\gamma_{S2}, \alpha_{R_2}$, and β_{R_2} on the space discretization parameter h is less clear (see Table II).

Figure 21c shows the amplitude of q_1 of the solution obtained with the two integrators R2 and S2 using $N = 16$ and $t = 10^{-2}$. Solutions of the AL system exhibit regular quasi-periodic motion due to the fact that the AL flow occurs in general on an N-torus. For $t = 0.01$, a phase lag develops using R2 which becomes more pronounced as the system evolves. However, using $t = 0.001$ the solutions from the two integrators are virtually indistinguishable on the time scale examined. The amplitudes of the other lattice sites show similar qualitative behavior.

TABLE II: Error in the AL Hamiltonian for S2 and R2.

N	16	16	32	32	64	64
t	1.0E-02	1.0E-03	1.0E-03	1.0E-04	5.0E-04	1.0E-04
S2	2.7E-04	2.7E-06	3.7E-06	5.1E-08	1.0E-06	1.0E-07
R2	q 2.2E-04	5.2E-07	6.0E-07	4.1E-09	1.2E-07	4.1E-09

The conjugacy relation $q = p^*$ arises in the applications of the NLS of physical interest [21, 61], thus preserving this additional constraint can potentially be as important as preserving the symplectic structure. It is of interest then to consider initial data of this form and to determine which of the schemes minimizes $|p - q^*|$, the deviation from conjugacy. Figure 21d shows that the deviation in $|p_1 - q_1^*|$ for $N = 16$ and $t = 10^{-3}$ is of size 10^{-6} using S2, whereas with R2 it is on the order of roundoff (the deviation in $|p_n - q_n^*|$ is comparable for general n). Note: although $q(0) = p^*(0)$ and the semi-discrete AL flow preserves conjugacy, this condition is not imposed throughout the time evolution as the performance of the integrator degrades. In fact, if the relation is imposed and the implicit scheme is solved for just q_n at each time step, a linear error growth in the Hamiltonian occurs indicating that in this case the scheme is not symplectic [51].

Both schemes exhibit stability issues as can be seen from the $N = 4$ and $N = 16$ cases. Keeping the time step fixed and varying N (equivalently h), as h decreases the performance of both schemes degrades. This suggests that $t/h^2 < M$, for some M, is required for stability. The instability is more pronounced for the explicit scheme R2 than for either of the symplectic schemes. It is surprising then that R2 preserves conjugacy better, indicating that instabilities of R2 lie in the $p = q^*$ subspace, whereas for S2 they are transverse to it.

It should be mentioned that R2, being an explicit scheme, is faster than S2 and the difference in computation time becomes more significant as the dimension $2N$ of the semi-discrete system is increased. At the same time the difference in accuracy of the two schemes manifests on a longer time scale, making R2 attractive for intermediate integration times.

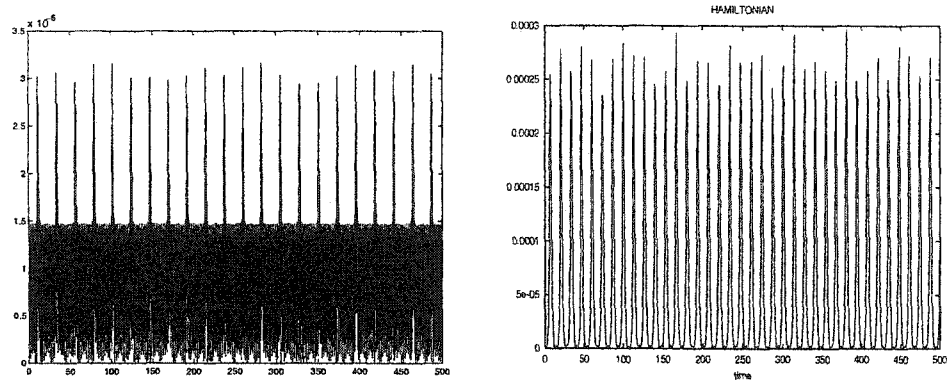

FIG. 22: The error in the Hamiltonian for (a) LF and (b) AL.

The symplectic integrators in non-canonical and canonical form

Next we compare the performance of the leapfrog method LF (124), the symplectic canonical implicit midpoint scheme CS2 (139) and the generating function symplectic scheme S2 (137) for the one mode case (140a). Initialization and comparison of the constants of motion and waveform for the various integration methods is done in the original coordinate system (p, q), i.e., we unwind all transformations before the AL Hamiltonian (117) is computed and output is generated. For the implicit schemes, the same criterion is used to accept a solution of the iterative procedure at each time step, namely, the L_1-norm of the error has to be less than 10^{-10}.

Both LF and CS2 exhibit the characteristic behavior of symplectic schemes. As an example, Figure 22 shows the error in the Hamiltonian, which is nicely bounded over long times obtained with a) LF using $N = 32$, $t = 10^{-4}$ and b) CS2 using $N = 32$, $t = 10^{-3}$, both for $T = 500$. Table III provides the maximum absolute error in the AL Hamiltonian (117) obtained with the symplectic schemes CS2, S2 and LF for mesh sizes $N = 32$ and 64, each for two time steps. For fixed h ($h = L/N$), halving the time step results in a decrease in the maximum error in H by a factor of 2^{-2}. An example of this is shown in the Table for $N = 32$. This supports the conjecture that for the LF and CS2 methods, the error in H is bounded by $\gamma_{LF}t^2$ and $\gamma_{CS2}t^2$, respectively, similar to the results for S2. However, the maximum error in H obtained with LF and CS2 is at least two orders of magnitude larger than with S2. Thus the error coefficients γ_{LF}, γ_{CS2} are significantly larger than γ_{S2}.

TABLE III: Error in the AL Hamiltonian for CS2, S2 and LF.

N	32	32	64	64
t	2.0E-03	1.0E-03	5.0E-04	1.0E-04
CS2	1.2E-03	3.0E-04	1.0E-03	4.5E-05
S2	1.5E-05	3.7E-06	1.0E-06	1.0E-07
LF	1.3E-03	3.2E-04	1.6E-03	6.4E-05

In Figure 22a small amplitude, high frequency background oscillations are visible against the dominant large amplitude, low frequency oscillations (whose frequency corresponds to that of the excited mode in the AL solution). The time-dependent map $u \mapsto w$ is responsible for the high frequency oscillations as well as the less accurate resolution of the Hamiltonian exhibited by LF and CS2.

In the experiments CS2 was found to be less efficient than S2 as it requires almost as much CPU time as S2 even though it is less accurate. On the other hand, LF is relatively fast and easy to implement but is also less accurate than S2. In addition, the method is based on a particular feature of (119) – its separable nature, which is not apparent from the original AL formulation, nor general enough. Although there is no loss of conjugacy when using LF and CS2, we emphasize the utility of the generating function method for its ability to handle a wide class of non-canonical Hamiltonian systems. To obtain a robust symplectic integrator which preserves $p_n = q_n^*$ exactly, the conjugacy condition should be imposed first. Then letting $q_n = a_n + ib_n$, the AL system can be written in real form and the generating function method developed in section B.1 can be applied to the real non-canonical system.

VITA

Alvaro Lucas Islas
Department of Mathematics and Statistics
Old Dominion University
Norfolk, VA 23529

Education

Ph. D. in Computational Applied Mathematics (2002) Department of Mathematics and Statistics, Old Dominion University

Teacher Certification in Mathematics (1995) State of Colorado

M.S. in Mathematics (1985) New York University

B.S. in Mathematical Physics (1981) National University of Mexico

Professional Employment

Instructor of Mathematics (8/96 - 6/98) Old Dominion University

Head of the Mathematics Program (1/94 - 6/96) New Vista High School, Boulder, Colorado

Professional Research Assistant (8/91 - 2/92) Department of Civil, Environmental and Architectural Engineering, University of Colorado

Instructor (9/85 - 8/86) New York University, HEOP

Publications

1. A.L. Islas, D. Karpeev and C.M. Schober, *J. Comput. Phys.* **173**, 116 (2001).
2. A.L. Islas and C.M. Schober, *LNCS* **2331**, 486 (Springer Verlag, 2001).
3. A.L. Islas and C.M. Schober, *Fut. Gen. Comp. Sys.* **19**, 403 (2003).
4. M.H. Nachabe, A.L. Islas and T.H. Illangasekare, *Groundw.* **33**, 304 (1995).
5. A.W. Warrick, D.O. Lomen and A.L. Islas, *Wat. Res. Res.* **27**, 763 (1991).

Typeset using LaTeX.